LONG RANGE ANISOTROPIC INTERACTIONS IN RYDBERG ATOMS AND MOLECULES

by

WILLIAM CLARK

B. S., University of Nevada, 1992

M. S., University of Colorado, 1994

A thesis submitted to the

Faculty of the Graduate School of the

University of Colorado in partial fulfillment

of the requirements for the degree of

Doctor of Philosophy

Department of Physics

1998

This thesis for the Doctor of Philosophy degree by

William Clark

has been approved for the

Department of

Physics

by

Chris H. Greene

Robert Parson

Date _____

The final copy of this thesis has been examined by the signators, and we find that both the content and the form meet acceptable presentation standards of scholarly work in the above mentioned discipline.

Clark, William (Ph. D., Physics)

Long Range Anisotropic Interactions in Rydberg Atoms and Molecules

Thesis directed by Professor Chris H. Greene

The study of subtle interactions in atomic and molecular systems has stirred scientific interest since the dawn of quantum mechanics. Even today, research into perturbative long range interactions continues to push into new territory, largely driven by the experimental capabilities of Rydberg state spectroscopy. However, theoretical investigations have also made significant contributions, suggesting that the motion of a charged particle in the field of an anisotropic core is far more complicated than previously thought.

In this work we present a new theoretical formulation of Rydberg atoms and molecules that confirms the existence of previously unknown interactions, including an unusual pseudo-vector interaction with an "orbit-orbit" operator structure. While static long-range multipole interactions have been studied for years, the presence of dynamic terms that involve both position and momentum operators has been demonstrated only recently. In contrast to the ordinary quadrupole or induced-dipole interaction terms, the existence of this vector interaction hinges on the motion of the distant charge as it roams far beyond the confines of the core. Physically, this interaction reflects an attempt of the Rydberg electron to "drag" the core polarization vector with it. This drag is hindered by the internal moment of inertia of the ion, and by the moment of inertia of the distant electron about the center-of-mass .

The theoretical work described below, for high-ℓ Rydberg states of Ne, in combination with experimental work performed elsewhere, has confirmed for the first time the existence of this vector interaction. Our analysis shows that details of the spectrum, at sub-MHz resolution, depend strongly on the tensorial structure of this unusual interaction. Our long range multichannel formulation has now been applied successfully to describe autoionization resonances in doubly excited Rydberg states of Mg, and, most recently, to describe

high-ℓ Rydberg states of H_2 and D_2. This work also presents the first complete adiabatic calculations of the ground ($\nu^+ = 0, N^+ = 0$) and first rotationally excited ($\nu^+ = 0, N^+ = 1$) state polarizabilities and hyperpolarizabilities of H_2^+ and D_2^+. An analysis of the energy shifts generated by the vector interaction and the relativistic retardation (or Casimir) interaction demonstrates that they cause clearly different patterns of energy level splittings that should be experimentally observable. This theoretical work, in combination with still more sensitive experiments that are currently underway, should reveal the quantitative nature of both of these subtle interactions in a Rydberg molecule.

DEDICATION

I dedicate this work to my niece Anastasia Clark King who has been a great source of love and inspiration, and who reminds me every day that life is an adventure that is to be enjoyed. Thanks Pooh!

ACKNOWLEDGEMENTS

I first want to thank my advisor Professor Chris H. Greene for his support over the past few years, support that has allowed me to mature as a scientist and that has allowed me to interact with some of the best people in this field. The work presented here originated from discussions with Chris regarding the work of Stephen R. Lundeen and Bernard Zygelman during the previous three years, and has developed into a complete theoretical description of Rydberg atoms and molecules that provides both spectroscopic accuracy and physical insight.

Secondly, I want thank Professor Bernard Zygelman for providing me with encouragement and enthusiasm throughout my undergraduate and graduate years. I thank Bernard for having genuine interest in me and my future, and for taking the time to make a difference. I also want to thank Professor Thomas Degrand, who like Bernard, has encouraged me and impressed me with his exceptional knowledge, intelligence, wit, and advise.

Thirdly, I want to thank the numerous people I have had the privilege to interact with at JILA. I thank Robert P. Wood, Kurt W. Meyer, Gregory Miecznik, Jeff Stephens, Brett D. Esry, James P. Burke, Stephanie Staley, Andrew Hooker, John L. Bohn, Brian Eleson Granger, and Hugo W. Van der Hart whom made up the Greene Research Group during my graduate years. I also thank, Professor Robert Parson and my other committee members for reading this manuscript and provided many useful suggestions.

Finally, I want to thank the National Science Foundation for supporting my research interests, for allowing me to publish my work in peer reviewed, international journals, and for making it possible to attend and present my research at international conferences.

CONTENTS

FIGURES

FIGURE

TABLES

TABLE

CHAPTER 1

INTRODUCTION

The subtle influences of tiny interactions have frequently served as probes of new physics and as a reminder of the complexity of nature. The discrepancy between the observed and calculated perihelion of the planet Mercury, a mere difference of $43''$ of arc per century, was the outstanding problem in Newtonian physics until the equations of planetary motion were modified by the general theory of relativity. The existence of the Lamb shift in the $2S_{\frac{1}{2}}$ and $2P_{\frac{1}{2}}$ states of hydrogen (≈ 1057MHz) [1, 2] was found to originate from the interaction between the bound electron and vacuum fluctuations, and lead to the first systematic removal of logarithmic divergences from early relativistic theories and to the creation of renormalization techniques in modern quantum field theory [3, 4, 5, 6, 7]. Even the spin of an electron, while in some way a subtle atomic property, was originally discovered through its effects in spectroscopy, and has had far reaching implications including the number of electrons that can occupy a give quantum state (Pauli's exclusion principle) and of course the basic chemical properties of atoms and molecules.

Since the first measurement of the Lamb shift [1, 2], a half-century ago, the ability of experiments to probe the weakest forces in nature has grown enormously. Today the electroweak interaction and the nuclear anapole moment can be measured in table top atomic physics experiments [8], thereby broadening the traditional scope of atomic physics and complementing studies in high energy and nuclear physics. The field of Rydberg state spectroscopy [9, 10, 11, 12, 13, 14, 15, 16, 17] has likewise grown tremendously, providing a revealing probe of the subtle interactions between atomic and molecular ionic cores and weakly bound Rydberg electrons. High resolution microwave spectroscopy can now resolve

Rydberg intervals with a precision of 1 kHz [9, 10, 11], yielding precise, indirect measurements of ionic core multipole moments and polarizabilities. And, as a consequence of these improvements in resolution, experiments are close to measuring, for the first time, the slight energy shifts of Rydberg states due to relativistic retardation, or "Casimir" forces [18, 19].

In recent years, new physics has been discovered in the long range interactions of anisotropic Rydberg atoms and molecules. The work presented here not only chronicles this new discovery, but essentially represents much of its history. To put this discovery in perspective let us begin by reviewing some simple features of high-ℓ Rydberg motion.

The unusual spatial nature of nonpenetrating Rydberg states provides a considerable degree of theoretical simplification. The strong centrifugal repulsion, associated with high-ℓ motion, forces the Rydberg electron to roam far beyond the confines of the core. In this distant region the electron primarily experiences a simple screened Coulomb attraction toward the ion. However, it is the structure of the ionic core that makes Rydberg physics interesting and surprisingly complicated.

In order to elucidate the importance of core structure, consider the simple case of a distant Rydberg electron attached to a spherically symmetric ground state ion, which possesses no permanent multipole moment. Apart from the long range $-\frac{1}{r}$ Coulomb attraction, the charge induces dipole moments in the ion that fall off, asymptotically, as $\frac{1}{r^2}$. The net effect of the induced dipole interaction is to further increase the interaction potential energy by $-\frac{\alpha_s}{2r^4}$, where α_s is the scalar dipole polarizability of the ionic core. As a result, the polarization interaction produces simple scalar shifts for each ℓ state, removing the hydrogenic degeneracy.

The physics of a Rydberg system changes substantially when anisotropic cores having nonzero total angular momentum are considered. The first important difference is the presence of a quadrupole Rydberg-core interaction of the form $-\frac{Q}{r^3}P_2(cos\theta)$, where θ is the relative angle between a symmetry axis of the ion and a unit vector pointing to

the Rydberg electron. Moreover, an additional tensor dipole polarization interaction of the form $-\frac{\alpha_t}{2r^4}P_2(cos\theta)$ appears that was absent in the spherically symmetric case. The tensorial dependence of these interactions produces coupling among different ionic core states and among the various Rydberg series attached to ionization thresholds of the core, which generally produces far richer and more complex spectra than are observed for systems with spherically symmetric ionic cores.

Most theoretical treatments of Rydberg systems have been restricted to interactions among charged particles and spherically symmetric closed-shell atoms or ions [20, 21, 22]. Theoretical extensions to nonpenetrating Rydberg states that involve an electron and an open-shell, anisotropic core have remained largely unexplored. A few notable exceptions in atomic and molecular physics are the perturbative polarization schemes of Schoenfeld and Sturrus [23, 13, 12, 11] and the more general nonperturbative multichannel approach of Herzberg and Jungen [24, 25, 26]. The lack of attention to anisotropic systems, and the need to better understand the long range nature of nonrelativistic physics, is highlighted by Zygelman's [27] recent prediction of a new nonrelativistic "orbit-orbit" type interaction in anisotropic Rydberg systems. In a pioneering study of long range atomic forces, Zygelman used non-Abelian gauge transformations and geometric phases to predict an effective long-range potential energy, now called the "vector" interaction, with the operator structure

$$V_{vector} = \beta_v \frac{\vec{L_c} \cdot \vec{\ell}}{r^6}. \tag{1.1}$$

Here $\vec{L_c}$ and $\vec{\ell}$ denote the orbital momentum of the ionic core and the Rydberg electron, respectively. The terminology "vector" interaction is somewhat misleading. The overall operator $\vec{L_c} \cdot \vec{\ell}$ is clearly a scalar, which conserves the total angular momentum of the Rydberg-core system. Moreover, $\vec{L}_c$ and $\vec{\ell}$ are *pseudovectors* that remain even under the spatial inversion of the core and Rydberg electronic degrees of freedom. Interestingly, this is the only nonzero term with odd tensorial structure in the effective long range potential out

to radial order $\frac{1}{r^6}$. Additional odd rank tensor terms such as the dipole or octupole terms of the Rydberg-core interaction fail to survive to this order in $\frac{1}{r}$, assuming, of course, the typical situation where ionic states possess a definite parity.

The analysis of Zygelman provided no analytic expression for the proportionality coefficient β_v, raising questions regarding not only the physical origin of this "vector" interaction, but also its existence since the coefficient could vanish. A term with this operator structure was introduced into atomic spectroscopy by Trees [28] and Racah [29], but only on semiempirical grounds and without an explicit derivation. However, they did correctly interpret this correction term as a polarization energy arising from second-order perturbative effects.

In a move to clarify the existence of this term and provide some explanation of its physical origin, we put forth a systematic derivation of this unusual interaction, using standard techniques in atomic and molecular physics. With the aid of high resolution Rydberg spectra we confirmed, for the first time, its existence in Rydberg states of Ne [30, 31, 10]. Our theory has not only established the existence of the vector interaction, but it has also spawned an extension of perturbative theories that enables us to treat effects due to coupling among Rydberg states, using a long range polarization methodology. The new multichannel Hamiltonian approach to Rydberg systems has now been successfully applied to Rydberg states of Ne [30, 31, 10], to autoionizing Rydberg states of Mg [33, 32] and, most recently, to Rydberg states of H_2 and D_2 [34, 9, 11]. Physically, the vector term is a dynamic angular interaction that reflects a coupling among the orbital motion of the Rydberg electron and the internal ionic angular momentum, mediated by the dipole portion of the electron-ion interaction. As the Rydberg electron orbits the core, it tries to drag the core polarization vector with it. This drag is hindered by the internal moment of inertia of the ion, and the moment of inertia of the distant Rydberg electron.

The theoretical description of Rydberg systems developed here differs from the

traditional perturbative approaches in two important ways. We abandon the use of Rayleigh-Schrödinger perturbation theory and approach the problem from a multichannel close-coupling perspective that is common in modern scattering theory. The multichannel formulation makes it possible to derive effective long range potentials without fully solving the complete atomic or molecular Rydberg problem. This differs from the Rayleigh-Schrödinger approaches [23, 13, 12, 11] in that we do not calculate shifts from pure hydrogenic levels, but rather systematically derive effective potentials and compute Rydberg states by diagonalizing an effective Hamiltonian. This last step provides a second important difference, in that coupling among different Rydberg states can be treated almost exactly. While it is true that the long range interaction between the Rydberg electron and the ionic core can be expanded in reciprocal powers of the Rydberg radial coordinate, Rydberg states attached to different ionization thresholds of the ionic core can still be strongly coupled to one another. Moreover, the fact that there can be near degeneracies among these strongly coupled Rydberg states invalidates the traditional nondegenerate perturbative approaches. This type of coupling is easily treated, however, with the multichannel formulation presented here.

We begin in Chapter 2 with a systematic derivation of the long range adiabatic potential between a Rydberg electron and an arbitrary anisotropic core. This derivation serves to demonstrate how a long range potential can be derived using standard techniques in atomic and molecular physics, and lays the groundwork for a theoretical prediction of the vector interaction, which is presented in Chapter 4. In Chapter 3 we generalize the single channel analysis of Chapter 2 and develop a multichannel diabatic approach to Rydberg systems that enables a systematic treatment of channel coupling. The proper treatment of channel coupling is essential in any modern theory that attempts to reproduce experimental observations with spectroscopic accuracy. In chapter 4 we use Wigner-Racah recoupling algebra to transform the potentials developed in Chapters 2 and 3 so that both their operator structure and their anisotropic nature can be easily identified. The tensor analysis also

enables the identification of channel dependent core properties that allow us to cast the long range potentials in a parametrized form. A systematic derivation of the vector interaction is then presented and its physical implications are discussed.

In Chapters 5 through 7 we apply our theoretical formulation to the description of Rydberg states in Ne, Mg, H_2, and D_2. The analysis of the $n = 10$, $\ell = 5, 6, 7$, and 8 Rydberg states of Ne, presented in Chapter 5, represents the first confirmation of the vector interaction within a Rydberg system. We show that by including the vector interaction in our analysis of the observed Ne Rydberg levels [10, 30, 31] a four fold reduction in the χ^2 comparison can be achieved, reproducing energy splittings with an accuracy of no worse that 0.5 MHz. Moreover, a comparison of our theoretical value for β_v and the value extracted from the experiment provides additional evidence for the existence of this subtle interaction.

Chapter 6 continues this investigation into anisotropic interactions by considering the doubly excited $3pnf$ Rydberg states of Mg where a Rydberg electron interacts with an excited Mg^+ $3p$ core [31, 32]. In this system the strong coupling among Rydberg states results in irregular behavior in the n-dependence of autoionization rates, which is accurately described by our diabatic formulation. While the coefficient of the vector interaction is thirty times larger for the Mg^+ $3p$ core than for the Ne^+ core, its effect is much less discernible owing to the large widths of the lower-ℓ autoionizing resonances that were examined in the Mg experiment.

Chapter 7 presents our most recent work on Rydberg states of the simple diatomic molecules H_2 and D_2. This work focuses primarily on Rydberg states attached to spherical ionic cores, namely the $(\nu^+ = 0, N^+ = 0)$ states of H_2^+ and D_2^+, since measurements with kHz resolution were recently performed by Jacobson [9]. These precise measurements give a stringent test of our diabatic formulation and our ability to accurately compute core multipole moments, polarizabilities, and hyperpolarizabilities. The first complete adiabatic calculations of polarizabilities and hyperpolarizabilities for the ground $(\nu^+ = 0, N^+ = 0)$ and

first rotationally excited ($\nu^+=0, \mathrm{N}^+=1$) states of H_2^+ and D_2^+ are presented. The strength of our treatment is demonstrated by our ability to reproduce Rydberg intervals with a accuracy of better than 0.3 MHz. We are hopeful that exact, or nonadiabatic, calculations of the polarizabilities and hyperpolarizabilities of H_2^+ and D_2^+ will help reduce the remaining discrepancies and provide the first clear signature of retardation, or a "Casimir" force, within a Rydberg molecule.

While very little data exits with kHz resolution for H_2 Rydberg states attached to an anisotropic core ($N^+ > 0$) [12, 11], we can still provide some interesting studies of the vector interaction. One of the more revealing new predictions is that the vector hyperpolarizability β_v is inversely proportional to the rotational inertia of an anisotropic homonuclear diatomic ion. This fact confirms our physical picture of the vector interaction. As the distant Rydberg electron revolves around the core, it tries to "drag" the core polarization vector with it. Unfortunately, the relatively large moment of inertia of the molecule strongly resists this drag, thereby minimizing the "torque" effect. As a result, the dynamic vector interaction is tiny in molecular Rydberg states. An analysis of the energy shifts generated by the vector interaction and by relativistic retardation interactions in Rydberg states of ($\nu^+=0, \mathrm{N}^+=1$) H_2 [19] demonstrates that they produce distinct patterns of energy level splittings that should be experimentally observable. This theoretical work, in combination with more sensitive experiments that are currently underway, should reveal the quantitative nature of both of these subtle interactions in Rydberg states of H_2.

CHAPTER 2

ADIABATIC DESCRIPTION OF RYDBERG SYSTEMS

In this chapter we present an adiabatic analysis of Rydberg systems that shows the origin of the vector interaction, and develop a multichannel formulation that generalizes perturbative polarization models. The goal here is to use techniques that are standard in atomic and molecular physics to derive a long range potential that describes how a slow, or adiabatic, Rydberg electron interacts with an arbitrary anisotropic ionic core.

2.1 Adiabatic Representation

The concept of adiabaticity has been used extensively in atomic and molecular physics. One of the earliest quantum mechanical application was the extremely useful Born-Oppenheimer approximation, which provides much of the framework used to understand the low vibrational states of diatomic molecules. The approximation essentially assumes that the relative motion of the nuclei is slow compared with the motion of the molecular electrons, and, as a consequence, the electronic properties of the system acquire a weak parametric dependence on the internuclear separation. In other words, the slow nuclear motion leads to an approximate separation of the nuclear and electronic degrees of freedom.

This approach can be extended to many problems in physics, provided there is at least one "slow" degree of freedom relative to all other degrees of freedom in the system. In Rydberg atoms and molecules it is the radial coordinate of the Rydberg electron that can serve as the adiabatic coordinate. A Rydberg atom or molecule is a simple quantum system involving an electron with high angular momentum ($\ell \geq 5$) and a relatively isolated ionic core. The slow moving Rydberg electron can be regarded as a probe of the electrostatic properties of the ionic core: specifically the permanent multipole moments and polarizabilities of the

relevant ionic states. The large spatial separation between high-ℓ Rydberg and core electronic states makes Rydberg electron spin effects (such as exchange) negligible. (These effects can be included perturbatively if they become appreciable.) The absence of exchange between the Rydberg and the core electrons leads to the $(J_c\ell)K$ coupling scheme [35, 36]. Here the total angular momentum J_c of the fast core electrons is coupled with the orbital momentum ℓ of the slow Rydberg electron to form a resultant K, which serves as the total angular momentum in most of the succeeding derivations.

The centrifugal repulsion associated with high-ℓ Rydberg states forces the Rydberg electron to roam beyond the confines of the core. In this distant region the radial coordinate of the Rydberg electron becomes distinct, both spatially and dynamically, from the coordinates of the ionic core. For these reasons, a useful expansion of the wave function for the entire system is

$$\Psi(r,\omega) = \sum_i \phi_i(\omega)\psi_i(r) \tag{2.1}$$

where the $\{\phi_i(\omega)\}$ representation is an r-independent basis set and ω represents all coordinates in the system except the Rydberg radial coordinate. This basis set is formed from a complete set of ionic energy eigenstates, whose angular momenta are coupled with the orbital functions Y_{lm} of the Rydberg electron. This *ansatz* for the wavefunction, combined with the Schrödinger equation, leads to a set of coupled radial equations that are usually called the "close-coupling equations" (without exchange) in atomic physics. The functions $\{\psi_i(r)\}$ in this primitive expansion can be viewed as the radial wavefunctions for motion within the ionic channels of the system. The potential curves that describe the radial motion of the Rydberg electron are formed from a combination of the diagonal matrix element $V_{ii}(r)$ of the Rydberg-core interaction potential, the repulsive centrifugal term, and the ionic threshold energy E_i in channel i. The off-diagonal matrix elements $V_{ji}(r)$ can then be viewed as causing Rydberg electron transitions from the $i-th$ to the $j-th$ Rydberg-core channel.

The full effective potential matrix that enters the conventional close-coupling (CC) equations without exchange is

$$V_{ij}^{CC}(r) = \left(\frac{\ell_i(\ell_i+1)}{2r^2} - \frac{1}{r} + E_i \right) \delta_{ij} + V_{ij}(r). \tag{2.2}$$

Here ℓ_i is the orbital momentum of the Rydberg electron in channel i. Unless stated otherwise, matrix elements involve integrals over all coordinates (ω) (and traces over all spins) in the problem, except for the radial coordinate of the Rydberg electron. Note that we have split off the dominant Coulomb interaction $-\frac{1}{r}$ so that the remaining potential matrix $V_{ij}(r)$ can be expanded as an asymptotic series in $\frac{1}{r}$.

2.2 Adiabatic Close-Coupling Equations

The primitive basis set $\{\phi_i(\omega)\}$ used in the conventional close-coupling equations is independent of the radial coordinate r of the Rydberg electron. As a consequence, this representation does not describe the radial variation in the polarization of the ionic core during close encounters with the Rydberg electron. That physics, however, is included in the standard close-coupling equations through off-diagonal channel coupling. Here we introduce a representation that builds the predominant dynamical effects of the Rydberg electron into a more useful effective potential. As in the molecular Born-Oppenheimer approach, these potential curves are obtained by diagonalizing an "adiabatic Hamiltonian" $\hat{H}_{r=const}$ in which derivative operators with respect to the adiabatic coordinate r are discarded. The resulting adiabatic eigenstates $\Phi_\mu(r;\omega)$ form (at every value of r) a complete orthonormal set in the coordinates ω. The adiabatic approximation is valid in our present context if the system remains confined within a single adiabatic channel as the Rydberg electron roams slowly beyond the confines of the core. Explicitly, the adiabatic potentials $U_\mu(r)$ and eigenstates $\Phi_\mu(r;\omega)$ are defined as r-dependent parametric solutions of the linear eigenvalue problem:

$$\hat{H}_{r=const}\Phi_\mu(r;\omega) = U_\mu(r)\Phi_\mu(r;\omega). \tag{2.3}$$

In the $\{\phi_i(\omega)\}$ representation, the matrix of the adiabatic Hamiltonian operator $\hat{H}_{r=const}$ reduces to $\underline{V}^{CC}(r)$. The adiabatic channel functions are r-dependent superpositions of the ionic core states and the orbital functions of the Rydberg electron. They contain information concerning the instantaneous interactions between the Rydberg electron and the core, and provided r varies slowly, concerning the approximately conserved properties of the electron-core system. An expansion of the total wavefunction for the system in terms of the adiabatic channel functions

$$\Psi(r,\omega) = \sum_\mu F_\mu(r)\Phi_\mu(r;\omega), \tag{2.4}$$

transforms the Schrödinger equation into a set of coupled radial equations. These can be written in matrix form as

$$\left[-\frac{1}{2}\left(\underline{I}\frac{d}{dr} + \underline{P}(r)\right)^2 - (E\underline{I} - \underline{U}(r))\right]\underline{F}(r) = 0, \tag{2.5}$$

where the derivative coupling matrix is defined by

$$P_{\mu\nu}(r) = \langle\Phi_\mu \mid \frac{\partial}{\partial r}\Phi_\nu\rangle. \tag{2.6}$$

Here we adopt Greek letters to label the adiabatic channels. At sufficiently large distances $r \to \infty$, each adiabatic channel converges to one of the ionic channels labeled by Roman letters in the primitive close-coupling representation.

In contrast to the primitive close-coupling representation, in which the coupling among the ionic channels enters through the potential matrix V^{CC}, the coupling among

our *adiabatic channels* derives from the derivative matrix $P_{\mu\nu}(r)$ that modifies the radial momentum operator. Thus the P-matrix accounts for all nonadiabatic or inelastic effects that arise because the slow Rydberg electron is not slow enough for the core electrons to instantaneously adjust within the time frame of Rydberg motion. For most of the regimes discussed here, the off-diagonal derivative couplings are small compared with the diagonal adiabatic potentials. Under these conditions, the motion of the system remains confined, to an excellent approximation, within a single adiabatic channel of the system. As we discuss later, the analogy between the modified radial momentum operator and a generalized momentum operator that involves both the usual mechanical momentum plus an additional term, such as an electromagnetic vector potential, [27, 37, 38] permits some of the long range interactions to be viewed as non-Abelian gauge fields.

2.3 Adiabatic Potentials and Post-Adiabatic Corrections

The Born-Oppenheimer approximation, which neglects the channel coupling matrix $\underline{P}(r)$ altogether, is adequate for many purposes. To achieve higher accuracy or to treat higher energy processes, however, it is important to include some effects of $\underline{P}(r)$. One natural approach to this problem attempts to write the radial Schrödinger equation in an approximate single channel form

$$\left[-\frac{1}{2}\frac{d^2}{dr^2} - (E - u_\mu(r,E))\right] F_\mu(r) = 0, \tag{2.7}$$

in which a new effective potential $u_\mu(r,E)$ is introduced that depends on the adiabatic potentials $\{U_\nu(r)\}$, the derivative couplings, and the energy of the system E in some simple algebraic way.

The post-adiabatic theory of Klar and Fano[39, 40], later generalized by Aquilanti [41], provides a means of including the perturbative effects of derivative coupling through an iterative algebraic procedure. The main idea is to transform the original adiabatic equation

Eq.(2.5) into a set of coupled single-channel equations where the new coupling arises from terms proportional to $\underline{P}(r)$ or $\frac{d}{dr}\underline{P}(r)$. This "postadiabatic procedure" can be iterated, in principle, which will (hopefully) reduce the coupling strength in each successive iteration.

For our purposes we use only the first iteration of the procedure, for which the effective potential is given by

$$u_\mu(r,E) \simeq U_\mu(r) - \frac{1}{2}\left(P^2\right)_{\mu\mu} + 2\left(E - U_\mu(r)\right)\sum_\nu \frac{\mid P_{\mu\nu} \mid^2}{U_\mu(r) - U_\nu(r)}. \tag{2.8}$$

The perturbative condition $P^2_{\mu\nu}(r) \ll \mid U_\mu(r) - U_\nu(r) \mid$ should be satisfied at all r relevant in the problem, which should always be the case for sufficiently high ℓ states of Rydberg systems. An immediate implication of the nonadiabatic corrections is an increase in the potential energy due to the repulsive energy-independent diagonal term $-P^2_{\mu\mu}$. Inclusion of this term in molecular problems is often called the "adiabatic approximation" as opposed to the strict Born-Oppenheimer approximation which neglects $\underline{P}(r)$ completely. This term is usually written as a second derivative coupling matrix in that context, but it is equivalent to our form as the square of the first-derivative coupling matrix [39]. An additional implication is the presence of an energy-dependent contribution; its sign can vary from state to state, but for the channel of lowest energy, it generally makes the effective post-adiabatic potential $u_\mu(r,E)$ *increasingly attractive* as the energy *increases* above threshold.

The derivative couplings $P_{\mu\nu}(r)$ can be computed from the radial partial derivative of the adiabatic Hamiltonian. The diagonal derivative couplings vanish, that is $P_{\mu\mu}(r) = 0$, since the P matrix is skew symmetric, and the off diagonal terms are given by

$$P_{\mu\nu}(r) = \frac{\langle \Phi_\mu \mid \frac{\partial}{\partial r}\hat{H}_{r=const} \mid \Phi_\nu \rangle}{U_\nu(r) - U_\mu(r)}, \tag{2.9}$$

which can be derived from the defining equation, Eq.(2.3), for the adiabatic potentials and eigenfunctions. The partial derivative of the adiabatic Hamiltonian is readily evaluated

analytically. This form of the derivative coupling matrix clearly demonstrates the apparently singular behavior when two channels of common symmetry are nearly degenerate ($U_\mu(r) \approx U_\nu(r)$). The avoided crossing redistributes radial flux among the strongly coupled, nearly degenerate channels.

2.4 Perturbative Adiabatic Diagonalization for Nondegenerate Channels

In Rydberg atoms and molecules of high orbital momentum ($\ell \geq 5$) the dominant electrostatic interaction between the Rydberg electron and the ionic core is the dipole moment which goes as $\frac{1}{r^2}$. Since a typical inner turning radius is $r \approx \frac{\ell(\ell+1)}{2}$ for a Rydberg electron near zero energy, all electrostatic interactions are perturbative compared to the screened Coulomb attraction $-\frac{1}{r}$. The small values of the electrostatic matrix elements $V_{ij}(r)$ compared with the ionic threshold splittings validates a perturbative diagonalization of the $\underline{V}^{CC}(r)$ matrix.

An important step in a systematic perturbative diagonalization of this matrix is the inclusion of diagonal elements $V_{ii}(r)$ in the unperturbed Hamiltonian (see the *modified iteration-perturbation* formulas of Morse and Feshbach[42]). This is immediately apparent when the long range coupling matrix is written as

$$V_{ij}^{CC}(r) = \left(\frac{\ell_i(\ell_i+1)}{2r^2} - \frac{1}{r} + E_i + V_{ii}(r) \right) \delta_{ij} + V_{ij}(r), \tag{2.10}$$

where the $V_{ij}(r)$ are now purely off-diagonal contributions. A spherical multipole expansion of $V_{ij}(r)$ now separates the ionic core and Rydberg electron coordinates

$$\begin{aligned} V_{ij}(r) &= \sum_{k=0}^{\infty} \langle \phi_i \mid \frac{r_i^k}{r^{k+1}} P_k(cos\theta_{ir}) \mid \phi_j \rangle \\ &= \sum_{k=0}^{\infty} \langle \phi_i \mid \frac{r_i^k}{r^{k+1}} C^{(k)}(\hat{r}_i) \cdot C^{(k)}(\hat{r}) \mid \phi_j \rangle \end{aligned} \tag{2.11}$$

where the $C^{(k)}$ are renormalized spherical harmonics [43].

The perturbative diagonalization of the $\underline{V}^{CC}(r)$ matrix, through second order in $V_{ij}(r)$, produces terms involving summations over intermediate channels ν with potential energy denominators $U_\mu(r) - U_\nu(r)$. These second order contributions can be classified as either degenerate or nondegenerate depending on whether an intermediate channel ν is degenerate with the physically relevant channel μ at $r \to \infty$ (i.e., $U_\nu = U_\mu$). In the nondegenerate case (i.e., $E_\nu \neq E_\mu$), this approach gives a long range potential with the structure

$$\begin{aligned} u_\mu(r) \qquad &= E_\mu - \frac{1}{r} + \frac{\ell_\mu(\ell_\mu+1)}{2r^2} + \frac{Q^{(2)}_{\mu\mu}}{r^3} - \frac{\alpha_\mu}{2r^4} + \frac{Q^{(4)}_{\mu\mu}}{r^5} \\ &+ \frac{\beta^{ad}_\mu + \beta^{nad}_\mu - 2(E-E_\mu)\lambda_\mu - \delta_\mu - \eta_\mu}{2r^6} + O\left(\frac{1}{r^8}\right) \end{aligned} \tag{2.12}$$

where *ad* (or *nad*) denotes adiabatic (or nonadiabatic). Every term in this potential can be written as a standard second-order perturbation sum, except for the diagonal quadrupole $Q^{(2)}_{\mu\mu}$ and hexadecapole $Q^{(4)}_{\mu\mu}$ terms which are diagonal (first-order) matrix elements of the ionic electric quadrupole and hexadecapole operators. Explicit expressions for these terms as infinite perturbation sums, over bound and continuum states of the core, can be obtained along the lines of the derivation given by Ref.[44], although there are differences in notation, in coupling scheme, and in the multipoles that were included. Each term $Q^{(2)}_{\mu\mu}$,$Q^{(4)}_{\mu\mu}$,α_μ, β^{ad}_μ, β^{nad}_μ, λ_μ, δ_μ, and η_μ depends on the various quantum numbers J_μ, ℓ_μ, and K in a relatively complicated fashion which is difficult to analyze:

$$Q^{(k)}_{\mu\nu} = \langle \mu \mid \sum_{i=1}^{N_c} r_i^k P_k(cos\theta_{ir}) \mid \nu \rangle, \tag{2.13}$$

$$\alpha_\mu = \sum_{\nu \neq \mu} \frac{2Q^{(1)}_{\mu\nu} Q^{(1)}_{\nu\mu}}{E_\nu - E_\mu}, \tag{2.14}$$

$$\beta^{a\,d}_\mu = \sum_{\nu \neq \mu} \frac{[\ell_\nu(\ell_\nu + 1) - \ell_\mu(\ell_\mu + 1)]}{(E_\nu - E_\mu)^2} Q^{(1)}_{\mu\nu} Q^{(1)}_{\nu\mu}, \tag{2.15}$$

$$\beta^{na\,d}_\mu = \sum_{\nu \neq \mu} \frac{4Q^{(1)}_{\mu\nu} Q^{(1)}_{\nu\mu}}{(E_\nu - E_\mu)^2}, \tag{2.16}$$

$$\lambda_\mu = \sum_{\nu \neq \mu} \frac{8Q^{(1)}_{\mu\nu} Q^{(1)}_{\nu\mu}}{(E_\nu - E_\mu)^3}, \tag{2.17}$$

$$\delta_\mu = \sum_{\nu \neq \mu} \frac{2Q^{(2)}_{\mu\nu} Q^{(2)}_{\nu\mu}}{E_\nu - E_\mu}, \tag{2.18}$$

and

$$\eta_\mu = \sum_{\nu \neq \mu} \frac{4Q^{(1)}_{\mu\nu} Q^{(3)}_{\nu\mu}}{E_\nu - E_\mu}. \tag{2.19}$$

In Eq. (2.13) N_c denotes the number of ionic core electrons, while the subscript r refers the Rydberg electron. One consequence of including nonadiabatic effects is the appearance of an energy dependent term in the long range potential. This energy dependence has generated a small controversy because different treatments disagree in multiplicative constants[21, 22]. Ref.[22] shows, however, that the energy dependent term of order $\frac{1}{r^6}$ can be written as an ℓ-dependent linear combination of $\frac{1}{r^7}$ and $\frac{1}{r^8}$, implying that the energy dependent term can be regarded as a contribution of higher order than $\frac{1}{r^6}$.

2.5 Degenerate Channel Contributions

The nature of the long range potential changes qualitatively when degenerate terms are present. For instance, in Mg the 3pnf and 3pnh channels are degenerate. Second order degenerate contributions appear when intermediate channels ν share the same threshold energies $E_\nu = E_\mu$, K-value and parity with the physically relevant channel μ at $r \to \infty$. However, for simplicity we assume that (as in the Mg case cited above) the intermediate Rydberg electron orbital momentum ℓ_ν differs from ℓ_μ, for all degenerate channels. A derivation similar to that given above produces two additional contributions to the potential $u_\mu(r)$ that originate in coupling to the degenerate channels:

$$u'_\mu(r) = u_\mu(r) + \frac{a_\mu}{r^4} + \frac{b_\mu}{r^6} + O\left(\frac{1}{r^8}\right) \tag{2.20}$$

where the a_μ and b_μ terms are explicitly

$$a_\mu = \sum_{\nu \neq \mu} \frac{2Q^{(2)}_{\mu\nu} Q^{(2)}_{\nu\mu}}{\ell_\mu(\ell_\mu+1) - \ell_\nu(\ell_\nu+1)} \tag{2.21}$$

and

$$b_\mu = \sum_{\nu \neq \mu} \frac{4Q^{(2)}_{\mu\nu} Q^{(4)}_{\nu\mu}}{\ell_\mu(\ell_\mu+1) - \ell_\nu(\ell_\nu+1)}. \tag{2.22}$$

Eq.(2.20) excludes one important type of degenerate channel coupling that arises when two or more ionic states of opposite parity are degenerate and can consequently support a permanent dipole moment. The resulting degenerate dipole-coupling of channels can be important, e.g. in the properties of doubly-excited states of the hydrogen negative ion. In this case a diagonalization within the degenerate channel space should be performed as in Refs.[45, 21]. After transformationing to a representation where the long-range dipole

coupling is diagonal, however, the effects of other (non-dipole) multipoles can be handled using the present techniques.

2.6 Advantages and Disadvantages

An adiabatic analysis is not quantitatively accurate in situations where curve crossings arise, because of the neglect of channel coupling. However, the qualitative insight provided by the single channel description can be a helpful tool when it comes to interpretation of the dynamics. For a Rydberg atom or molecule, the simple form of the long range adiabatic potential offers physical insight into the Rydberg-core interaction. Specifically, if the core of a Rydberg system is spherically symmetric (total angular momentum zero), then the interaction between the Rydberg electron and the many core electrons is purely scalar and the dominant interaction is induced dipole polarization. In anisotropic systems where the core is nonspherical (nonzero total angular momentum) the dominant interaction is the tensor quadrupole interaction followed by scalar and tensor dipole polarization. In chapter 4 we show that a new type of interaction arises when the core is anisotropic. The new vector interaction

$$V_{vector} = \beta_v \frac{\vec{L}_c \cdot \vec{\ell}}{r^6} \tag{2.23}$$

couples the angular momentum of the core with the orbital momentum of the Rydberg electron. The vector hyperpolarizability β_v depends on the dipole moments of the core and arises as a dynamic angular interaction due to the motion of the Rydberg electron.

CHAPTER 3

DIABATIC FORMULATION OF THE RYDBERG CHANNEL INTERACTIONS

In this chapter we present a multichannel diabatic formulation that provides an effective means of treating coupling among different Rydberg-core channels. By "eliminating" a class of channels, we use a Green's function expansion to derive an effective Hamiltonian with a potential matrix that can couple different μ and μ' channels. The resulting structure resembles that of the nondegenerate long range potential developed in the previous chapter.

3.1 Diabatic Representation

In the previous chapter the description of a Rydberg system began with the choice of a primitive representation $\{\phi_i(\omega)\}$ in the Hilbert space of the ion and of the angular degrees of freedom of the Rydberg electron. This basis set is independent of the radial coordinate r of the Rydberg electron. Through a diagonalization of the ionic Hamiltonian matrix (at every value of r) we form an adiabatic representation where each eigenstate is a superposition of the ionic core states and the orbital functions of the Rydberg electron. These adiabatic eigenstates contain information concerning the instantaneous Rydberg-core interaction and, provided channel coupling is weak, concerning the approximately conserved properties of the system. Unfortunately, an adiabatic analysis that involves a single adiabatic channel is usually only appropriate when channel coupling is weak, implying an approximate separability of the problem. In general, an accurate description of a Rydberg system requires the inclusion of channel coupling, either through the derivative coupling matrix elements $P_{\mu\nu}(r)$ of an adiabatic formulation or through the off-diagonal $V_{ij}(r)$ matrix elements in our primitive basis set expansion. Examples of this situation arise in our applications of these methods to Rydberg states of Ne[30, 31], to doubly excited autoionizing Rydberg states of

Mg[33], and finally to Rydberg states of H_2 and D_2 [34].

Our theoretical description of Rydberg systems is based on the primitive $\{\phi_i(\omega)\}$ basis set, which is often referred to as a "diabatic" representation. Adiabatic formulations and their corresponding potential curves are useful for developing a qualitative understanding of radial motion and for providing insight into perturbations and resonance structure. Unfortunately, the derivative coupling matrix elements of an adiabatic formulation can become nearly singular, when channels of common symmetry possess close avoided crossings. Such crossings occur ubiquitously in open shell atoms with fine structure and can lead to numerical difficulties; consequently, a diabatic formulation is often preferable for quantitative calculations.

The channel structure provided by the primitive close-coupling equations enables physically dominant channels to be separated from those that play only a perturbative role in the physics of a Rydberg system. Since most experiments devoted to the study of Rydberg energy levels focus on Rydberg series that converge to specific ionization thresholds of the core (typically split by fine structure or rotational interactions in the case of molecules), the total channel space can be partitioned into a P subspace of physically dominant channels and a complementary Q subspace (see Figure 3.1) that is needed to describe core multipole moments induced by the electric field of the Rydberg electron. In what follows, the interactions among channels belonging to the P subspace are treated "exactly", while couplings to the Q subspace are described perturbatively.

3.2 Diabatic Close-Coupling Equations

The diabatic close-coupling equations connecting all channels with specified total angular momentum K (excluding the Rydberg electron spin) and specified parity π can be written in the partitioned form

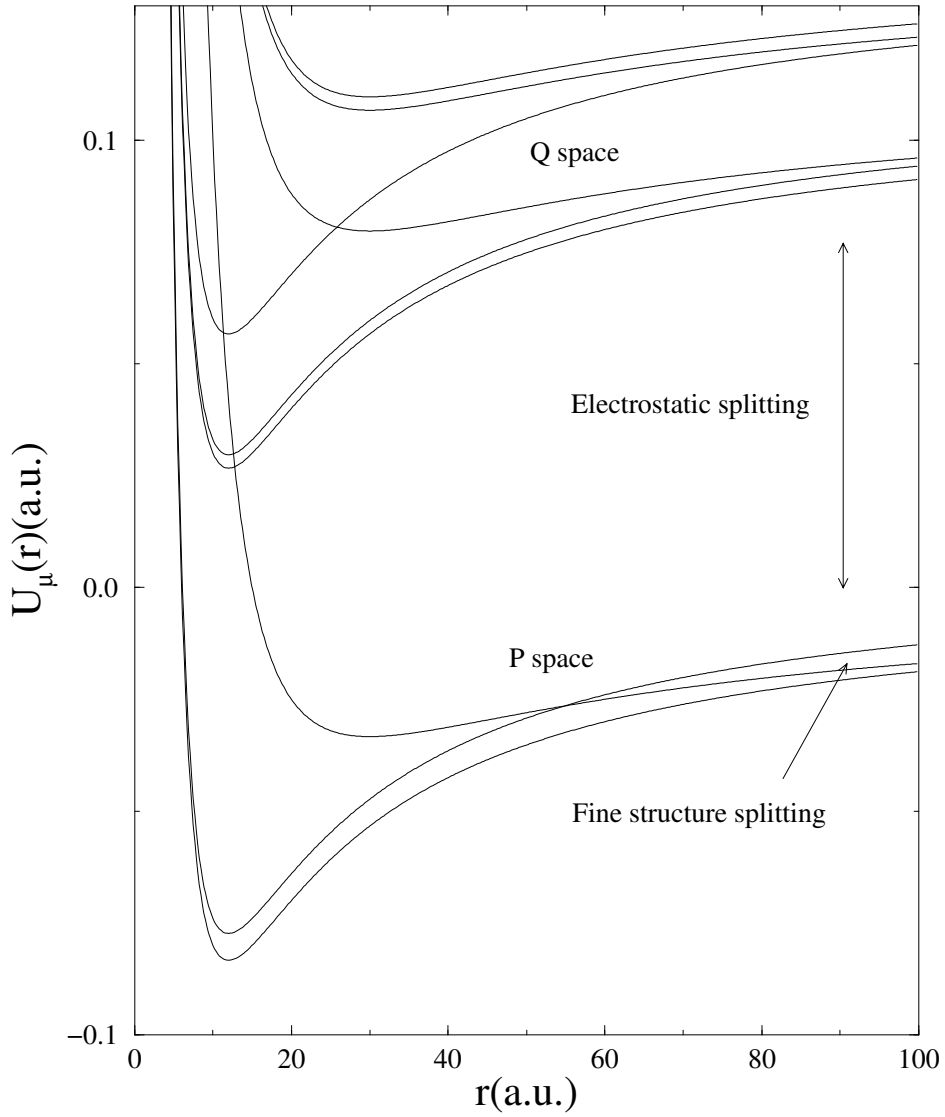

Figure 3.1. Generic radial potentials, with electrostatic (or vibrational) and fine-structure (or rotational) splittings, that demonstrate the natural separation of physically dominant channels from those that play only a perturbative role in the physics of a Rydberg system.

$$\left[-\frac{1}{2}\underline{I}\frac{d^2}{dr^2} - E\underline{I} + \begin{pmatrix} V^{QQ} & V^{QP} \\ V^{PQ} & V^{PP} \end{pmatrix}\right] \begin{pmatrix} \psi_Q \\ \psi_P \end{pmatrix} = 0, \tag{3.1}$$

where V is the coupling matrix V^{CC} in Eq.(2.2), and $\underline{I}$ is the identity matrix.

The number of these equations is generally infinite and for practical reasons must be truncated in some sensible way. The object is to derive a set of equations and an effective Hamiltonian that describe the motion of a Rydberg electron within the physical channel subspace. For this approach to be useful, the Hamiltonian must include coupling among the channels of the physical P subspace, and incorporate effects of the perturbative Q subspace channels, which manifest themselves through polarization and hyperpolarization interactions.

An equation describing the P subspace wavefunction and an effective Hamiltonian can be obtained through the standard technique of channel elimination [46, 47, 48]

$$H^{PP}\psi_P = E\psi_P, \tag{3.2}$$

using a Green's functions [49, 50]. The energy dependence of the effective Hamiltonian H^{PP}

$$H^{PP} = -\frac{1}{2}I^{PP}\frac{d^2}{dr^2} + V^{PP} + V^{PQ}G^{QQ}(E)V^{QP}, \tag{3.3}$$

is a consequence of the channel elimination, and enters through the radial Green's function matrix $G^{QQ}(E)$ that satisfies the equation

$$\left[-\frac{1}{2}I^{QQ}\frac{d^2}{dr^2} - EI^{QQ} + V^{QQ}\right] G^{QQ}(r, r', E) = -I^{QQ}\delta(r - r'), \tag{3.4}$$

subject to closed-channel boundary conditions. The dominant coupling among P subspace channels enters through the first order terms V^{PP}, while the perturbative effects of the Q subspace channels enters through the second-order terms involving the energy-dependent Green's function. The Green's function of equation (3.4) can be written in the operator form

$$G^{QQ}(r, r', E) = \left[E - H^{QQ}(r)\right]^{-1} \delta(r - r') \tag{3.5}$$

where the inverse operator $\left[E - H^{QQ}(r)\right]^{-1}$ is an integral operator with the boundary conditions built into it [49, 50]. In the next section we use a binomial expansion of this inverse operator to obtain an energy-independent effective Hamiltonian that can be used to accurately describe Rydberg motion within the physical channel subspace.

3.3 Generalized Eigenvalue Problem

The form of the effective Hamiltonian in equation (3.3) is neither very appealing nor useful, because of its nonlinear dependence on energy. Since we are interested in Rydberg states that converge to specific ionic thresholds of the core, this nonlinear energy dependence can be approximately removed through a binomial expansion of the Green's function and a simple energy transformation.

Channels in the P subspace are typically split by fine structure interactions (rotational interactions in the context of Rydberg molecules) while the energy difference between a channel in the P subspace and a channel in the Q subspace basically originates from electrostatic interactions (vibrational interactions). The difference in magnitude of fine structure and electrostatic splittings enables us to expand the Green's function in reciprocal powers of $E - E_Q$, where E_Q is an ionization threshold in the Q subspace. In addition to this expansion we also replace the energy of the system E with $E_{P_0} + \varepsilon$ where E_{P_0} is typically the ionic threshold within the P channel subspace under experimental study and ε is a small Rydberg energy shift. The resulting Green's function takes the simple, analytic form

$$G^{QQ}(r, r', E) = g^{QQ}(r, \varepsilon)\delta(r - r') \tag{3.6}$$

where

$$g^{QQ}(r,\varepsilon) \equiv \left[E - H^{QQ}(r)\right]^{-1} = \left[(E - E_Q) - (H^{QQ}(r) - E_Q)\right]^{-1}$$

$$= \frac{I^{QQ}}{E - E_Q} + \frac{I^{QQ}}{E - E_Q}(H^{QQ}(r) - E_Q)\frac{I^{QQ}}{E - E_Q} + \cdots$$

$$= \frac{I^{QQ}}{E_{P_0} - E_Q} + \frac{I^{QQ}}{E_{P_0} - E_Q}(H^{QQ}(r) - E_Q)\frac{I^{QQ}}{E_{P_0} - E_Q}$$

$$-\varepsilon\frac{I^{QQ}}{(E_{P_0} - E_Q)^2} + \cdots. \tag{3.7}$$

This formally exact analytic expression for the Green's function can be obtained, alternatively, through an eigenfunction expansion, for example, using the bound and continuum states of hydrogen [49, 50]. Since we are considering high-ℓ Rydberg states within the P subspace, the Green's function for the Rydberg electron can only couple to high-ℓ states of the Q subspace. The high-ℓ nature of this coupling suggests that only near threshold bound and continuum states within the Q subspace will contribute to the Green's function. In this sense, the $H^{QQ}(r) - E_Q$ operator represents a Rydberg energy that is small compared with the large electrostatic splittings. These arguments are supported by the fact that all dynamic or nonadiabatic effects arising from terms proportional to $\frac{1}{(E_{P_0} - E_Q)^2}$ are typically an order of magnitude smaller than the static or adiabatic terms proportional to $\frac{1}{E_{P_0} - E_Q}$. This will become clear in the later chapters where numerical calculations support these arguments.

The preceding analysis enables us to cast our original close-coupling equation, Eq.(3.2), involving an energy-dependent Hamiltonian, in the form of a generalized eigensystem (linear in ε) where the eigenvalue is the Rydberg energy ε

$$\bar{H}^{PP}\psi_P = \varepsilon\Lambda^{PP}\psi_P. \tag{3.8}$$

The energy-independent "effective Hamiltonian" $\bar{H}^{PP}$ is

$$\bar{H}^{PP} = -\frac{1}{2} I^{PP} \frac{d^2}{dr^2} - E_{P_0} I^{PP} + V^{PP} + V^{PQ} g^{QQ}(r,0) V^{QP}. \tag{3.9}$$

(Note: the $g^{QQ}(r,0)$ matrix in $\bar{H}^{PP}$ is evaluated at $\varepsilon = 0$, since we have collected all ε terms on the right-hand side of the generalized eigenvalue equation.) The Λ^{PP} matrix, whose presence in the eigenvalue equation is reminiscent of an overlap matrix in a nonorthogonal representation, is

$$\Lambda^{PP} = I^{PP} + V^{PQ} \frac{I^{QQ}}{(E_{P_0} - E_Q)^2} V^{QP}. \tag{3.10}$$

As in the adiabatic formulation, a spherical expansion of the electrostatic matrix V can be performed that separates all the core electronic and Rydberg coordinates. Such an expansion for the diabatic formulation is postponed until the next chapter where we present the recoupling theory and an effective parametrization of the long-range electron-core potential energy.

The interaction terms within the effective Hamiltonian and the Λ matrices are classified as permanent electric multipole , and induced "static" and "dynamic" polarization interactions (sometimes referred to as polarization and hyperpolarization). The static and dynamic polarization interactions comprise all second-order contributions, and are distinguished from one another by their dependence on information regarding the motion of the Rydberg electron. Specifically, *dynamic* terms involve either radial or angular kinetic energy operators of the Rydberg electron, while *static* terms depend solely upon the electrostatic interaction between the Rydberg electron and the ionic core. The dynamic terms can be viewed as representing coupling due to the *motion* of the Rydberg electron.

In principle, the expansion of the Green's function can be carried out to higher-order in ε. Unfortunately, such an expansion only complicates the description of Rydberg electron motion by introducing higher-order nonlinear energy dependence with no significant improvement in energy level nor wavefunction information. Another point deserving attention is the connection between our approach and that of others like W.G. Sturrus [12, 11]

and W.G. Schoenfeld [23]. While our derivation differs from their theoretical analysis, the final effective Hamiltonians exhibit similarities. The notable difference between our approach and that of Sturrus is our nonperturbative inclusion of coupling among channels, and consequently among different Rydberg series. In the approach of Sturrus, the effect of the core on the positions of Rydberg levels is incorporated through diagonal matrix elements of the effective Hamiltonian within a hydrogenic basis; this is tantamount to traditional second-order Rayleigh-Schrödinger perturbation theory. The coupling among different $n\ell$ states is included perturbatively, which breaks down when there are near-degeneracies among Rydberg states. In our formulation the coupling among Rydberg levels converging to thresholds within our physical channel subspace is treated to all orders by diagonalizing the generalized eigensystem. Sturrus' evaluation of dynamic corrections relies upon the approximation that ε can be replaced with the effective radial hydrogenic Hamiltonian $\varepsilon \rightarrow -\frac{1}{2}\frac{d^2}{dr^2} + \frac{\ell(\ell+1)}{2r^2} - \frac{1}{r}$. By collecting all terms involving ε on the right hand side of our coupled equations, no such approximation is needed and all coupling among channels can be effectively included. This permits a more realistic description of Rydberg electron motion in the presence of an arbitrary ionic core. It might be noted that this type of rearrangement and energy linearization can also be applied to the post-adiabatic formulation of Klar and Fano [39, 40].

3.4 Autoionization Rates

In anticipation of Chapter 6, where we discuss autoionization in doubly excited Rydberg systems, we present a final section on the calculation of autoionization rates. The excited electrons in a doubly excited Rydberg system may exchange energy through their electron-electron interaction, forcing one or more core electrons to drop into a lower state, while ejecting the remaining electron into the continuum. (This does not involve the emission of electromagnetic radiation.) The total initial state wavefunction for the Rydberg system involves both $|\psi_P\rangle$ and $|\psi_Q\rangle$, components of the wavefunction distributed among all channels. Although $|\psi_P\rangle$ represents the dominant portion of the total wavefunction, the perturbative

contribution $|\psi_Q\rangle$ should be included for consistency and to ensure complete convergence in the calculation of decay rates.

The rate for a perturbative transition from the initial state $|\psi\rangle$ to a final energy normalized state $|\phi\rangle$, associated with a channel energetically below the P subspace, is given by the "Fermi Golden Rule"

$$\Gamma = 2\pi \mid \langle \phi \mid V \mid \psi \rangle \mid^2, \tag{3.11}$$

where V is the electrostatic interaction minus the screening $\frac{1}{r_>}$ potential. Expressing $|\psi\rangle$ in terms of P and Q subspace components this rate can be written as

$$\Gamma = 2\pi \mid \langle \phi \mid T^{QP} \mid \psi_P \rangle \mid^2, \tag{3.12}$$

where the transition matrix T^{QP} is

$$T^{QP} = V^{QP} + V^{QQ} g^{QQ} V^{QP}. \tag{3.13}$$

This final expression for the autoionization rate Γ shows that once $|\psi_P\rangle$ is known, the perturbative effects of $|\psi_Q\rangle$ can be included through use of the Green's function developed in the previous section.

3.5 Advantages

The primary advantage of a diabatic formulation over an adiabatic formulation is the ease with which channel coupling can be included. For many systems, channel coupling is essential for accuracy. The polarization models introduced by Sturrus [11, 12] and Schoenfeld [23] are attractive from a physical standpoint, but they have difficulty achieving the spectroscopic accuracy needed to compare theory with experiment. On the other hand,

the fact that electric multipole and induced polarization interactions are involved in these theories offers a simple physical picture of Rydberg and core electron interaction. The developments presented in the next chapter enable us to recast our multichannel theory in terms of multipole and polarization properties of the ionic core. However, our retention of channel coupling allows us to utilize both the physical insight of polarization interactions and the spectroscopic accuracy of a multichannel approach.

CHAPTER 4

RECOUPLING AND PARAMETRIZATION

In this chapter we disentangle the operator structure and the anisotropic nature of the long range potentials developed in the two previous chapters. The analysis presented here enables us to systematically derive, for the first time, the complete vector interaction, and to explain its physical origin and implications.

4.1 Motivation

The forms of the effective adiabatic potential developed in Chapter 2 and the effective diabatic Hamiltonian developed in Chapter 3 are simple from an algebraic standpoint, but each term in them depends on the various quantum numbers J_c, ℓ, and K in a relatively complicated fashion that is difficult to analyze. The objective in this chapter is to reveal the operator structure and to clarify the dependence of each interaction term on the various core and Rydberg quantum numbers. Once this recoupling is accomplished the concept of parametrization, which is the identification of channel dependent core properties, can be developed.

Each term within the adiabatic potential and diabatic Hamiltonian can be written in terms of spherical tensor operators that act on states of the core and the Rydberg electron. Using standard Wigner-Racah recoupling algebra these terms can be recoupled so that information pertaining to the core is separated from information pertaining to the Rydberg electron. As an example, the adiabatic dipole polarizability α_μ in Eq.(2.14) is proportional to the expectation value, in $|\mu\rangle$, of

$$(r_c^{(1)} \cdot r_r^{(1)}) P (r'^{(1)}_c \cdot r'^{(1)}_r) \tag{4.1}$$

where P is a weighted (scalar) projection operator. This expression can be recoupled into

$$\sum_k (-1)^k \left[r_c^{(1)} \otimes P_c r'^{(1)}_c \right]^{(k)} \cdot \left[r_r^{(1)} \otimes P_r r'^{(1)}_r \right]^{(k)}, \tag{4.2}$$

where factors appear with net multipole moment k acting on the core and Rydberg electron, respectively. The validity of this derivation relies on the fact that the infinite summation over intermediate states ν is itself a "scalar" object that contributes no multipolarity to any term. The expectation value in $|\mu\rangle$ of this expression can be written as

$$\alpha_\mu = \alpha_s^\mu + \alpha_t^\mu \mathcal{A}^{(2)}_{\mu\mu} \tag{4.3}$$

where α_s^μ and α_t^μ are the scalar and tensor dipole polarizabilities of the core in the adiabatic channel μ, and $\mathcal{A}^{(2)}_{\mu\mu}$ is an angular coupling factor, which is the mean value of a second-rank tensorial operator.

In the next few sections we demonstrate how a similar analysis can be extended to all interaction terms in the adiabatic potential and the diabatic Hamiltonian. Just as the Wigner-Eckart theorem enables the factorization of angular matrix elements into purely geometric and dynamic contributions, the tensorial analysis presented here enables a factorization of the bulk ionic properties of the core from the dynamic coupling of the Rydberg and core electronic interaction. Moreover, the scalar and tensor parameters, which represent bulk properties of the ionic core, can be computed from first principles, and indirectly extracted from experimental Rydberg spectra, thereby providing an important test of theoretical core wavefunction information.

4.2 Recoupling of Spherical Tensor Operators

Spherical tensor operators and the Wigner-Racah algebra used to manipulate them play a central role in atomic and molecular physics. A spherical tensor operator of rank k is defined to be a set of $2k+1$ functions $T_q^{(k)}$ with components $q = -k, -k+1, \cdots, k-1, k$ that transform under a coordinate frame rotation as

$$\underline{R} T_q^{(k)} \underline{R}^{-1} = \sum_p T_p^{(k)} D_{pq}^k(R) \tag{4.4}$$

where the expansion coefficients are the Wigner rotation matrix elements $D_{pq}^k(R)$ and R is a set of Euler angles.

The primary reason for introducing spherical tensor operators is that they greatly simplify the evaluation of angular matrix elements through the use of the Wigner-Eckart theorem. The Wigner-Eckart theorem disentangles matrix elements into a product of two factors; one that is purely geometric, expressing the symmetry and selection rules of the system, and another that contains the dynamics. The Wigner-Eckart theorem reads:

$$\langle \gamma j m \mid T_q^{(k)} \mid \gamma' j' m' \rangle = (-1)^{j-m} \begin{pmatrix} j & k & j' \\ -m & q & m' \end{pmatrix} \langle \gamma j \parallel T^{(k)} \parallel \gamma' j' \rangle, \tag{4.5}$$

where the phase and normalization conventions are those of Refs.[43, 51, 52]. Since the reduced matrix element does not depend of the magnetic quantum numbers m, m', and q it can be found once and for all by evaluating the full matrix element for a specific set of $\{m, m', q\}$, provided the matrix element is nonzero.

A key spherical tensor operator for our analysis is the renormalized spherical harmonic $C_q^{(k)}$

$$C_q^{(k)} = \left(\frac{4\pi}{2k+1} \right)^{\frac{1}{2}} Y_{k,q}(\theta, \phi) \tag{4.6}$$

where $Y_{k,q}(\theta,\phi)$ is the standard spherical harmonic function. The reduced matrix element of $C_q^{(k)}$ is [43]

$$\langle \ell \parallel C^{(k)} \parallel \ell' \rangle = (-1)^{\ell} \left[(2l+1)(2\ell'+1)\right]^{\frac{1}{2}} \begin{pmatrix} \ell & k & \ell' \\ 0 & 0 & 0 \end{pmatrix}. \tag{4.7}$$

Moreover, the spherical harmonic addition theorem, which is used in the spherical expansion of $\frac{1}{r_{ij}}$, is written in this notation as

$$\begin{aligned} P_k(cos\theta_{ij}) \qquad &= C^{(k)}(\hat{r}_i) \cdot C^{(k)}(\hat{r}_j) \\ &\equiv \sum_q (-1)^q C_q^{(k)}(\hat{r}_i) C_{-q}^{(k)}(\hat{r}_j), \end{aligned} \tag{4.8}$$

as defined in Ref.[43].

4.2.1 Recoupling of First-Order Terms The general form of all first-order terms in our perturbative expansion of the Rydberg-core interaction potential is

$$W^1(k) = A_c^{(k)} \cdot B_r^{(k)} \tag{4.9}$$

where $A_c^{(k)}$ and $B_r^{(k)}$ are spherical operators of rank k that act on the core and the Rydberg electron respectively. As is clearly seen these first-order operators are already written in a factorized form, making the evaluation of matrix elements rather trivial. The angular matrix element of this operator expression is [43]

$$\begin{aligned} W^1(k)_{\mu\mu'} \qquad &= \langle \mu \mid A_c^{(k)} \cdot B_r^{(k)} \mid \mu' \rangle = \langle \gamma(J_c \ell) K M \mid A_c^{(k)} \cdot B_r^{(k)} \mid \gamma'(J_c' \ell') K' M' \rangle \\ &= \delta_{K,K'} \delta_{M,M'} (-1)^{J_c' + \ell + K} \begin{Bmatrix} J_c & \ell & K \\ \ell' & J_c' & k \end{Bmatrix} \langle \gamma J_c \parallel A_c^{(k)} \parallel \gamma' J_c' \rangle \langle \ell \parallel B_r^{(k)} \parallel \ell' \rangle. \end{aligned}$$

(4.10)

4.2.2 Recoupling of Second-Order Terms The general form of all second-order terms in our perturbative expansion of the Rydberg-core interaction is

$$W^2(k,k') = (T_c^{(k)} \cdot T_r^{(k)}) S^{(0)} (T_c^{(k')} \cdot T_r^{(k')}) \tag{4.11}$$

where $S^{(0)}$ is a weighted scalar projection operator that includes the energy denominators, *e.g.* of Eqs.(2.14) through (2.19). For a Rydberg system, this scalar operator can be written as a summation of projection operators, where each projection operator is product of two operators: one that projects onto the angular states of the Rydberg electron, and another that involves the energy denominators and projections onto the states of the core,

$$S^{(0)} = P_r P_c. \tag{4.12}$$

Then $W^2(k,k')$ can be rewritten as

$$W^2(k,k') = \left[T_c^{(k)} \cdot (T_r^{(k)} P_r)\right] \left[(P_c T_c^{(k')}) \cdot T_r^{(k')}\right] \equiv (A_c^{(k)} \cdot B_r^{(k)})(C_c^{(k')} \cdot D_r^{(k')}). \tag{4.13}$$

or in tensorial coupling notation as [53, 43, 51]

$$W^2(k,k') = (-1)^{k+k'} \left[(2k+1)(2k'+1)\right]^{\frac{1}{2}} \left[\left[A_c^{(k)} \otimes B_r^{(k)}\right]^{(0)} \otimes \left[C_c^{(k')} \otimes D_r^{(k')}\right]^{(0)}\right]_0^{(0)}. \tag{4.14}$$

Finally, a recoupling of the tensor products leads to the following form for the matrix element

$$W^2(k,k')_{\mu\mu'} \qquad = \langle \gamma(J_c \ell) K M \mid W^2(k,k') \mid \gamma'(J_c' \ell') K' M' \rangle$$

$$= (-1)^{k+k'} \sum_q (-1)^q \langle \mu \mid \left[A_c^{(k)} \otimes C_c^{(k')} \right]^{(q)} \cdot \left[B_r^{(k)} \otimes D_r^{(k')} \right]^{(q)} \mid \mu' \rangle$$

$$= (-1)^{k+k'+J_c'+\ell+K} \delta_{K,K'} \delta_{M,M'} \sum_q (-1)^q \left\{ \begin{array}{ccc} J_c & \ell & K \\ \ell' & J_c' & q \end{array} \right\}$$

$$\langle \gamma J_c \parallel \left[A_c^{(k)} \otimes C_c^{(k')} \right]^{(q)} \parallel \gamma' J_c' \rangle \langle \ell \parallel \left[B_r^{(k)} \otimes D_r^{(k')} \right]^{(q)} \parallel \ell' \rangle. \tag{4.15}$$

4.2.3 Unit Tensor Notation In this subsection we introduce a unit tensor notation that allows us to write both $W^1(k)_{\mu\mu'}$ and $W^2(k,k')_{\mu\mu'}$ in terms of a common set of unit tensor operators. Let us define $X^{(k)}$ and $Y^{(k)}$ as "unit tensor operators" (spatial) of rank k that act on the ionic core and the Rydberg electron, respectively, such that

$$\begin{aligned} \langle X^{(k)} \cdot Y^{(k)} \rangle_{\mu\mu'} \quad &= \langle (J_c \ell) K \mid X^{(k)} \cdot Y^{(k)} \mid (J_c' \ell') K \rangle \\ &\equiv \delta_{K,K'} \delta_{M,M'} (-1)^{J_c'+\ell+K} \langle J_c \parallel X^{(k)} \parallel J' \rangle \langle \ell \parallel Y^{(k)} \parallel \ell' \rangle \left\{ \begin{array}{ccc} J_c & \ell & K \\ \ell' & J_c' & k \end{array} \right\} \end{aligned} \tag{4.16}$$

with the reduced matrix elements [54]

$$\langle J_c \parallel X^{(k)} \parallel J_c' \rangle = \left\{ \begin{array}{ll} 1, & if\ \Delta(J_c, k, J_c') \\ 0, & otherwise \end{array} \right\} \tag{4.17}$$

and

$$\langle \ell \parallel Y^{(k)} \parallel \ell' \rangle = \left\{ \begin{array}{ll} 1, & if\ \Delta(\ell, k, \ell') \\ 0, & otherwise \end{array} \right\}. \tag{4.18}$$

Here $\Delta(x,y,z)$ denotes the condition of triangularity among the quantum numbers $\{x,y,z\}$, *i.e.* $\Delta =$"true" if $\mid x-y \mid \leq z \leq x+y$, and if $x+y+z =$integer.

In this notation the first-order terms $W^1(k)_{\mu\mu'}$ in our perturbative expansion of the Rydberg-core interaction become

$$W^1(k)_{\mu\mu'} = \langle \gamma J_c \parallel A_c^{(k)} \parallel \gamma' J_c' \rangle \, \langle \ell \parallel B_r^{(k)} \parallel \ell' \rangle \, \langle X^{(k)} \cdot Y^{(k)} \rangle_{\mu\mu'}. \tag{4.19}$$

Likewise, the second-order terms $W^2(k,k')_{\mu\mu'}$ are

$$\begin{aligned} W^2(k,k')_{\mu\mu'} \quad &= \sum_q (-1)^{k+k'+q} \langle \gamma J_c \parallel \left[A_c^{(k)} \otimes C_c^{(k')} \right]^{(q)} \parallel \gamma' J_c' \rangle \langle \ell \parallel \left[B_r^{(k)} \otimes D_r^{(k')} \right]^{(q)} \parallel \ell' \rangle \\ &\quad \times \langle X^{(q)} \cdot Y^{(q)} \rangle_{\mu\mu'}. \end{aligned} \tag{4.20}$$

The unit tensor notation helps elucidate the separation of each interaction into a product of three factors: one factor that depends on properties of the ionic core, another term that relates only to the Rydberg electron, and finally a simple angular factor that couples the angular momentum properties of the core with the orbital angular momentum of the Rydberg electron. It is important to note that no approximation has been introduced as a result of the tensorial analysis presented here. In the following sections we show that in special circumstances these unit tensor operators can be replaced with angular momentum operators that generate the same coupling.

4.3 Parametrization of Interactions

At this stage all first and second-order interaction terms in the effective adiabatic potential and diabatic Hamiltonian have been recoupled which factors out information pertaining to the ionic core from information relating to the Rydberg electron. However, the matrix elements that depend on core wavefunction information are still channel dependent. The channel dependence of these interactions is not strictly a problem, since in more traditional approaches like multichannel quantum defect theory and R-matrix methods [55, 56],

a multichannel reactance-matrix or scattering-matrix is formed that provides essentially the same information. Unfortunately, it is difficult to extract physical insight from large basis set and R-matrix calculations.

The tensorial analysis of the preceding section facilitates a parametrization of each interaction. Specifically, the ionic core properties of the first-order terms in our perturbative expansion of the Rydberg-core interaction are simply the permanent multipole moments of the ionic core. Similarly, the ionic properties of the second-order interaction terms can be identified as the channel dependent polarizabilities and hyperpolarizabilities that characterize the multipole moments of the core induced by the Rydberg electron.

For some systems, further approximations make it possible to approximately remove the channel dependence of each parameter. In atoms with low-Z atomic nuclear charge, the spin-orbit interaction is small compared with electrostatic interactions. Therefore the total orbital angular momentum L_c and the total spin S_c of the core are approximately good quantum numbers. For such light systems each parameter can be replaced with an $LS-$coupled version so that channel dependence arises only from the simple angular coupling factor.

4.4 Tensor Analysis of Adiabatic Potential

In the adiabatic theory of chapter 2 we developed both nondegenerate and degenerate contributions to the long range adiabatic potential that describes the interaction of a slow charge with an aribitrary anisotropic core. Each term in the adiabatic potential depends on quantum numbers of both the ionic core and the Rydberg electron in a rather complicated way. To clarify the dependence of each term on J_c, ℓ, and K, and to reveal the operator structure of the full potential, we apply the tensor recoupling theory of the previous sections so that each term takes the form

$$\sum_k (-1)^k c_k \langle X^{(k)} \cdot Y^{(k)} \rangle_\mu , \tag{4.21}$$

where $X^{(k)}$ and $Y^{(k)}$ are the unit tensor operators defined in subsection 4.2.3 that operate on the core and the Rydberg electron, respectively. Next, because of the single channel nature of the adiabatic potential we follow the spirit of the Fano-Macek [53] treatment of alignment and orientation and replace the tensorial structure by coupled angular-momentum operators of the same rank. Each such replacement introduces a compensating ratio of reduced matrix elements

$$\sum_k (-1)^k \frac{\langle \mu \parallel X^{(k)} \cdot Y^{(k)} \parallel \mu \rangle}{\langle \mu \parallel J_c^{(k)} \cdot \ell^{(k)} \parallel \mu \rangle} \langle J_c^{(k)} \cdot \ell^{(k)} \rangle_\mu = \sum_k C_k \langle J_c^{(k)} \cdot \ell^{(k)} \rangle_\mu , \tag{4.22}$$

where the choice of the $J_c^{(k)} \cdot \ell^{(k)}$ operator representation is motivated by the fact that adiabatic potentials involve specific values of J_c and ℓ_μ. In general, the choice of a particular operator representation depends on whether the formulation is adiabatic or diabatic. In our diabatic formulation the "unit tensor operator" notation is appropriate, and only under special circumstances, as in the case of low-Z atomic systems, can the unit operators be replaced with simpler angular momentum operators of the same rank that generate the same coupling among the Rydberg channels and reflect the basic symmetry properties of the system.

4.4.1 Nondegenerate Channel Contributions Keeping powers of $\frac{1}{r}$ up to radial order $\frac{1}{r^6}$ and grouping terms of the same tensorial structure allows us to present the nondegenerate long-range adiabatic potential in a form that better displays its anisotropic nature

$$u_\mu(r) = E_\mu - \frac{1}{r} + \frac{\ell_\mu(\ell_\mu+1)}{2r^2} + \frac{C^{4\mu}_{0(1,1)}}{r^4} + \frac{C^{6\mu}_{0[(1,1),(2,2)]}}{r^6} + \frac{C^{6\mu}_{1(1,1)}}{r^6} \langle J_c^{(1)} \cdot \ell^{(1)} \rangle_\mu$$

$$+\left(\frac{C^{3\mu}_{2(2,0)}}{r^3}+\frac{C^{4\mu}_{2(1,1)}}{r^4}+\frac{C^{6\mu}_{2[(1,1),(2,2),(1,3)]}}{r^6}\right)\langle J_c^{(2)}\cdot\ell^{(2)}\rangle_\mu$$

$$+\left(\frac{C^{5\mu}_{4(4,0)}}{r^5}+\frac{C^{6\mu}_{4[(2,2),(1,3)]}}{r^6}\right)\langle J_c^{(4)}\cdot\ell^{(4)}\rangle_\mu. \tag{4.23}$$

Here the terms $C^{n\mu}_{k(a,b)}$, corresponding to *even* tensorial rank k, of radial order $\left(\frac{1}{r}\right)^n$, and formed from the electric a-multipole and b-multipole moment contributions from $\frac{1}{r_{ij}}$, are given by

$$C^{n\mu}_{k(a,b)}=\frac{(-1)^{2J_c+\ell_\mu}(2\ell_\mu+1)(2k+1)}{\langle\ell_\mu\parallel\ell^{(k)}\parallel\ell_\mu\rangle\langle J_c\parallel J_c^{(k)}\parallel J_c\rangle}\begin{pmatrix}\ell_\mu & \ell_\mu & k\\ 0 & 0 & 0\end{pmatrix}\begin{pmatrix}a & b & k\\ 0 & 0 & 0\end{pmatrix}$$

$$\sum_{\gamma_\nu J_\nu}\Gamma^n_k(a,b)\begin{Bmatrix}a & b & k\\ J_c & J_c & J_\nu\end{Bmatrix}\langle\gamma_c J_c\parallel\sum_{i=1}^{N_c}r_i^aC^{(a)}(\hat{r}_i)\parallel\gamma_\nu J_\nu\rangle$$

$$\langle\gamma_\nu J_\nu\parallel\sum_{j=1}^{N_c}r_j^bC^{(b)}(\hat{r}_j)\parallel\gamma_c J_c\rangle \tag{4.24}$$

where $C^{(a)}(\hat{r}_i)$ are renormalized spherical harmonics. Terms that share the same tensorial rank and power of $\frac{1}{r}$ but differ in multipole dependence are combined additively into a single net coefficient:

$$C^{n\mu}_{k[(a_1,b_1),(a_2,b_2),\cdots]}=C^{n\mu}_{k(a_1,b_1)}+C^{n\mu}_{k(a_2,b_2)}+\cdots. \tag{4.25}$$

The matrix elements $\langle J_c^{(k)}\cdot\ell^{(k)}\rangle_\mu$ are

$$\langle J_c^{(k)}\cdot\ell^{(k)}\rangle_\mu = \langle(J_c\ell_\mu)K\mid J_c^{(k)}\cdot\ell^{(k)}\mid(J_c\ell_\mu)K\rangle$$

$$=(-1)^{J_c+\ell_\mu+K}\langle J_c\parallel J_c^{(k)}\parallel J_c\rangle\langle\ell_\mu\parallel\ell^{(k)}\parallel\ell_\mu\rangle\begin{Bmatrix}J_c & \ell_\mu & K\\ \ell_\mu & J_c & k\end{Bmatrix}, \tag{4.26}$$

Ref.[43, 51], and explicit expressions for particular $\Gamma_k^n(a,b)$'s with even k in Eq. (4.24) are given by

$$\Gamma_k^3(2,0) = \Gamma_k^5(4,0) = 1, \tag{4.27}$$

$$\Gamma_k^4(1,1) = \Gamma_k^6(2,2) = \frac{1}{E_\mu - E_\nu}, \tag{4.28}$$

$$\Gamma_k^6(1,3) = 2\Gamma_k^4(1,1), \tag{4.29}$$

$$\Gamma_0^6(1,1) = \frac{6}{2(E_\nu - E_\mu)^2} - \frac{8(E - E_\mu)}{(E_\nu - E_\mu)^3}, \tag{4.30}$$

and

$$\Gamma_2^6(1,1) = \frac{3}{2(E_\nu - E_\mu)^2} - \frac{8(E - E_\mu)}{(E_\nu - E_\mu)^3}. \tag{4.31}$$

In contrast to the long-range potential presented in Eq.(2.12), the operator form of the anisotropic potential in Eq.(4.23) possesses a very simple dependence on the various quantum numbers J_c, ℓ, and K. Along with the factorization of the orbital angular momentum ℓ of the Rydberg electron from information pertaining to the ionic core, all terms of the same *even* tensorial rank k share the same ℓ-dependence. In addition, all dependence on K appears in a single $6-j$ symbol originating from the matrix element $\langle J_c^{(k)} \cdot \ell^{(k)} \rangle_\mu$, and accounts for the splitting of the $\mid K + J_c \mid - \mid K - J_c \mid +1$ number of ℓ levels of common K. Unfortunately, the terms $C^{n\mu}_{k(a_1,b_1)}, C^{n\mu}_{k(a_2,b_2)}, \cdots$ that make up $C^{n\mu}_{k[(a_1,b_1),(a_2,b_2),\cdots]}$ are not distinguishable from one another since they share the same tensorial rank, power of $\frac{1}{r}$, and ℓ-dependence.

The angular momentum representation of the nondegenerate long-range potential in Eq.(4.23) immediately shows the appearance of a vector contribution whose structure is

similar to a term predicted by Zygelman[27]. And, as noted in the Introduction, a term of this tensorial structure was introduced into atomic spectroscopy by Trees [28] and Racah [29], but on purely semiempirical grounds, with no explicit derivation or formal justification. As a complement and extension of the work of Zygelman, we provide an explicit expression for the coefficient of this unusual interaction and interpret its physical origin. The term $C^{6\mu}_{1(1,1)}$ is the *only* one, out to radial order $\frac{1}{r^6}$, with *odd* tensorial rank k $(k = 1)$

$$C^{6\mu}_{1(1,1)} = (-1)^{2J_c}\frac{\sqrt{6}}{\langle J_c \parallel J_c^{(1)} \parallel J_c\rangle}\sum_{\gamma_\nu J_\nu}\frac{1}{2(E_\nu - E_\mu)^2}\begin{Bmatrix} 1 & 1 & 1 \\ J_c & J_c & J_\nu \end{Bmatrix}$$

$$\langle\gamma_c J_c \parallel \sum_{i=1}^{N_e} r_i C^{(1)}(\hat{r}_i) \parallel \gamma_\nu J_\nu\rangle\langle\gamma_\nu J_\nu \parallel \sum_{j=1}^{N_e} r_j C^{(1)}(\hat{r}_j) \parallel \gamma_c J_c\rangle. \tag{4.32}$$

The existence of this term has been controversial [10, 11] since a simple parity argument might seem to negate the existence of any odd-rank tensor interaction in the long-range potential. The parity argument, however, fails since the "vector" interaction is an *even parity pseudovector* in the ionic core degrees of freedom. Surprisingly, this interaction would vanish if it were not for the $\ell_\nu(\ell_\nu + 1)$ factor in the summation for $\beta^{a\,d}_{\mu}$, which allows the vector coefficient $C^{6\mu}_{1(1,1)}$ to survive.

Next we demonstrate that the untransformed potential, in Eq.(2.12), cannot support odd tensorial contributions, such as $J_c^{(1)}\cdot\ell^{(1)}$, without such an additional ℓ dependence. The ℓ_ν summation can be evaluated explicitly

$$\sum_{\ell_\nu}(-1)^{\ell_\nu}(2\ell_\nu+1)\begin{pmatrix} \ell_\mu & a & \ell_\nu \\ 0 & 0 & 0 \end{pmatrix}\begin{pmatrix} \ell_\nu & b & \ell_\mu \\ 0 & 0 & 0 \end{pmatrix}\begin{Bmatrix} a & b & k \\ \ell_\mu & \ell_\mu & \ell_\nu \end{Bmatrix}$$

$$= (-1)^{a+b-k}\begin{pmatrix} a & b & k \\ 0 & 0 & 0 \end{pmatrix}\begin{pmatrix} \ell_\mu & \ell_\mu & k \\ 0 & 0 & 0 \end{pmatrix}. \tag{4.33}$$

Since each contribution to our long-range potentials involves a and b multipole moments that add up to an even number the tensorial rank k must be even in this case.

However, if there is an addition ℓ_ν dependence, such as $\ell_\nu(\ell_\nu+1)$ in β_μ^{ad}, the summation becomes

$$\sum_{\ell_\nu}(-1)^{\ell_\nu}\ell_\nu(\ell_\nu+1)(2\ell_\nu+1)\begin{pmatrix}\ell_\mu & 1 & \ell_\nu\\ 0 & 0 & 0\end{pmatrix}\begin{pmatrix}\ell_\nu & 1 & \ell_\mu\\ 0 & 0 & 0\end{pmatrix}\begin{Bmatrix}1 & 1 & 1\\ \ell_\mu & \ell_\mu & \ell_\nu\end{Bmatrix}$$

$$=(-1)^{\ell_\mu+1}\left[\frac{2}{3}\frac{\ell_\mu(\ell_\mu+1)}{(2\ell_\mu+1)}\right]^{\frac{1}{2}} \tag{4.34}$$

which is nonzero for Rydberg states with $\ell_\mu \neq 0$. Thus it is the centrifugal energy of the Rydberg electron, or angular motion, that generates the vector interaction.

4.4.2 Degenerate Channel Contributions The nature of the long range adiabatic potential changes qualitatively when second order degenerate contributions appear from intermediate channels ν that share the same ionization thresholds, K-value and parity with the physically relevant channel μ at $r \to \infty$. For example, the $3pnf$ and $3pnh$ channels in Mg are degenerate. However, as detailed in section 2.5, we assume that the intermediate Rydberg electron orbital momentum ℓ_ν differs from ℓ_μ, for all degenerate channels. The additional degenerate contributions to the long range adiabatic potential can be analyzed, as in the preceding subsection, to reveal their tensorial structure, which can then be replaced with coupled angular momentum operators of the same rank. Keeping powers of $\frac{1}{r}$ up to radial order $\frac{1}{r^6}$ and grouping terms of the same tensorial rank allows us to present these terms in the long range adiabatic potential that derive from the degenerate channels. The resulting degenerate terms, which are understood to be added to the nondegenerate potential of Eq.(2.12), are:

$$U_{\mu}^{degen}(r) = \frac{D_{0(2,2)}^{4\mu}}{r^4} + \frac{D_{1(2,2)}^{4\mu}}{r^4}\langle J_c^{(1)} \cdot \ell^{(1)} \rangle_{\mu} + \left(\frac{D_{2(2,0)}^{3\mu}}{r^3} + \frac{D_{2(2,2)}^{4\mu}}{r^4} + \frac{D_{2(2,4)}^{6\mu}}{r^6} \right) \langle J_c^{(2)} \cdot \ell^{(2)} \rangle_{\mu}$$

$$+ \left(\frac{D_{3(2,2)}^{4\mu}}{r^4} + \frac{D_{3(2,4)}^{6\mu}}{r^6} \right) \langle J_c^{(3)} \cdot \ell^{(3)} \rangle_{\mu} + \left(\frac{D_{4(2,2)}^{4\mu}}{r^4} + \frac{D_{4(4,0)}^{5\mu}}{r^5} + \frac{D_{4(2,4)}^{6\mu}}{r^6} \right) \langle J_c^{(4)} \cdot \ell^{(4)} \rangle_{\mu}$$

$$+ \frac{D_{5(2,4)}^{6\mu}}{r^6}\langle J_c^{(5)} \cdot \ell^{(5)} \rangle_{\mu} + \frac{D_{6(2,4)}^{6\mu}}{r^6}\langle J_c^{(6)} \cdot \ell^{(6)} \rangle_{\mu}. \tag{4.35}$$

Since the degenerate contributions arise within the context of a single channel adiabatic analysis of Rydberg motion, these terms do not appear in the more general multichannel Hamiltonian treatment of Chapter 3, and are, therefore, not included in the numerical studies presented in Chapters 5 through 7. Here the terms $D_{k(a,b)}^{n\mu}$ corresponding to tensorial rank k, of radial order $\left(\frac{1}{r}\right)^n$, and with electric a-multipole and b-multipole moment contributions are given by

$$D_{k(a,b)}^{n\mu} = \frac{(-1)^{k+2J_c+\ell_\mu}(2k+1)(2\ell_\mu+1)}{\langle \ell_\mu \parallel \ell^{(k)} \parallel \ell_\mu \rangle \langle J_c \parallel J_c^{(k)} \parallel J_c \rangle} \sum_{\ell_\nu} \Delta_{\mu\nu}^{n}(a,b)(-1)^{\ell_\nu}(2\ell_\nu+1)$$

$$\begin{pmatrix} \ell_\mu & a & \ell_\nu \\ 0 & 0 & 0 \end{pmatrix} \begin{pmatrix} \ell_\nu & b & \ell_\mu \\ 0 & 0 & 0 \end{pmatrix} \begin{Bmatrix} a & b & k \\ \ell_\mu & \ell_\mu & \ell_\nu \end{Bmatrix} \begin{Bmatrix} a & b & k \\ J_c & J_c & J_c \end{Bmatrix}$$

$$\langle \gamma_c J_c \parallel \sum_{i=1}^{N_e} r_i^a C^{(a)}(\hat{r}_i) \parallel \gamma_c J_c \rangle \langle \gamma_c J_c \parallel \sum_{j=1}^{N_e} r_j^b C^{(b)}(\hat{r}_j) \parallel \gamma_c J_c \rangle, \tag{4.36}$$

where the $\Delta_{\mu\nu}^{n}(a,b)$'s are

$$\Delta_{\mu\nu}^{3}(2,0) = \Delta_{\mu\nu}^{5}(4,0) = 1, \tag{4.37}$$

$$\Delta_{\mu\nu}^{4}(2,2) = \frac{2}{\ell_\mu(\ell_\mu+1) - \ell_\nu(\ell_\nu+1)}, \tag{4.38}$$

$$\Delta^6_{\mu\nu}(2,4) = 2\Delta^4_{\mu\nu}(2,2). \tag{4.39}$$

Like the terms in the nondegenerate case these degenerate coefficients $D^{n\mu}_{k(a,b)}$ exhibit a factorization of ionic core and the Rydberg information. These degenerate coefficients depend on quadrupole and/or hexadecapole moments of the ionic core, but like the vector term, they also depend of the orbital momentum of the Rydberg electron. The additional ℓ_ν dependence generates odd tensorial terms with ranks 3 and 5. However, the combination of quadrupole and hexadecapole moments and the reciprocal ℓ-dependence of the $\Delta^4_{\mu\nu}(2,2)$ term suggests that these degenerate contribution are generally small, but they cannot be neglected if a single channel adiabatic analyis is used to interpret experimental Rydberg energy distributions.

4.5 Tensor Analysis of Diabatic Hamiltonian

Generally, the coupling of nearly degenerate Rydberg states attached to different ionization thresholds of a ionic core results in complex perturbed spectra, which are difficult to treat using a single channel adiabatic formulation. For this reason, the diabatic formulation of Chapter 3 is more robust than the adiabatic approach of Chapter 2 for explicit calculations and for the achievement of spectroscopic accuracy. As with the adiabatic theory we perform a spherical expansion of each term in the diabatic Hamiltonian in powers of $\frac{1}{r}$, and then disentangle all core and Rydberg information through the use of the tensor recoupling techniques presented in section 4.2. However, instead of transforming to an angular momentum operator representation, we retain the unit tensor notation introduced in subsection 4.2.3 so that coupling among the Rydberg-core channels can be properly treated. Furthermore, we treat here the special case of low-Z atomic Rydberg systems. Later in Chapter 7 we present a diabatic formulation for Rydberg states of H_2 and D_2 that assumes no special circumstances and that displays the channel dependence of the core polarizabilities and hyperpolarizabilities.

4.5.1 High ℓ States of Low Z Atoms In low-Z atomic systems where the spin-orbit interaction is small relative to electrostatic interactions, the total orbital angular momentum L_c and the total spin S_c of the core are approximately good quantum numbers. In these systems, the effective diabatic Hamiltonian that describes high-ℓ Rydberg states takes the parametrized form

$$\begin{aligned}\bar{H}^{\mu\mu'} &= \left(-\frac{1}{2}\frac{d^2}{dr^2} + \frac{\ell_\mu(\ell_\mu+1)}{2r^2} - \frac{1}{r} + \Delta E_{\mu\mu_0} - \frac{\alpha_s}{2r^4} - \frac{\eta_s}{r^6}\right)\delta_{\mu\mu'} - \left(\frac{Q}{r^3} + \frac{\alpha_t}{2r^4} + \frac{\eta_t}{r^6}\right)\mathcal{A}^{(2)}_{\mu\mu'} \\ &+ \left(\frac{\beta_s\mathcal{B}^{(0)}_{\mu\mu'} + \beta_t\mathcal{B}^{(2)}_{\mu\mu'}}{r^6}\right) + \frac{\beta_v}{r^6}\langle\vec{L}_c\cdot\vec{\ell}\rangle_{\mu\mu'} \\ &- 2\left(\frac{\beta_s\delta_{\mu\mu'} + \beta_t\mathcal{A}^{(2)}_{\mu\mu'}}{r^5}\right) + p_r\left(\frac{\beta_s\delta_{\mu\mu'} + \beta_t\mathcal{A}^{(2)}_{\mu\mu'}}{r^4}\right)p_r,\end{aligned} \tag{4.40}$$

where $p_r \equiv -i\frac{d}{dr}$ and where $\Delta E_{\mu\mu_0} \equiv E_\mu - E_{\mu_0}$. Similarly, the matrix $\Lambda_{\mu\mu'}$ that appears on the right-hand side of the generalized eigensystem is given by

$$\Lambda_{\mu\mu'} = \delta_{\mu\mu'} + 2\left(\frac{\beta_s\delta_{\mu\mu'} + \beta_t\mathcal{A}^{(2)}_{\mu\mu'}}{r^4}\right). \tag{4.41}$$

(Note: the effective operators $\bar{H}$ and Λ act on the reduced radial wavefunction $\psi_\mu = r\Psi_\mu$ within the P subspace.) The indices μ and μ' refer to channels within the P subspace.

Here we adopt the convention in which α_s and α_t are the standard scalar and tensor dipole polarizabilities, Q is the quadrupole moment, and η_s and η_t are higher-order scalar and tensor hyperpolarizabilities of the ionic core. Explicit expressions for all terms, including the angular factors such as $\mathcal{A}^{(2)}_{\mu\mu'}$ and $\mathcal{B}^{(2)}_{\mu\mu'}$, are given in Appendix A.

The β_s, β_v, and β_t terms that involve $\frac{1}{r^6}$ in Eq.(4.40) represent nonadiabatic scalar, vector, and tensor induced-polarization corrections due to the angular motion of the Rydberg

electron, while the β_s and β_t terms that involve $\frac{1}{r^4}$ and $\frac{1}{r^5}$ represent scalar and tensor nonadiabatic corrections that are associated with the radial motion of the Rydberg electron. The proportionality coefficient β_v (vector hyperpolarizability) of the vector interaction $\vec{L_c} \cdot \vec{\ell}$ deserves special attention. This vector hyperpolarizability depends on the dipole moments of the ionic core and its existence hinges on the centrifugal repulsion experienced by the Rydberg electron. Physically, the vector interaction describes a coupling among the orbital motion of the Rydberg electron and the internal angular momentum of the ionic core, which is mediated by the dipole portion of the Rydberg-core interaction. As the distant Rydberg electron orbits the core, it tries to "drag" the core polarization vector with it. However, this drag is hindered by the internal moment of inertia of the core, and by the moment of inertia of the Rydberg electron. Stated another way, this interaction reflects the inability of the ionic core to instantaneously adjust to the angular motion of the Rydberg electron. The vector nature and the $\frac{1}{r^6}$ behavior of the interaction are independent of representation. However, the core angular momentum operator which appears in $\vec{L_c} \cdot \vec{\ell}$, *does* depend on the choice of representation. Specifically, in an adiabatic representation the core operator is $\vec{J_c}$, while in a diabatic representation the operator is $\vec{L_c}$. This artificial dependence arises because of the difference in the channel coupling appropriate for these representations.

The combination of r-dependence and tensorial structure provide a great deal of insight into the distribution of Rydberg levels. The Coulomb interaction is the dominant term and accounts for the nearly hydrogenic nature of Rydberg systems. Provided the ionic core is nonspherical, the quadrupole interaction, which is the dominant anisotropic term, follows in importance and has the effect of spreading Rydberg levels. Scalar quantities like α_s produce simple shifts of different ℓ-levels, while higher order tensor terms like α_t cause additional spreading, although to a lesser degree than the quadrupole term. The vector term has the effect of further splitting levels that share the same symmetry, but differ in their ℓ dependence. Moreover, the operator $\vec{L_c} \cdot \vec{\ell}$ has the effect of splitting levels that are degenerate

in the quantum number associated with the projection of $\vec{\ell}$ onto $\vec{L_c}$.

The operator structure of the effective Hamiltonian and Λ matrices, and the coupling among P subspace channels that they describe, improves significantly over earlier perturbative formulations. The perturbations among Rydberg levels and the resulting complex spectra can be easily understood and described within this coupled-channel framework. For instance, the wave function of a Rydberg electron may be thought of as distributed among the various channels (paths). The combination of amplitudes from the various channels can result in interference and, consequently, complex spectra. The degree to which this takes place depends on the coupling among channels and whether the channels support strongly overlapping series converging to the various thresholds.

4.6 Qualitative Interpretation of the Vector Interaction

One of the most difficult challenges of our analysis has been to provide a qualitative interpretation of the new vector interaction term in the potential energy. In this section we present a qualitative discussion of this interaction from four perspectives: first by analytically rearranging the operator structure of the adiabatic β_μ^{ad} term, then by considering a two electron example from both a classical and quantum mechanical perspective [31], and finally from the non-Abelian gauge perspective of Zygelman[27].

4.6.1 Analytic Recoupling Analysis In the adiabatic formulation of Chapter 2, only the radial coordinate of the Rydberg electron was treated adiabatically. For this reason, effects arising from Rydberg angular motion can be considered as nonadiabatic. As mentioned in Chapter 2, the vector interaction originated from the radially-adiabatic β_μ^{ad} term. Here we show that this term can be directly recast in an analytic form in which a cross product of the ionic core electric dipole operators appear as a projection onto the orbital momentum of the Rydberg electron. This cross product suggests that torques are present in the dynamics of the nonadiabatic Rydberg-core interaction. In order to see how torques can arise in a Rydberg system, we begin by writing β_μ^{ad} as

$$\beta_\mu^{ad} = \sum_{\nu\neq\mu} \frac{[\ell_\nu(\ell_\nu+1)-\ell_\mu(\ell_\mu+1)]}{(E_\nu-E_\mu)^2} Q^{(1)}_{\mu\nu} Q^{(1)}_{\nu\mu}$$

$$= \sum_{\nu\neq\mu} \frac{\langle\mu \mid \left[\hat{r}_r, \vec{\ell}^2\right]\cdot\vec{r}_c \mid \nu\rangle\langle\nu \mid \hat{r}'_r\cdot\vec{r}'_c \mid \mu\rangle}{(E_\nu-E_\mu)^2}. \tag{4.42}$$

The commutator of $\hat{r}_r$ and $\vec{\ell}^2$ is [51]

$$\left[\hat{r}_r, \vec{\ell}^2\right] = i(\vec{\ell}\times\hat{r}_r - \hat{r}_r\times\vec{\ell}), \tag{4.43}$$

and with a little tensor recoupling the term with a vector structure in β_μ^{ad} is seen to be proportional to

$$\left(\left[\hat{r}_r, \vec{\ell}^2\right]\times P_r\hat{r}'_r\right)\cdot(\vec{r}_c\times P_c\vec{r}'_c) \tag{4.44}$$

Using

$$\left[\hat{r}_r, \vec{\ell}^2\right]\times P_r\hat{r}'_r = -2i(\hat{r}_r\cdot P_r\hat{r}'_r)\vec{\ell} + 2i\hat{r}_r(\vec{\ell}\cdot P_r\hat{r}'_r) - 2\hat{r}_r\times P_r\hat{r}'_r \tag{4.45}$$

we see the appearance of a $\frac{1}{r^6}$ vector interaction that is proportional to

$$\sim \vec{\ell}\cdot(\vec{r}_c\times P_c\vec{r}'_c) \tag{4.46}$$

The existence of this vector interaction hinges on the presence of the centrifugal $\ell_\nu(\ell_\nu+1)$ term within β_μ^{ad}, which again supports our conclusion that the vector interaction results from the angular motion of the Rydberg electron. In addition, the vector cross product on the right hand side of Eq.(4.43) suggests that the Rydberg electron exerts a torque on the ionic

core as the Rydberg electron attempts to "drag" the polarization vector of the spinning core. This idea of the Rydberg electron torquing the core will be more fully explored in chapter 6 where the concept of orbital planes is introduced, and the relative orientation of the core and Rydberg orbital planes is studied within the adiabatic representation [57, 58].

4.6.2 A Two-Electron Example Treated Classically Next we turn to a classical example with two nonoverlapping coplanar electrons that move in the field of a $Z = 2$ charged nucleus as shown in Figure 4.1. The inner electron is initially in a circular Bohr orbit with $n_1 = 2$ and $\ell_1 = 1$, while the outer electron is started in a circular orbit with $n_2 = 7$ and $\ell_2 = 6$. The zeroth-order Hamiltonian for this system then looks like:

$$H_0 = \frac{1}{2}\overrightarrow{p_1}^2 + \frac{1}{2}\overrightarrow{p_2}^2 - \frac{2}{r_1} - \frac{1}{r_2}. \tag{4.47}$$

We assume here that $r_2 >> r_1$, so that the inner electron ($r_1 \approx 2$) fully screens the outer electron ($r_2 \approx 49$), and the leading order perturbation to H_0 is the dipole component of the electron-electron interaction:

$$V = \frac{r_1 \cos\theta_{12}}{{r_2}^2}. \tag{4.48}$$

In order to find the energy shift of the system due to the perturbative dipole interaction V, we propagate classical trajectories for the Hamiltonian $H_0 + R(t)V$, where R(t) is an adiabatic "ramp-on" that is zero at time $t = 0$ and becomes unity after many orbit periods of the outer electron. (This method of evaluating perturbation energies in conjunction with classical mechanics has been used successfully in a different context by Hooker [59].) Figure 4.2 shows that the resulting perturbation in the energy of the system has opposite sign for the two geometries of Figure 4.1. In particular, the energy shift is negative when the two angular momenta $\overrightarrow{\ell_1}$ and $\overrightarrow{\ell_2}$ are parallel (left-hand case in Figure 4.1, while the energy shift has nearly the same magnitude but is positive when these angular

momenta are antiparallel (right-hand case in Figure 4.1).

4.6.3 Two-Electron Example Treated Using Quantum Mechanics The same system just considered classically possesses a simple quantum mechanical description. One quantitative difference between this example of a one-electron ionic core in the $n_1 = 2$ state of He^+ and the cases formulated in Chapters 2 and 3, is that a one-electron hydrogenic ion possesses the unusual "accidental degeneracy" (when fine structure is neglected) of the $2s$ and $2p$ substates. It is well known that this degeneracy magnifies the effect of the dipole interaction between a distant electron and the hydrogenic ion, which is one reason we have chosen this example. At the same time, this system can be treated simply using 2x2 matrices in an LS-coupled representation. In the following, we let r stand for r_2, the distance of the outer electron from the nucleus, while ℓ is the orbital angular momentum of that outer electron. The leading order term at $r \to \infty$ in the potential accordingly contributes in order r^{-2}, *i.e.* on a par with the centrifugal term in the Rydberg electron Hamiltonian.

The quantum mechanical channel describing this $2pn\ell$ two electron atom thus has the following character. When the angular momenta of the inner ($\ell_1 = 1$) and outer electron ($\ell = 6$) are "parallel", the zeroth-order state can be written as $|(2p, n\ \ell = 6)L = 7\rangle$, i.e. as an eigenstate of $\overrightarrow{L}^2 = L(L+1)$ with $L = 7$. The dominant channel that couples to this state is the channel $|(2s, n\ \ell + 1 = 7)L = 7\rangle$. The correction to the long-range Coulomb potential of the outermost electron is therefore a dipolar $\propto \frac{1}{r^2}$ potential for this example, whose coefficient is obtained by diagonalization of the combined centrifugal and dipole-interaction potentials. Through dipolar order, neglecting terms of radial order $\frac{1}{r^3}$, the effective potential appropriate for parallel angular momenta is the smaller eigenvalue of:

$$V^{eff}(r) = -\frac{1}{r} + \begin{pmatrix} \frac{\ell(\ell+1)}{2r^2} & \frac{d}{r^2} \\ \frac{d}{r^2} & \frac{(\ell+1)(\ell+2)}{2r^2} \end{pmatrix}.$$

Here d is a matrix element of the core electric dipole operator between the two coupled channels, $d = \langle 2p|r_1|2s\rangle\langle(1\ell)L = \ell+1|\cos\theta_{12}|(0,\ell+1)L = \ell+1\rangle = -\sqrt{\frac{21}{20}}$. The analogous

effective potential relevant for antiparallel angular momenta of the core and the Rydberg electron is the larger eigenvalue of:

$$V^{eff}(r) = -\frac{1}{r} + \begin{pmatrix} \frac{\ell(\ell+1)}{2r^2} & \frac{d'}{r^2} \\ \frac{d'}{r^2} & \frac{(\ell-1)\ell}{2r^2} \end{pmatrix},$$

where $d' = \langle 2p|r_1|2s\rangle\langle(1\ell)L = \ell - 1|\cos\theta_{12}|(0,\ell-1)L = \ell - 1\rangle = \sqrt{\frac{27}{22}}$. The resulting eigenvalues give effective potentials for the outer ($\ell = 6$) electron:

$$V^{eff}_{\uparrow\uparrow}(r) = -\frac{1}{r} + \frac{\ell(\ell+1)}{2r^2} - \frac{0.147}{r^2},$$

$$V^{eff}_{\uparrow\downarrow}(r) = -\frac{1}{r} + \frac{\ell(\ell+1)}{2r^2} + \frac{0.198}{r^2}.$$

The last term in each potential gives the effect of the perturbation. The quantum mechanical estimate of the perturbation energy is obtained by averaging the last term in the above two potentials over the radial $n = 7, \ell = 6$ orbital, which gives: $\Delta^{QM}_{\uparrow\uparrow} = -6.6\times10^{-5} a.u.$, and $\Delta^{QM}_{\uparrow\downarrow} = 8.9 \times 10^{-5} a.u.$ These quantum mechanical energy shifts for this example are within about a factor of two of the classically-estimated energy shifts, confirming that the basic classical picture presented above is qualitatively correct. Interestingly, the quantum mechanical interpretation for this prototype two-electron example shows that the different sign of the energy perturbation for parallel and antiparallel angular momenta is a consequence of differential level repulsion. The state $2pn\ell[L = \ell + 1]$, with parallel angular momenta, is pushed down in energy by its interaction with the higher-lying $2sn'(\ell+1)[L = \ell + 1]$ state, whereas the state $2pn\ell[L = \ell - 1]$, with antiparallel angular momenta, is pushed up in energy by the lower $2sn'(\ell-1)[L = \ell - 1]$ state. This qualitative interpretation remains similar when the ionic s and p levels are not degenerate, except that the differential level repulsion then causes the ℓ-dependence in the potential to begin at the r^{-6}level rather than the r^{-2} level.

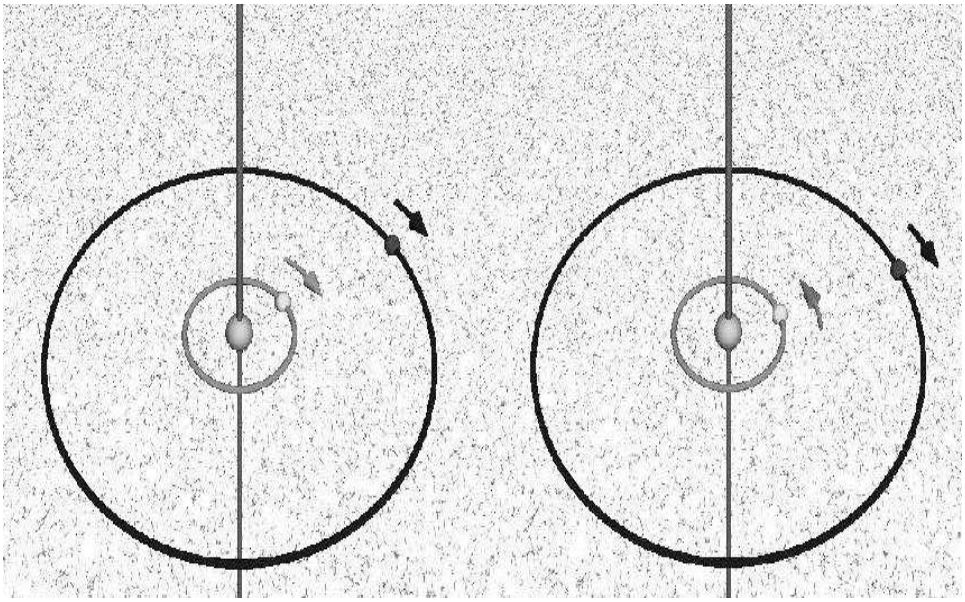

Figure 4.1. Classical orbits of a Rydberg electron around a core consisting of an electron with angular momentum circling about a nucleus. The interaction energy associated with the vector interaction term has opposite sign depending on whether the angular momenta are parallel (left) or antiparallel (right).

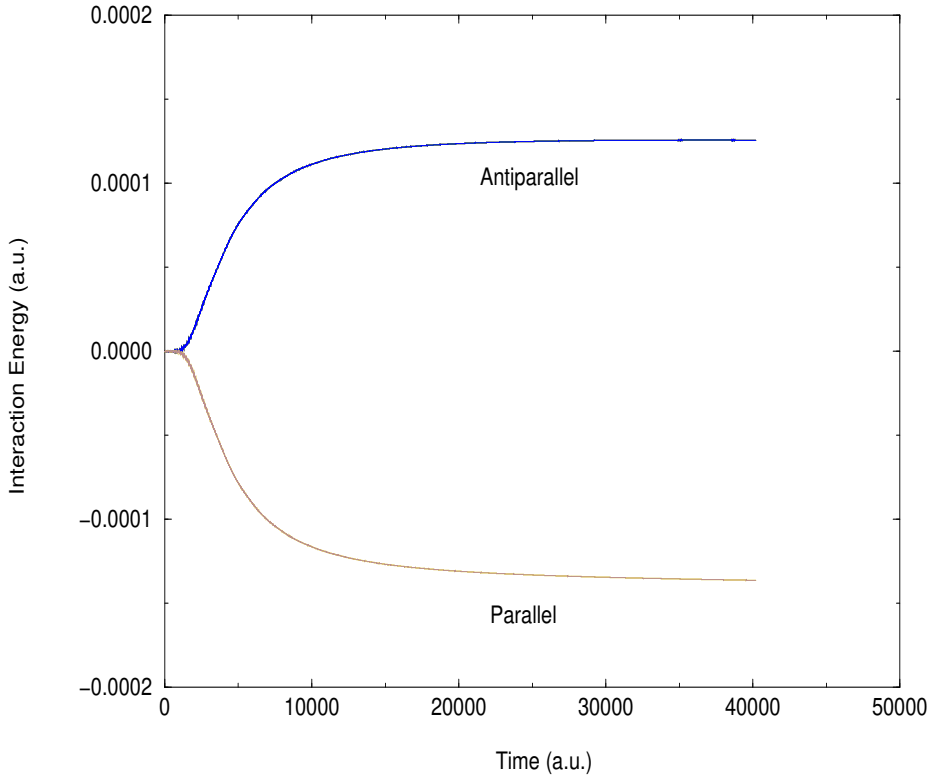

Figure 4.2. Resulting perturbation in the energies of the parallel and antiparallel classical orbits versus time.

4.7 Non-Abelian Gauge Formulation

Zygelman [27] was the first to predict the existence of the vector interaction and to estimate the magnitude of the proportionality constant. In an original and pioneering approach, Zygelman used ideas of non-Abelian gauge fields and geometric phases to study long range atomic forces. Extending the work of Berry [60], Wilczek and Zee[61], Moody [62] and Jackiw [63] Zygelman realized that the derivative coupling matrix $\underline{P}(r)$ within an adiabatic representation resembles an electromagnetic vector potential or a non-Abelian gauge field,

$$\left[-\frac{1}{2}\left(\underline{I}\frac{d}{dr}+\underline{P}(r)\right)^2-(E\underline{I}-\underline{U}(r))\right]\underline{F}(r)=0.$$

As in the classical dynamics of charged particles in electromagnetic fields, [27, 37, 38], a gauge transformation can in principle be found that gauges away the derivative coupling matrix. However, if the channel space is finite or truncated the derivative coupling can be only approximately gauged away, leaving, as in our formulation, an effective potential. It was within this framework that Zygelman first suggested that a vector interaction involving $\vec{L_c}\cdot\vec{\ell}$ does exist as a long range interaction between a charge and an anisotropic system. However, an explicit expression for the coefficient of proportionality was not provided, leaving questions regarding the physical origin of this interaction and to some extent even the fundamental reality of this term, since the coefficient could be zero.

CHAPTER 5

RYDBERG STATES OF NEON

In this Chapter we present the first experimental and theoretical confirmation of the vector interaction in a Rydberg system. The analysis presented here both establishes the importance of this subtle interaction and demonstrates the utility of an effective Hamiltonian approach.

5.1 Application to Neon

The importance of the vector interaction and the channel coupling provided by the effective Hamiltonian approach have been demonstrated in the $n = 10$ Rydberg states of Ne with orbital angular momenta of $\ell = 5, 6, 7$ and 8. These states have been studied in recent experiments by Ward *et al* [10], and interpreted by our theoretical analysis[30]. The most important aspect of this analysis is the capability of our parametrized long-range potential to describe the Rydberg energy levels that are attached to the lowest ionization threshold of the Ne^+ ionic core. The theoretical computation of Rydberg energies is accomplished by diagonalization of the multichannel Hamiltonian

$$H_{\mu\mu'} = \left(-\frac{1}{2}\frac{d^2}{dr^2} + \frac{\ell_\mu(\ell_\mu+1)}{2r^2} - \frac{1}{r} + E_\mu - \frac{\alpha_s}{2r^4} - \frac{\eta_s}{r^6}\right)\delta_{\mu\mu'}$$

$$- \left(\frac{Q}{r^3} + \frac{\alpha_t}{2r^4} + \frac{\eta_t}{r^6}\right)\mathcal{A}^{(2)}_{\mu\mu'} + \frac{\beta_v}{r^6}\langle\vec{L}_c\cdot\vec{\ell}\rangle_{\mu\mu'}, \tag{5.1}$$

followed by a minimization of the weighted χ^2 function (involving differences between the observed and computed energy levels) with respect to the parameters α_s, α_t, β_v, $\cdots$. This version of the effective Hamiltonian can be easily derived from our more general diabatic

Hamiltonian by treating ε, in the Green's functions expansion, as a hydrogenic Hamiltonian. We do this here so that the diagonal elements of our multichannel Hamiltonian exactly correspond with the perturbative Hamiltonian used in the Ward analysis [10]. It is worth noting that there is nothing *ad-hoc* in the parametrized theory. Analytic expressions for each parameter are given in Refs.[30, 31] and in Appendix A, and each can be computed from first principles. In fact, *ab initio* calculations of α_s, α_t, β_v, $\cdots$ using multiconfiguration Hartree-Fock atomic wavefunctions, presented in the next section, confirm the analysis and the interpretation presented here.

The experimentally observed spin splittings were resolved only partially in the Ward *et al* experiment and were analyzed by the experimental group to extract spinless transition frequencies. We neglect all spin-orbit terms in the Rydberg electron Hamiltonian, and all Rydberg electron exchange interactions. The dominant perturbative effects that must be added to our computed Rydberg levels are the relativistic "mass correction" arising from the p^4 term in the kinetic energy of the Rydberg electron, and the magnetic interaction between the Rydberg electron and the ionic core given by

$$H_{mag} = -\frac{g_J}{2}\alpha^2 \frac{\vec{J}_c \cdot \vec{\ell}}{r^3}, \tag{5.2}$$

where α is the fine-structure constant and g_J is the g factor of the ionic core.

The results of our analysis are summarized by Tables 5.1 and 5.2. Table 5.1 compares the various fitted parameters for Ne^+ with those obtained in a fit carried out by Ward *et al* [10]. Our analysis, which nonperturbatively includes coupling between Rydberg series attached to different ionization thresholds, improves the χ^2 by nearly 80% over the fit performed by Ward *et al.*. The fact that the χ^2 per degree of freedom (per parameter) is now approximately *one* is a strong indication that the anisotropic multichannel Hamiltonian correctly accounts for the energetics of these Rydberg levels. Moreover, it also suggests that our nonperturbative treatment of channel coupling is an improvement on the perturbative

description of Rydberg levels used by Ward *et al*, since our fit and their fit were based on the same Hamiltonian, apart from the vector contribution to the potential energy. Our computed levels are compared in Table 5.2 with those of Ref. [10], for the n = 10 Rydberg states of Ne with $\ell = 5, 6, 7$ and 8. These parameters reproduce all observed energy levels to 0.5 MHz or better.

In order to determine the importance of the vector interaction, it is instructive to repeat the same least-squares fitting analysis described in the previous paragraph, but with the constraint that the vector hyperpolarizability β_v must vanish. Table 5.1 lists the various fitted parameters obtained from this analysis without the vector interaction. The greatest change among the parameters occurs in the Ne^+ $^2P_{\frac{3}{2}}$ gyromagnetic ratio g_J, which changes from 1.342 to 1.307. The tensorial structure of the gyromagnetic term is similar to that of the vector interaction and it is plausible that the resulting fit modifies g_J to "mock up" the effects omitted by setting β_v equal to zero. However, since both the radial dependence of these two interactions are different, a change in g_J can only approximately compensate for the omission of β_v from our nonlinear fit. Note that the LS coupling value of g_J is precisely $\frac{4}{3}$, but the effects spin-orbit coupling can change this value from this limiting LS-coupled value. (An independent, linear Zeeman effect measurement could easily test the fitted g_J value.)

The Rydberg levels computed without the vector interaction are given in Table 5.2. The largest discrepancies among the computed and observed levels appear in the lower ℓ states, where the largest deviation is -1.43 MHz in $(\frac{3}{2})10H_{\frac{9}{2}}$. A clear difference is apparent, though, between this analysis and that obtained with the vector hyperpolarizability included. The new least-squares fit obtained without the vector interaction results in $\chi^2 = 27.5$, a χ^2 per degree of freedom approximately four times worse than the χ^2 for the fit including the vector interaction. We interpret this as strong evidence that the existence of the vector interaction has been confirmed in the Ward *et al* experiment on Ne Rydberg states.

Table 5.1. Comparison of fitted (experimental) and theoretical parameters for Ne^+. L refers to length form and V refers to velocity form. The value of g_J in column 4 is based on pure LS-coupling*. The values labelled "present" are from our earlier work (Clark *et al.* 1996), as are the unlabelled theoretical values for α_s, α_t, and β_v.

	Present Fit	Present Fit without β_v	Ward *et.al.* fit	Theoretical
Q	-0.204020(5)	-0.204001(11)	-0.20403(5)	-0.1964 [66] -0.2032(5) [66] -0.2117 [10]
α_s	1.3018(2)	1.3011(6)	1.3028(13)	1.23 (L) 1.19 (V) 1.27 [65]
α_t	-0.0259(3)	-0.0261(3)	-0.026(5)	-0.0374 (L) -0.0396 (V) -0.035 [10]
β_v	0.059(2)	'0'	0.045(29)	0.0678 (L) 0.0719 (V)
η_s	-0.10(1)	-0.10(1)	-0.29(24)	-1.44 [67]
η_t	0.274(5)	0.264(3)	0.5(5)	
g_J	1.342(12)	1.307(24)	1.354(21)	$\frac{4}{3}$ *
χ^2	7.1	27.5	35.7	

Table 5.2. Comparison of calculated (with and without β_v, see Clark *et al.* (1996)) and experimentally observed (Ward *et al.* 1996) energies (MHz) of $n = 10$ Rydberg neon with $J_c = \frac{3}{2}$ and $\ell = 5, 6, 7$, and 8. $\Delta E = E_{obs} - E_{calc}$.

States	$E_{obs}(MHz)$ [7]	E_{calc}	ΔE	$E_{calc}^{\beta_v=0}$	$\Delta E^{\beta_v=0}$
$H_{\frac{9}{2}}$	-145.58(77)	-145.63	0.05	-144.15	-1.43
$H_{\frac{11}{2}}$	2142.67(10)	2142.60	0.07	2142.81	-0.14
$H_{\frac{13}{2}}$	-6022.24(19)	-6022.02	0.22	-6022.66	0.42
$I_{\frac{9}{2}}$	-5267.15(35)	-5267.38	0.23	-5266.64	-0.51
$I_{\frac{11}{2}}$	-356.30(24)	-356.18	-0.12	-355.91	-0.39
$I_{\frac{13}{2}}$	800.52(5)	800.50	0.02	800.55	-0.03
$I_{\frac{15}{2}}$	-4131.36(15)	-4131.35	-0.01	-4131.10	-0.26
$K_{\frac{11}{2}}$	-3838.06(35)	-3838.50	0.44	-3838.26	0.20
$K_{\frac{13}{2}}$	-646.41(8)	-646.37	-0.04	-646.36	-0.05
$K_{\frac{15}{2}}$	'0'	'0'	'0'	'0'	'0'
$K_{\frac{17}{2}}$	-3205.01(16)	-3204.97	-0.04	-3204.68	-0.33
$L_{\frac{13}{2}}$	-3073.14(35)	-3073.64	0.50	-3073.56	0.42
$L_{\frac{15}{2}}$	-883.09(8)	-883.04	-0.05	-883.08	-0.01
$L_{\frac{17}{2}}$	-494.04(5)	-494.04	0.00	-494.05	0.01
$L_{\frac{19}{2}}$	-2693.41(18)	-2693.38	-0.03	-2693.14	-0.27

To complement our analysis of this Rydberg system we present *ab initio* theoretical values for α_s, α_t, and β_v, in Table 5.1 for comparison with other theoretical and experimental results. Our theoretical results are presented in both the length and velocity forms of the electric dipole matrix elements. The details of these calculations are presented in the next section. In view of the difficulty of the *ab initio* calculation of such parameters for a many-electron ion, the calculated values for Ne^+ are in reasonably good agreement, both in magnitude and in sign, with the values extracted from the measurements of Ward *et al* [10]. This agreement strengthens the argument that the vector interaction does exist and has experimental implications in certain features of Rydberg spectra.

As another demonstration of the importance of channel coupling in the Rydberg states of Ne, we display in Figures 5.1 and 5.2 two sets of adiabatic potentials for Ne, which exhibit clear qualitative differences. In Figure 5.1 the adiabatic potentials correspond to $K^\pi = \frac{9}{2}^-$ and are labeled from top to bottom with $(J_c, \ell) = (\frac{1}{2}, 5)$, $(\frac{3}{2}, 5)$, and $(\frac{3}{2}, 3)$. The absence of avoided crossings and the smoothly decaying behavior of the derivative couplings suggest that an adiabatic analysis is justifiable in this case. However, Figure 5.2 demonstrates that adiabatic potentials for different symmetries can differ in a crucial manner. In Figure 5.2 the adiabatic potentials corresponding to $K^\pi = \frac{11}{2}^-$ and are labeled from top to bottom with $(J_c, \ell) = (\frac{1}{2}, 5)$, $(\frac{3}{2}, 7)$, and $(\frac{3}{2}, 5)$. In this case, the presence of a close avoided crossing and a corresponding sharp derivative coupling indicate that a simple adiabatic analysis cannot account for the strong coupling among the nearly degenerate channels. For these reasons, the effective diabatic Hamiltonian approach is preferable, as has been demonstrated in this section.

It should be noted, though, that an adiabatic analysis can be very useful for developing a qualitative understanding of simple and complex spectra. For example, the wave function of a Rydberg electron moving in the presence of these potentials will be distributed among the various channels (paths). The coherent superposition of amplitudes from the

various paths can lead to interference that results in complex spectra. The extent to which such perturbations influence the spectrum depends on the coupling between channels, and on whether the Rydberg series converging to the various ionization thresholds overlap extensively.

5.2 First Calculation of the Vector Hyperpolarizability β_v

In this section we discuss the calculation of the reduced dipole matrix elements necessary to evaluate the vector hyperpolarizability β_v, the standard dipole scalar polarizability α_s, and the second-rank tensor polarizability α_t of Ne^+. The theoretical values for α_s, α_t, and β_v are presented in both length and velocity form in Table 5.1 for comparison with other theoretical and experimental results. Reduced dipole matrix elements are calculated for the ground state ($2s^2 2p^5\ ^2P^o$) of Ne^+. The dipole operator $r^{(1)}C_q^{(1)}$ connects states of the opposite parity which differ by at most one orbital, and such that $\Delta L_c = 0, \pm 1$ (except for $L_c = 0$ to $L_c = 0$ transitions) and $\Delta S_c = 0$. Thus only the ^2S, ^2P, and ^2D final states are needed, which are generated from the ground state by $2s \rightarrow np$, $2p \rightarrow ns$ and $2p \rightarrow nd$ substitutions. Excitations of the $1s$ core are ignored since these give negligible contributions to reduced dipole matrix elements. These final states of Ne^+ are represented by $2s2p^6$, $2s2p^5np$, $2s^2 2p^4 ns$ and $2s^2 2p^4 nd$ configurations, which can be constructed (including the ground state $2s^2 2p^5$) from a product of Ne^{2+} states $2s2p^5$ or $2s^2 2p^4$, and an outer s, p or d electron. These Ne^{2+} configurations are referred to as physical target states.

The summations over bound and continuum states of Ne^+ are accomplished using the eigenchannel R-matrix method [55]. This allows us to construct a complete set of orthogonal basis functions, vanishing at the boundary of the R-matrix sphere of radius r_0. Such functions represent a bound spectrum and a discretized continuum of Ne^+. The target states of Ne^{2+} are calculated using the multiconfiguration Hartree-Fock approximation [68], in which both spectroscopic and correlation orbitals are included. First, spectroscopic

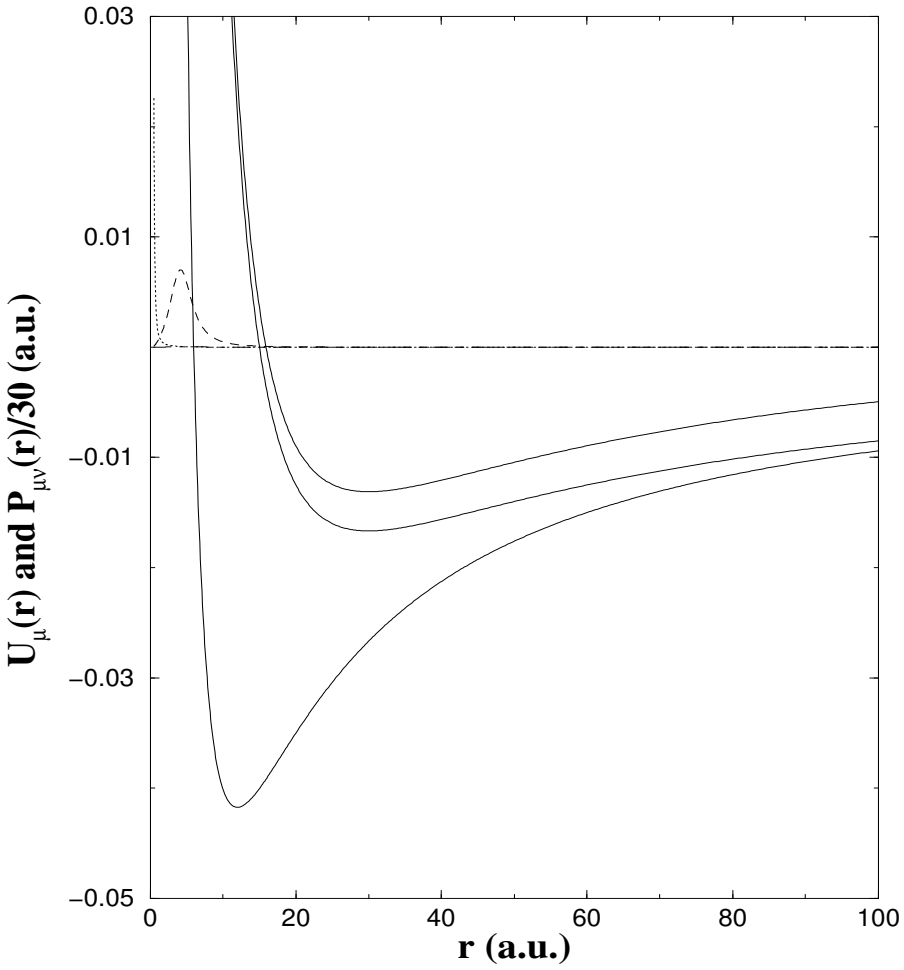

Figure 5.1. Adiabatic potential curves and derivative couplings for Rydberg Ne. The adiabatic potentials correspond to $K^\pi = \frac{9}{2}^-$ and are labeled from top to bottom with $(J_c, \ell) = (\frac{1}{2}, 5)$, $(\frac{3}{2}, 5)$, and $(\frac{3}{2}, 3)$. The derivative couplings $P_{\mu\mu'}(r)/30$ are given by the broken lines: $P_{top,middle}(r)$, dashed; $P_{middle,bottom}(r)$, dotted; and $P_{top,bottom}(r)$, dot-dashed

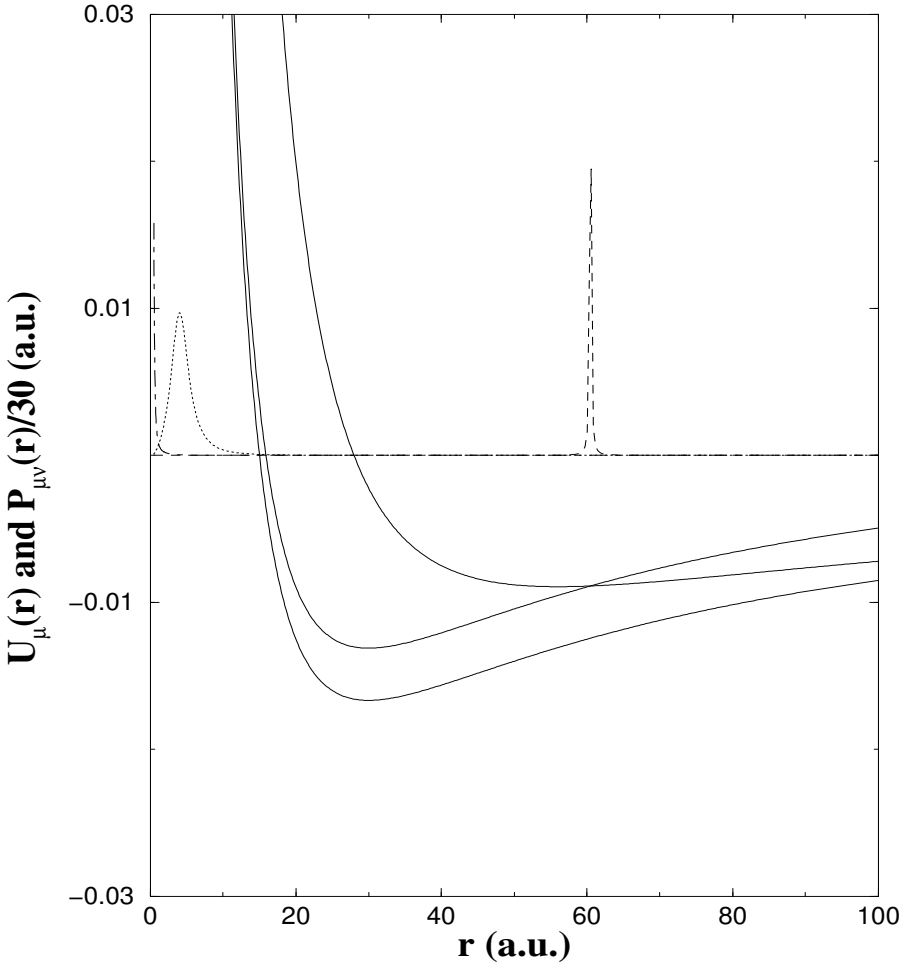

Figure 5.2. Adiabatic potential curves and derivative couplings for Rydberg Ne. The adiabatic potentials correspond to $K^\pi = \frac{11}{2}^-$ and are labeled from top to bottom with $(J_c, \ell) = (\frac{1}{2}, 5)$, $(\frac{3}{2}, 7)$, and $(\frac{3}{2}, 5)$. The derivative couplings $P_{\mu\mu'}(r)/30$ are given by the broken lines: $P_{top,middle}(r)$, dashed; $P_{middle,bottom}(r)$, dotted; and $P_{top,bottom}(r)$, dot-dashed.

orbitals $1s$, $2s$ and $2p$ are optimized on a single $2s^2 2p^4$ configuration. Then, a correlation $\underline{3d}$ orbital is optimized on $2s2p^5\,{}^3P^o$, whose CI expansion includes the main perturber $2s^2 2p^3 3d\,{}^3P^o$. Finally, $\underline{3s}$ and $\underline{3p}$ correlation orbitals are optimized on $2s^2 2p^4\,{}^3P$, where singly- and doubly-excited configurations allowed by parity and spin-angular momentum coupling rules are included.

We then set up an initial CI expansion for each LS-term in the $2s^2 2p^4$ and $2s2p^5$ configuration, including all allowed (by parity and LS-symmetry conservation rules) singly- and doubly-excited configurations of $2s$, $2p$, $\underline{3s}$, $\underline{3p}$ and $\underline{3d}$ orbitals. After diagonalizing a Hamiltonian, this initial CI set is condensed; from each eigenvector representing a physical target state, we delete those configurations whose weight is less than 0.0005. In the final step, extra configurations representing the target polarization are added. These are constructed from single-electron excitations from $2s^2 2p^4$ and $2s2p^5$, involving a change in the parity as $2s \rightarrow 2p$, $2p \rightarrow 3s$ and $2p \rightarrow 3d$. Table 5.3 shows energies and dominant configurations for each physical target state in the condensed basis. Comparing with experiment [69], our relative energies are accurate to at least 5%. As in previous eigenchannel R-matrix calculations [55], a discretized basis of outer-electron orbitals ns, np, nd, nf and ng is used. These are determined inside the R-matrix sphere of radius $r_0 = 7$ Bohr radii. The size of r_0 is chosen to contain all physical target states and the ground state of Ne^+, and to ensure an exponential decay of $rP_{nl}(r)$, where $P_{nl}(r)$ are the ground-state radial functions. A set of radial basis functions for the outermost electron is obtained from a Hartree equation

$$\left(-\frac{1}{2}\frac{d^2}{dr^2} + \frac{l(l+1)}{2r^2} - \frac{Z}{r} + V_H(r)\right) P_{nl}(r) = E_{nl} P_{nl}(r) + \sum_{n'} \lambda_{nn'} P_{n'l}(r),$$

where

$$V_H(r) = \sum_{n'} q_{n'l} \left[\int_0^r \frac{1}{r} P_{n'l}^2(s)ds + \int_r^\infty \frac{r^2}{s^2} P_{n'l}^2(s)ds\right].$$

Here, $q_{n'l}$ are occupation numbers of spectroscopic orbitals representing the $2s^22p^4$ target, and $\lambda_{nn'}$ are Lagrange multipliers needed to orthogonalize the outer-electron and target orbitals (including the correlation orbitals).

All new "box" orbitals are forced to vanish at the R-matrix surface. These constitute a complete orthogonal basis, representing an electron outside the residual Ne^{2+} ion. Those orbitals, which have positive energies $E_{nl} > -\frac{Z_{eff}}{r_0} + \frac{l(l+1)}{2r_0^2}$ not only describe bound states but also represent a discretized continuum of the Ne^+ spectrum. The ground state of Ne^+ is constructed from an antisymmetrized product of the target states and outer-electron orbitals. The energies and atomic wave functions of Ne^+ are just eigenvalues and eigenvectors, respectively, of the Hamiltonian. The ionization energy of $Ne^+(2s^22p^5\,{}^2P^o)$ obtained in this calculation is 334460 cm^{-1}, whereas the experimental value is 331350 cm^{-1}. The accuracy can be tested more thoroughly by analyzing errors in the whole calculated Rydberg series, instead of a singel level. The theoretical and experimental effective quantum numbers of a $2p$ electron in $2s^22p^5\,{}^2P^o$ are 0.573 and 0.572, respectively, giving a difference of 0.001 in the quantum defect.

The final ${}^2S$, ${}^2P$ and ${}^2D$ states are constructed in the same way as the ground state. However, a similar estimate of errors can only be made for the lowest eigenstates whose atomic wave functions fit inside 7 Bohr radii and thus represent physical states of Ne^+. For the lowest, even-parity state $2s2p^6\,{}^2S$ we obtain an excitation energy of 215953 cm^{-1}, whereas the experimental energy is 217050 cm^{-1}. The corresponding error in the quantum defect is only 0.01, well within the range of errors expected for such a strongly correlated state. Note that $2s2p^6\,{}^2S$ is correlated predominantly with a $2s^22p^4\underline{3d}\,{}^2S$ perturber, which contributes nearly 25% of the CI expansion. No similar error analysis can be carried out for higher excited states, of course, since those no longer fit within the R-matrix box. Our final results are obtained with 11 orbitals for each angular momentum l. However, a different number of the box orbitals was initially used to test convergence of the dipole scalar polarizability. For

Table 5.3. Theoretical and experimental energies Ref.[24] in cm^{-1} (upper and lower entry in first column, respectively) of some Ne^{2+} states, relative to the ground state $2s^2 2p^4\ ^3P$, and shortened CI expansions for each of these states.

Energy	Composition		
0.0	$2s^2 2p^4\ ^3P$	$2s2p^4(\ ^2D)3d\ ^3P$	$2s2p^4(\ ^2P)3d\ ^3P$
0.0	0.98605	0.00410	0.00160
25559	$2s^2 2p^4\ ^1D$	$2s2p^4(\ ^2P)3d\ ^1D$	$2s^2 2p^2(\ ^1D)3p^2(\ ^3P)\ ^1D$
25521	0.98406	0.00672	0.00176
53096	$2s^2 2p^4\ ^1S$	$2p^6\ ^1S$	$2s^2 2p^2(\ ^1S)3d^2(\ ^1S)\ ^1S$
55427	0.95453	0.03386	0.00303
203471	$2s2p^5\ ^3P$	$2s^2 2p^3(\ ^2D)3d\ ^3P$	$2s^2 2p^3(\ ^2P)3d\ ^3P$
204589	0.97417	0.01000	0.00397
291435	$2s2p^5\ ^1P$	$2s^2 2p^3(\ ^2D)3d\ ^1P$	$2s^2 2p^3(\ ^2P)3d\ ^1P$
289159	0.96629	0.01300	0.00314

the ^2S and ^2P symmetries, whose calculations consume the least CPU-time and memory, we increased the number of box states to 13. This changed the scalar polarizability by about 2%. We also tested the importance of g-waves, since these, along with f-waves, were neglected in earlier theoretical calculations [65]. The g-waves were found to contribute about 3% to the scalar dipole polarizability, and even greater effects are expected from f-waves. Therefore, these are kept in the present calculations.

Our final value of the scalar polarizability is 1.23 a.u. in length form and 1.19 a.u. in velocity form, which should agree if the wavefunctions are exact eigenfunctions of the Hamiltonian. The scalar polarizability in length form differs by about 6% from the experimental results and by about 3% with other theoretical results (see Table 5.1). In velocity form, the scalar polarizability differs by about 9% with experimental results and by about 6% with theoretical results. The slightly better results obtained in Ref.[65] can be attributed to the implicit summation over Rydberg series and continuua, whereas our method uses a CI expansion which in general converges more slowly.

CHAPTER 6

AUTOIONIZING RYDBERG STATES OF MAGNESIUM

In this chapter we continue our investigation of anisotropic interactions by considering the doubly-excited, autoionizing $3pnf$ states of Mg. Here a Rydberg electron interacts with an excited Mg^+ $3p$ ionic core. In this system, strong coupling among Rydberg states results in irregular behavior in the autoionization rates; we show that the irregularity is accurately described by the effective diabatic Hamiltonian formulation. As discussed in Chapter 4 we explore further the idea that the electric dipole moment of the ionic core experiences a torque as the distant Rydberg electron "revolves" around the core.

6.1 Modification for Low ℓ Rydberg States

In most circumstances, an accurate description of low-ℓ Rydberg states is difficult to achieve using a long-range adiabatic potential or an effective Hamiltonian. The difficulty arises because the short-range physics is described inadequately. However, there are special symmetries of Rydberg systems that are amenable to the methods we have developed. The $3p_{\frac{1}{2}}nf_{\frac{7}{2}}(J=4)$, $3p_{\frac{3}{2}}nf_{\frac{7}{2}}(J=4)$, and $3p_{\frac{3}{2}}nf_{\frac{9}{2}}(J=4)$ Rydberg states of Mg, with $n \geq 9$, fall into this latter category [32]. For these symmetries an f Rydberg electron can only couple to other f and h states, which means that the Rydberg-core interaction can still be treated perturbatively.

For f and g Rydberg states the inner classical turning point ranges from 6–$10 a.u.$. Exchange can still be reasonably neglected, but the asymptotic expansion of the Rydberg-core interaction in powers of $\frac{1}{r}$ becomes problematic when r becomes comparable to the physical size of the ionic core. In order to treat this small r region better it is preferable to expand in $r_< = min\{r, r_i\}$ and $r_> = max\{r, r_i\}$, where r_i is the radial position of a core

electron.

An analysis identical to that given in Chapters 3 and 4 for the diabatic Hamiltonian can be carried out for this case, with the simple modification that we perform a spherical expansion in $r_<$ and $r_>$. This expansion necessarily makes all electric multipole moments and induced polarizabilities radially-dependent, but this dependence rapidly falls off for $r > 10 a.u.$. The effective diabatic Hamiltonian for low-ℓ states of low-Z atoms is

$$\begin{aligned}
\bar{H}^{\mu\mu'} \quad &= \left(-\frac{1}{2}\frac{d^2}{dr^2} + \frac{\ell_\mu(\ell_\mu+1)}{2r^2} + \frac{C_c(r)}{r} + \Delta E_{\mu\mu_0} - \frac{\alpha_s(r)}{2r^4} - \frac{\eta_s(r)}{r^6} \right) \delta_{\mu\mu'} \\
&- \left(\frac{Q(r)}{r^3} + \frac{\alpha_t(r)}{2r^4} + \frac{\eta_t(r)}{r^6} \right) \mathcal{A}^{(2)}_{\mu\mu'} \\
&+ \left(\frac{\beta_s(r)\mathcal{B}^{(0)}_{\mu\mu'} + \beta_t(r)\mathcal{B}^{(2)}_{\mu\mu'}}{r^6} \right) + \frac{\beta_v(r)}{r^6} \langle \vec{L}_c \cdot \vec{\ell} \rangle_{\mu\mu'} \\
&- 2 \left(\frac{\beta_s(r)\delta_{\mu\mu'} + \beta_t(r)\mathcal{A}^{(2)}_{\mu\mu'}}{r^5} \right) + p_r \left(\frac{\beta_s(r)\delta_{\mu\mu'} + \beta_t(r)\mathcal{A}^{(2)}_{\mu\mu'}}{r^4} \right) p_r, \qquad (6.1)
\end{aligned}$$

where $\Delta E_{\mu\mu_0} \equiv E_\mu - E_{\mu_0}$. Similarly, the matrix $\Lambda_{\mu\mu'}$ is

$$\Lambda_{\mu\mu'} = \delta_{\mu\mu'} + 2 \left(\frac{\beta_s(r)\delta_{\mu\mu'} + \beta_t(r)\mathcal{A}^{(2)}_{\mu\mu'}}{r^4} \right). \qquad (6.2)$$

The additional term $C_c(r)$ represents the partially screened Coulomb charge seen by the Rydberg electron as a function of the radial coordinate. These channel independent radial parameters converge to *zero* in the limit $r \to 0$, except for $C_c(r)$ which converges to $-Z$. In the asymptotic limit $r \to \infty$ each radial parameter converges to its appropriate constant value, as in Eqs. (4.40) and (4.41). For example, $lim_{r\to\infty}\alpha_s(r) = \alpha_s$, and $lim_{r\to\infty}C_c(r) = -1$. In addition, when r becomes much larger than the physical extent of the ionic core, $r_>$ coincides with the radial coordinate of the Rydberg electron, and the radial parameters

Table 6.1: $e - Mg^{++}$ model potential parameters.

	ℓ	α_1^ℓ	α_2^ℓ	α_3^ℓ	r_c^ℓ
Mg^{++}	0	4.51367	11.81954	2.97141	1.447764
$\alpha_d = 0.49$	1	4.71475	10.71581	2.59888	1.71333
	≥ 2	2.99158	7.69976	4.38828	1.730930
Ref.[71]					

assume their constant asymptotic values. Analytic expressions for these radial parameters are given in Appendix A.

6.2 Radial Dependence of Core Parameters

The accurate calculation of electronic properties for a many-electron ion is generally very difficult. Fortunately, Mg^+ is an alkaline-earth ion, for which simple and effective model potentials [70, 56, 71] can be utilized. The model potential $V(r)$ describing the interaction between a valence electron and a closed-shell ionic core is chosen to have the analytic form

$$V(r) = -\frac{1}{r}\left[2 + (Z-2)exp(-\alpha_1^\ell r) + \alpha_2^\ell r\ exp(-\alpha_3^\ell r)\right] - \frac{\alpha_d}{2r^4}\left[1 - exp\left(-\left(\frac{r}{r_c^\ell}\right)^6\right)\right], \quad (6.3)$$

where Z is the nuclear charge and α_d is the scalar dipole polarizability of the doubly charged positive ion [70, 56, 71]. The parameters α_i^ℓ and r_c^ℓ are empirically fitted to obtain agreement between the energy eigenvalues of the one-electron model Hamiltonian and the experimental energy levels of the alkaline-earth ion. The values of the parameters for the interaction of Mg^{++} and a valence electron are given in Table 6.1. As noted in Ref.[70, 56] the ℓ dependence of these parameters makes the model potential formally a nonlocal potential, although in a trivial way.

The core wavefunctions are computed by diagonalizing the model Hamiltonian in a finite basis set of radial Sturmian functions (see Appendix C)

$$S_{n\ell}^{(\zeta)}(r) = \left[\frac{(n-\ell-1)!}{(n+\ell)!}\right]^{1/2} e^{-\zeta r/2}(\zeta r)^{\ell+1} L_{n-\ell-1}^{(2\ell+1)}(\zeta r), \tag{6.4}$$

where the $L_{n-\ell-1}^{(2\ell+1)}(\zeta r)$ are associated Laguerre polynomials defined by

$$L_n^{(k)}(x) = \sum_{\nu=0}^{n} \binom{n+k}{n-\nu} \frac{(-x)^\nu}{\nu!}, \tag{6.5}$$

and ζ is a parameter chosen to enhance convergence. Expanding each desired radial wavefunction as a linear combination of these Sturmians, the radial Schrödinger equation becomes a generalized eigenvalue problem

$$H_{model}\psi = EO\psi. \tag{6.6}$$

H_{model} and O are matrices of the model Hamiltonian and overlap operators, calculated in the Sturmian basis [110]. The asymptotic permanent multipole moments, polarizabilities, and hyperpolarizabilities for the $Mg^+(3p)$ ionic core computed with this wavefunction information are presented in Table 6.2.

A comparison with our earlier work on the Ne^+ ion reveals that the Mg^+3p ionic parameters are from one to two orders of magnitude larger. In particular, the vector hyperpolarizability β_v is $1.885 a.u.$ for the $Mg^+(3p)$, as opposed to $0.059(2) a.u.$ for the ground state Ne^+ ionic core [30, 31]. Unfortunately, as we will demonstrate later, the large autoionization widths of the $3pnf$ Rydberg states obscure the importance of this subtle interaction.

The channel independent radial parameters are also computed with this wavefunction information and are presented in Figure 6.1. In order to emphasize their radial variation, we have multiplied each parameter by a suitable constant. They converge rapidly to their asymptotic values, i.e. reasonably well by $r \sim 10$ a.u.. Nevertheless, the variations for $r < 10$ a.u. are sufficiently strong to shift the $3pnf$ Rydberg levels of magnesium with $n \sim 10$ by a few wavenumbers. For states with higher ℓ values, the centrifugal barrier excludes the

Table 6.2: Mg^+ $3p$ ionic core parameters.

Parameters	Calculated (a.u.)
C_c	-1
Q	2.752
α_s	31.514
α_t	1.531
η_s	677.205
η_t	-583.541
β_s	84.418
β_v	1.885
β_t	-34.144

Rydberg electron from the small radial region where these short range variations play an important role. These calculations were accurately converged, to $0.001 a.u.$ for each parameter, with 100 radial Sturmian functions per channel.

6.3 Rydberg Levels and Rates: Mg $3pnf$

The interactions among Rydberg channels generally increase in importance as the ionic core becomes larger and more polarizable. In this case the $3pnf$ Rydberg states of magnesium would appear ideal for the study of anisotropic interactions like $\frac{\vec{L_c}\cdot\vec{\ell}}{r^6}$. However, the small energy shifts generated by this vector interaction are difficult to observe in these states, because of the large autoionization widths. This could, in principle, be partially resolved by studying high ℓ states of a given n so that the decay rate is dominated by radiative decay, which is independent of n and ℓ [72]. In fact, this is preferable provided the natural linewidth for the $3p$ state is smaller than the splittings and energy shifts caused by the anisotropic terms.

Fortunately, the $3pnf$ states of Mg are still interesting, since strong coupling arises from the quadrupole interaction. This coupling gives rise to irregular behavior in the positions and the decay widths of the autoionization resonances, which can be clearly seen in the recent experiments of Lyons *et.al.* [32]. In fact, the coupling is strong enough that traditional perturbative treatments of Rydberg states are unable to account for the observed effects.

We compute the magnesium $3pnf$ Rydberg energy levels and the corresponding wavefunction information by diagonalizing the generalized eigenvalue equation, Eq.(3.8), with the computed radial functions shown in Figure 6.1. Once again we use a radial Sturmian basis for convenience. The autoionization rates (widths) are computed using the T-matrix formulation developed in Section 3.12. Since we exclusively consider Rydberg states with total angular momentum $J = 4$, only g final states contribute to these calculated rates.

The fine structure splitting between the Mg^+ $3p_{\frac{1}{2}}$ and $3p_{\frac{3}{2}}$ ionization thresholds was taken to be $91.57 cm^{-1}$ [73, 74]. The Rydberg energy levels, rates, and quantum defects

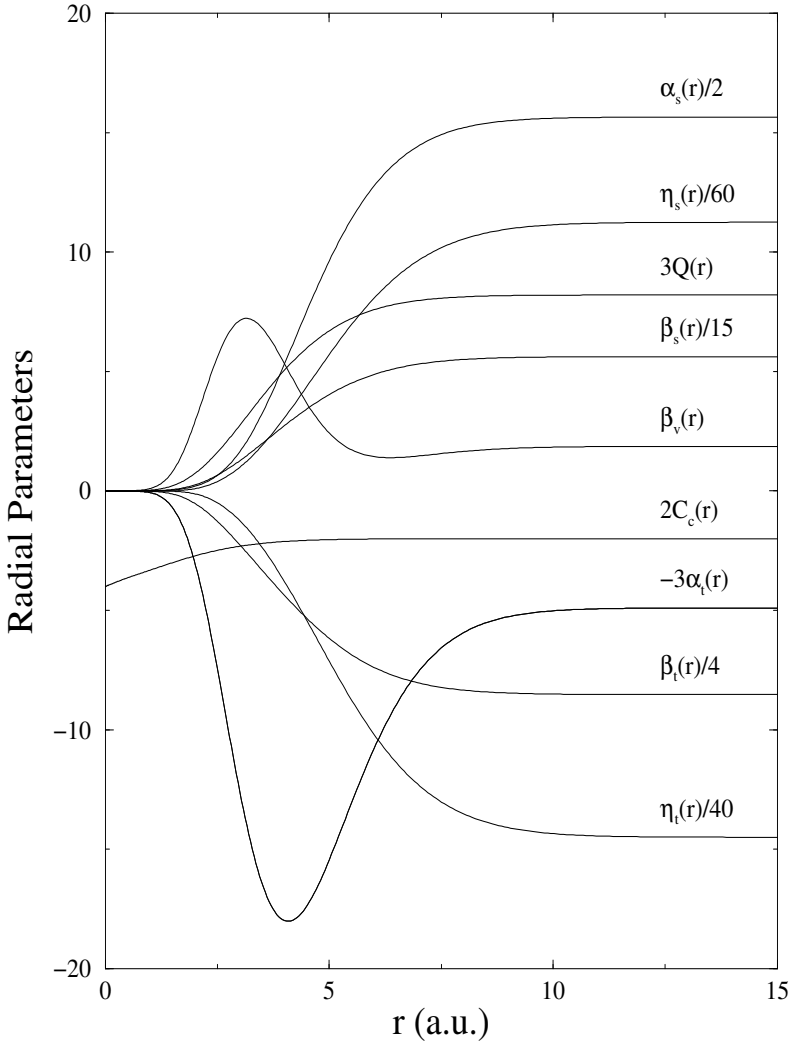

Figure 6.1: Channel-independent radial parameters for the Mg^+ $3p$ ion.

for the Mg $3p_{\frac{1}{2}}nf_{\frac{7}{2}}(J=4)$, $3p_{\frac{3}{2}}nf_{\frac{7}{2}}(J=4)$, and $3p_{\frac{3}{2}}nf_{\frac{9}{2}}(J=4)$ resonances are presented in Tables 6.3 through 6.5. The agreement between our computed and the measured levels is good to about $1cm^{-1}$. Since the measured rates have uncertainties of 20% and range from 5 to $10cm^{-1}$, depending on the symmetry, this agreement between our theory and experiment is reasonably good. The theoretical errors are primarily due to the neglect of exchange, which is of borderline importance for f states, and the use of a model potential to compute electronic properties of the Mg^+ $3p$ ion.

The irregular behavior of the $3p_{\frac{1}{2}}14f_{\frac{7}{2}}$ and $3p_{\frac{1}{2}}18f_{\frac{7}{2}}$ states, and of the $3p_{\frac{3}{2}}14f_{\frac{7}{2}}$ and $3p_{\frac{3}{2}}17f_{\frac{7}{2}}$ states is clearly seen in the n-dependence of their autoionization rates. To better visualize the distribution of these rates, we plot them as functions of the principal quantum number n in Figures 6.2 through 6.4, respectively. The principal quantum number n and the effective quantum number n^* are related by the quantum defect (QD) μ ($n^* = n - \mu$).

Apart from the occasional perturbation, the general decrease of these rates with increasing n is consistent with the $\frac{1}{n^3}$ trend when $n \gg \ell$ [72]. The irregular behavior is caused by strong channel coupling, which is primarily due to the quadrupole interaction, and by the near degeneracies of the Rydberg levels in different channels, such as the $3p_{\frac{1}{2}}14f_{\frac{7}{2}}$ and the $3p_{\frac{3}{2}}13f_K$ states. For comparison, we also present in Figures 6.2 through 6.4, the results of an R-matrix, multichannel quantum defect theory (MQDT) calculation, which agrees well with the effective Hamiltonian approach. The R-matrix results were based on reaction matrices calculated (inside a reaction volume of $20a.u.$) in an earlier study [75].

This comparison between the effective Hamiltonian approach and the more traditional and well tested R-matrix method is revealing. In general the positions and widths computed using $\bar{H}^{PP}$ agree better with experiment. This may not be surprising since R-matrix methods restrict the coordinate space to a reaction volume that may not necessarily be large enough to describe the spatial distribution of high $n\ell$ Rydberg states. The Hamiltonian approach simply requires an increase in the number of radial Sturmian functions per

Table 6.3: Mg $3p_{\frac{1}{2}}nf_{\frac{7}{2}}J=4$ energies (cm^{-1}), widths (cm^{-1}), and quantum defects.

n	E expt. [32]	E theory	Γ expt. [32]	Γ theory	QD expt. [32]	QD theory
9	95967.83	95969.94	6.48	8.326	0.053	0.0457
10	96231.89	96231.30	5.60	6.534	0.042	0.0449
11	96424.39	96424.35	4.90	5.193	0.044	0.0441
12	96571.94	96571.01	3.69	4.223	0.036	0.0431
13	96686.31	96685.11	3.43	3.597	0.030	0.0411
14	96778.00	96776.80	4.95	3.627	0.009	0.0235
15	96848.72	96847.71	1.62	1.805	0.033	0.0480
16	96907.94	96907.48	1.55	1.709	0.037	0.0451
17	96957.11	96956.93	1.38	1.559	0.039	0.0430
18	96999.49	96999.07	3.60	1.798	0.010	0.0212
19	97033.17	97033.09	0.73	0.972	0.044	0.0466

Table 6.4: Mg $3p_{\frac{3}{2}}nf_{\frac{7}{2}}J=4$ energies (cm^{-1}), widths (cm^{-1}), and quantum defects.

n	E expt. [32]	E theory	Γ expt. [32]	Γ theory	QD expt. [32]	QD theory
9	96050.34	96052.63	3.63	3.898	0.082	0.0746
10	96314.82	96315.89	2.54	2.504	0.081	0.0761
11	96509.75	96510.33	1.19	1.636	0.081	0.0774
12	96658.25	96657.90	0.54	0.969	0.076	0.0794
13	96771.41	96771.34		0.00150	0.093	0.0938
14	96865.43	96864.23	1.48	1.114	0.060	0.0748
15	96938.06	96937.32	0.95	0.639	0.066	0.0779
16	96996.76	96996.41	0.37	0.000619	0.087	0.0938
17	97046.97	97046.97	1.19	0.505	0.076	0.0769
18	97088.3	97087.75	0.59	0.0159	0.082	0.0974
19		97123.63	0.66	0.295		0.0785

Table 6.5: Mg $3p_{\frac{3}{2}}nf_{\frac{9}{2}}J=4$ energies (cm^{-1}), widths (cm^{-1}), and quantum defects.

n	E expt. [32]	E theory	Γ expt. [32]	Γ theory	QD expt. [32]	QD theory
9	96065.66	96067.23	11.53	12.212	0.032	0.0269
10	96326.73	96326.72	9.25	9.053	0.027	0.0275
11	96518.26	96518.61	6.28	6.882	0.030	0.0279
12	96665.55	96664.49	5.26	5.349	0.020	0.0282
13	96778.31	96777.98	5.05	3.932	0.025	0.0282
14	96869.47	96867.96	3.07	3.405	0.010	0.0286
15	96941.58	96940.54	2.13	2.781	0.012	0.0288
16	97000.40	96999.93	2.64	2.264	0.020	0.0288
17	97049.01	97049.13	1.73	1.921	0.031	0.0290
18	97090.85	97090.35	2.15	1.615	0.015	0.0291
19		97125.22	2.36	1.382		0.0292

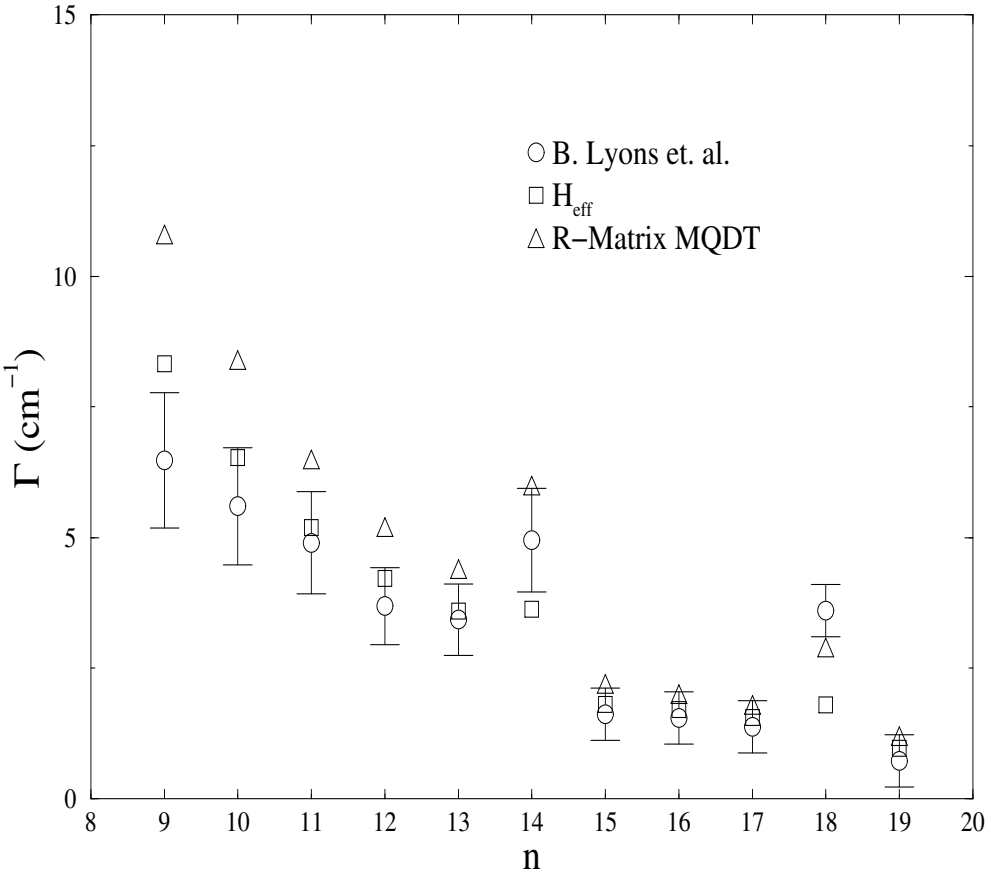

Figure 6.2. Plot of the Mg $3p_{\frac{1}{2}}nf_{\frac{7}{2}}(J=4)$ autoionization rates as a function of the principal quantum number n. The circled data points with error bars are experimental results [32].

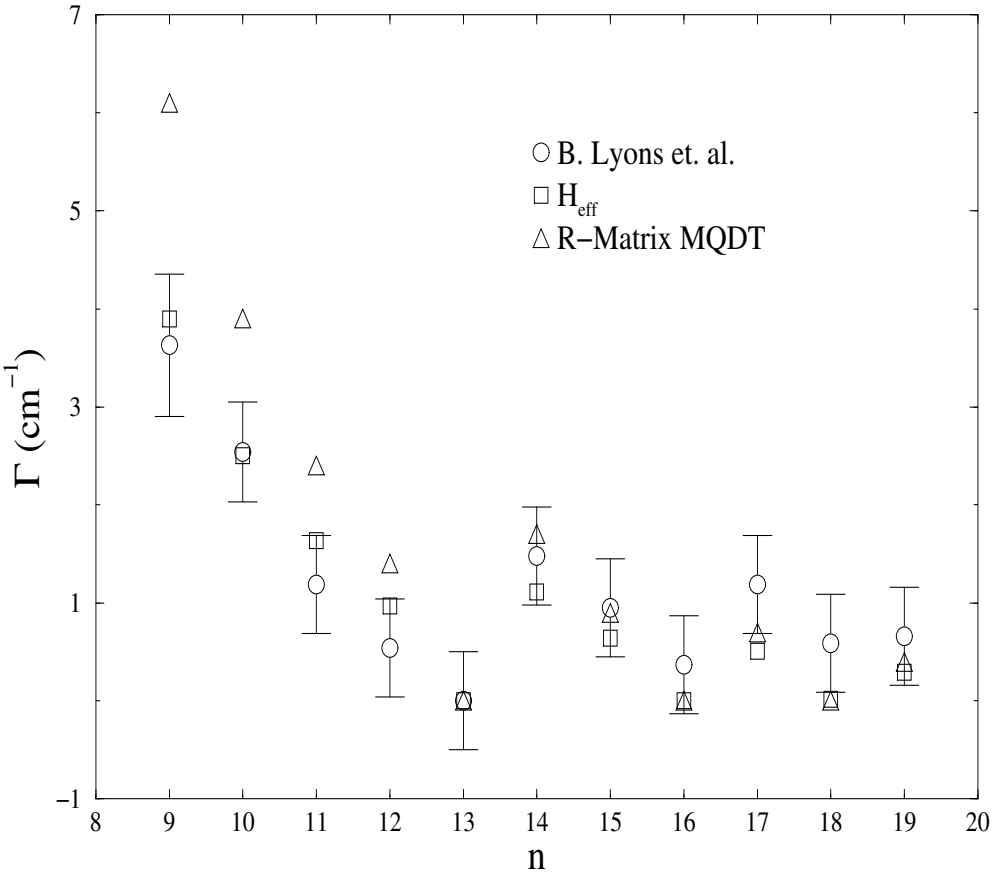

Figure 6.3. Plot of the Mg $3p_{\frac{3}{2}}nf_{\frac{7}{2}}(J=4)$ autoionization rates as a function of the principal quantum number n. The circled data points with error bars are experimental results [32].

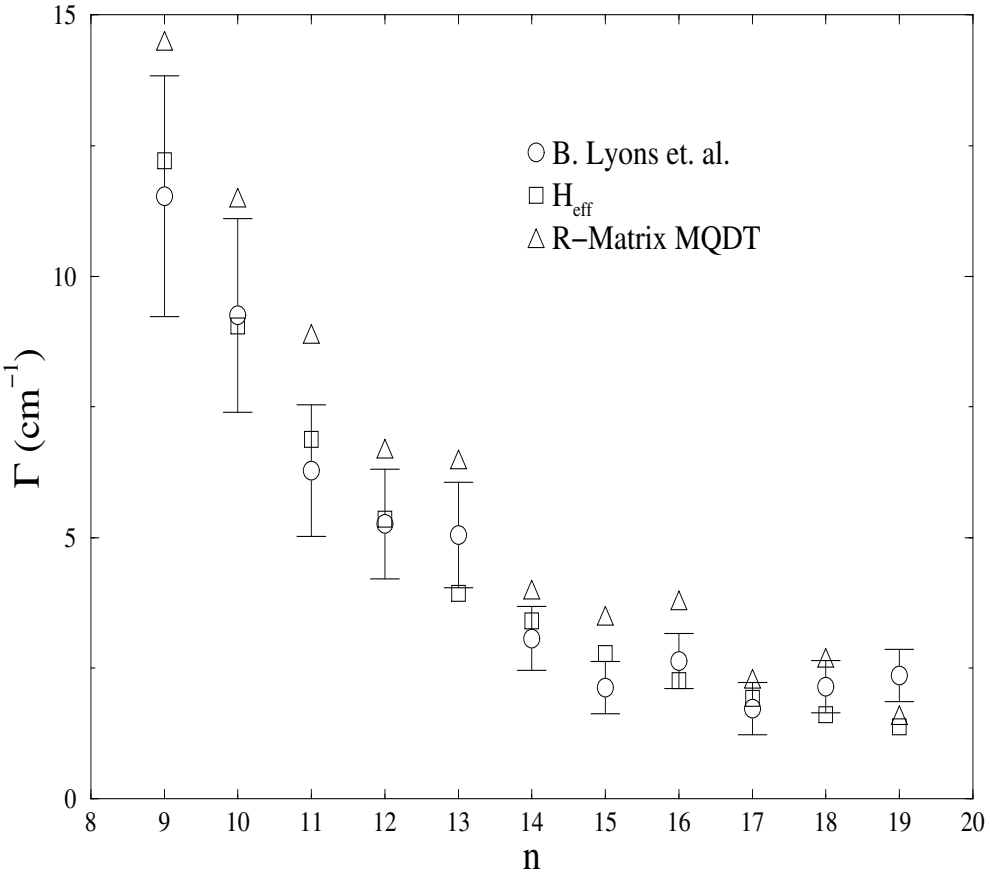

Figure 6.4. Plot of the Mg $3p_{\frac{3}{2}}nf_{\frac{9}{2}}(J=4)$ autoionization rates as a function of the principal quantum number n. The circled data points with error bars are experimental results [32].

channel to treat higher $n\ell$ states.

6.4 Adiabatic Torquing of Orbital Planes

In this section we more fully explore the idea that the ionic core of a Rydberg system experiences a torque from the distant, slow moving Rydberg electron. Here we turn to an adiabatic analysis to study how the orbital planes of the ionic core and the Rydberg electron orient themselves as the Rydberg electron adiabatically changes its radial position. Explicitly, the adiabatic potentials $U_\mu(r)$ and eigenstates $\Phi_\mu(r;\Omega)$ are defined as the r-dependent solutions of the generalized eigenvalue problem:

$$\bar{H}^{PP}_{r=const}\Phi_\mu(r;\Omega) = U_\mu(r)\Lambda^{PP}_{r=cont}\Phi_\mu(r;\Omega). \tag{6.7}$$

The adiabatic channel functions $\{\Phi_\mu(r;\Omega)\}$ are superpositions of the ionic core states and the orbital functions of the Rydberg electron; they contain information relating to the instantaneous interactions between the ionic core and the distant electron.

The $K^\pi = \frac{7}{2}^-$ and $K^\pi = \frac{9}{2}^-$ adiabatic potentials for Rydberg Mg, shown in Figures 6.5 and 6.6, exhibit very broad and smooth avoided crossings, and derivative couplings with similar qualitative behavior. In order to fit the potential curves and the couplings in the same figure we have divided the derivative couplings by a factor of twenty. The large magnitude of these couplings once again suggests that a diabatic treatment, where the coupling is still relatively small, is preferable. As a result of this coupling, Rydberg states attached to these potential curves should strongly interfere with one another and produce irregular behavior in the positions and decay widths of the autoionization resonances, as described in the previous section.

The orbital angular momentum of the Rydberg electron and that of the ionic core can be viewed as defining orbital planes as in classical mechanics. Here we investigate how the orientation of these orbital planes, or the projection of the Rydberg orbital momentum

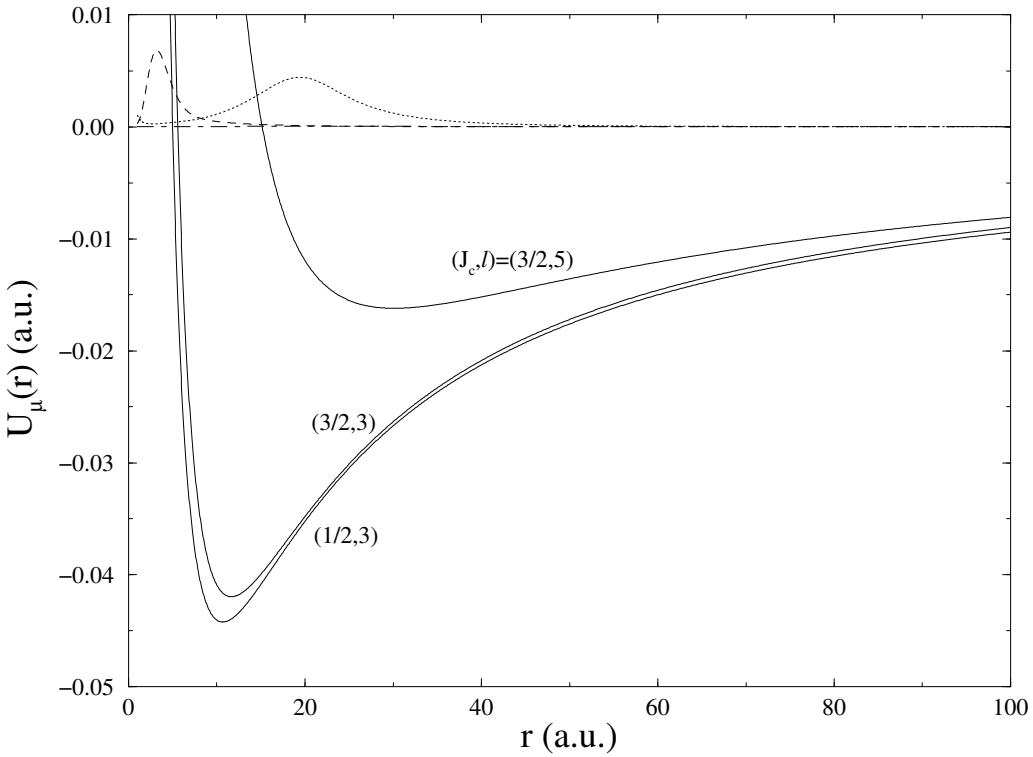

Figure 6.5. Radial adiabatic potential curves and derivative couplings for the $K^\pi = \frac{7}{2}^-$ Rydberg states of Mg. The derivative couplings $P_{\mu\mu'}(r)/20$ are given by the broken lines; $P_{bottom,middle}(r)$, dotted; $P_{middle,top}(r)$, dashed; and $P_{bottom,top}(r)$, dot-dashed.

,

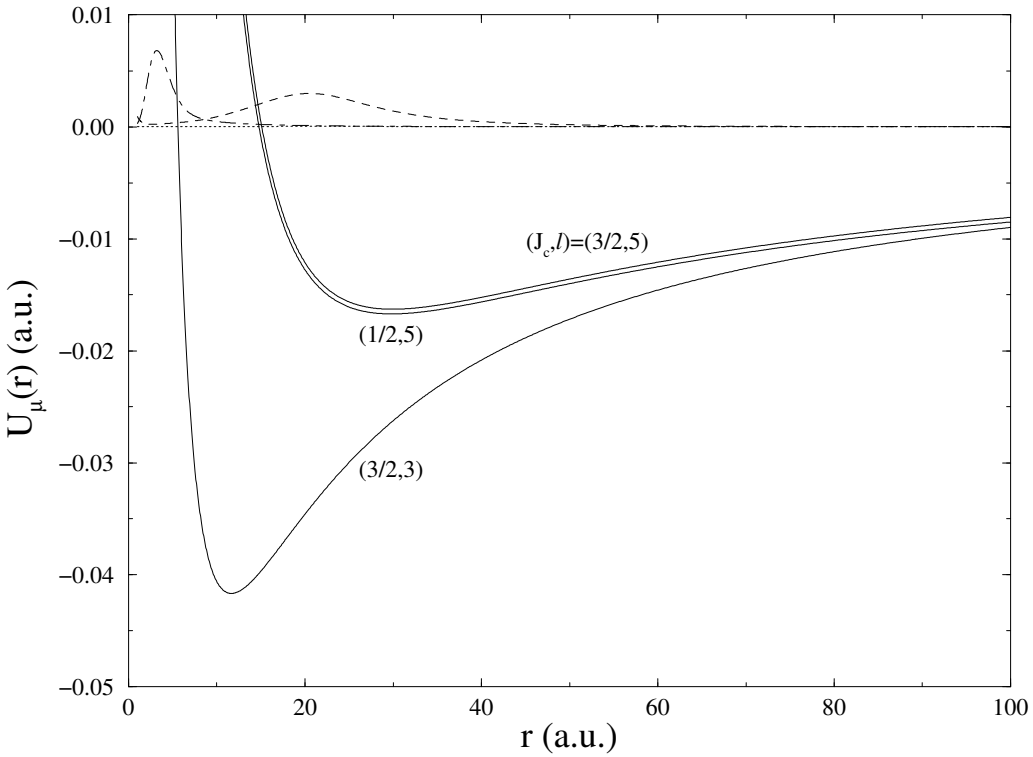

Figure 6.6. Radial adiabatic potential curves and derivative coupling for the $K^\pi = \frac{9}{2}^-$ Rydberg states of Mg. The derivative couplings $P_{\mu\mu'}(r)/20$ are given by the broken lines; $P_{bottom,middle}(r)$, dotted; $P_{middle,top}(r)$, dashed; and $P_{bottom,top}(r)$, dot-dashed.

onto the core orbital momentum, varies in a radial adiabatic analysis of Rydberg Mg. The matrix element of interest is:

$$\langle \vec{L_c} \cdot \vec{\ell} \rangle_\mu = \langle \Phi_\mu \mid \vec{L_c} \cdot \vec{\ell} \mid \Phi_\mu \rangle, \tag{6.8}$$

which varies with r for each of the $K^\pi = \frac{7}{2}^-$ and $K^\pi = \frac{9}{2}^-$ channels of Rydberg Mg.

In Figure 6.7 we plot $\langle \vec{L_c} \cdot \vec{\ell} \rangle_\mu$ versus r for the three adiabatic channels $(J_c, \ell) = (\frac{1}{2}, 3)$, $(\frac{3}{2}, 3)$, and $(\frac{3}{2}, 5)$ of $K^\pi = \frac{7}{2}^-$ Mg. In the isolated channel $(J_c, \ell) = (\frac{3}{2}, 5)$ the relative orientation of $\vec{\ell}$ and $\vec{L_c}$ exhibits very little variation with r. In contrast, the orientation of these two vectors shows a dramatic variation in the $(J_c, \ell) = (\frac{1}{2}, 3)$ and $(J_c, \ell) = (\frac{3}{2}, 3)$ channels. In these cases the variation reflects the presence of an avoided crossing that can be attributed to the strong coupling between these two channels. One channel of particular interest is $(J_c, \ell) = (\frac{1}{2}, 3)$ where the relative orientation flips, or changes sign. We attribute this type of variation in orientation to the anisotropic interactions and to the spin-orbit coupling within the system, since without the additional spin angular momentum $\vec{L_c} \cdot \vec{\ell}$ would be conserved.

In Figure 6.8 we show another example where anisotropic interactions in combination with core spin-orbit coupling produce interesting effects. Here we plot $\langle \vec{L_c} \cdot \vec{\ell} \rangle_\mu$ versus r, but for the three adiabatic channels $(J_c, \ell) = (\frac{1}{2}, 5)$, $(\frac{3}{2}, 3)$, and $(\frac{3}{2}, 5)$ of $K^\pi = \frac{9}{2}^-$ Mg. Once again, the isolated channel $(J_c, \ell) = (\frac{3}{2}, 3)$ shows very little effect from the radial variation. However, the two remaining channels exhibit a crossing, but no sign reversals. For large radial distances the relative orientation of the core and Rydberg angular momenta remains relatively fixed. As the Rydberg electron approaches the ionic core their electrostatic interaction increases, causing the relative orientation of the two orbital planes to change, provided the core is anisotropic.

In these two examples, the orbital plane of the ionic core undergoes the largest reorientation. This can be understood by realizing that total angular momentum is conserved,

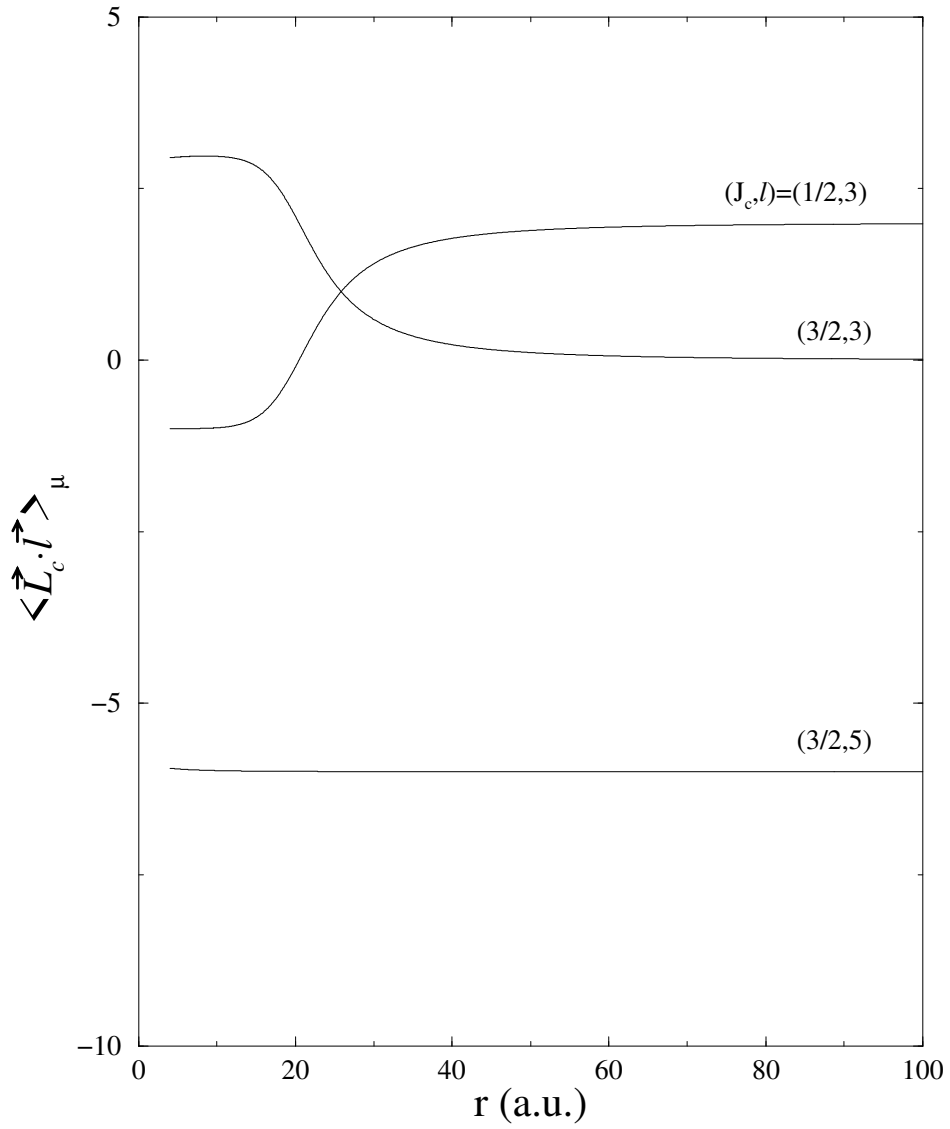

Figure 6.7. Adiabatic variation in the orientation of the ionic core and the Rydberg orbital planes for $K^\pi = \frac{7}{2}^-$ Rydberg Mg

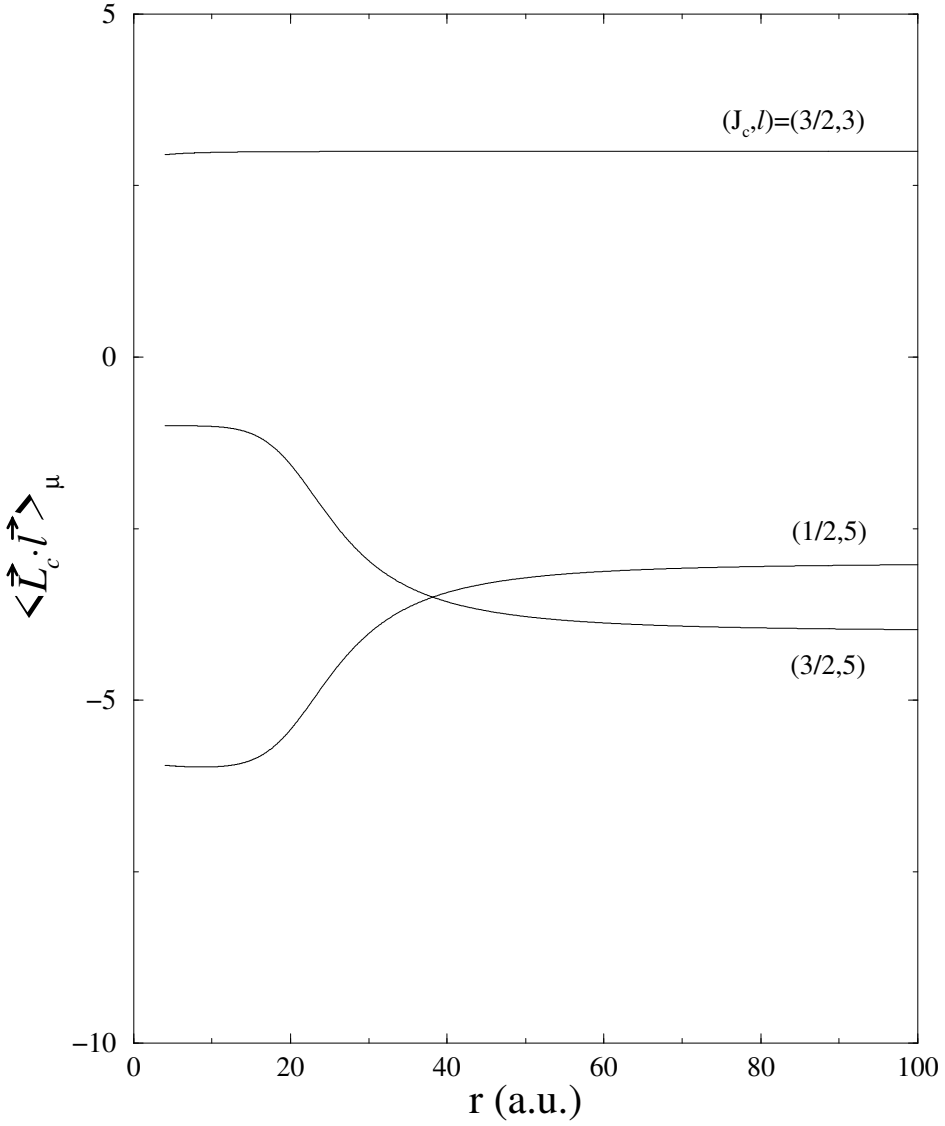

Figure 6.8. Adiabatic variation in the orientation of the ionic core and the Rydberg orbital planes for $K^{\pi} = \frac{9}{2}^{-}$ Rydberg Mg

and, therefore, only the much smaller angular momentum associated with the ionic core can exhibit a sign change. In this sense, we can view the orbit of the ionic core as being "flipped" by the approaching Rydberg electron.

CHAPTER 7

RYDBERG STATES OF THE HYDROGEN DIATOMIC MOLECULE

In this chapter we present our study on Rydberg states of H_2 and D_2. The recent high resolution measurements of Rydberg intervals in ground rovibrational state H_2 and D_2 [9] contain interesting physics for several reasons. The simplicity of the H_2^+ and D_2^+ ionic cores enables theory to compute all of the electric multipole and the induced polarization interactions with enough precision to be competitive with the best experimental measurements. Moreover, these measurements are tantalizingly close to resolving, for the first time, the slight energy shifts of Rydberg states due to relativistic retardation. The tiny interaction associated with retardation in this context is sometimes called a "Casimir force" [9, 19]. Excitement generated by this experimental progress has renewed theoretical interest in Rydberg state physics and in precise calculations of H_2^+ and D_2^+ ionic properties. This chapter develops the most extensive, complete adiabatic treatment of H_2^+ and D_2^+ ion properties presented to date. The resulting comparison with experiment gives a stringent test of our diabatic formulation of the Rydberg states physics.

7.1 Molecular Hamiltonian in Jacobi Coordinates

We begin by developing a general theory of the interactions in the generalized hydrogen Rydberg molecule. Much other work on molecular Rydberg systems has of course been done elsewhere [76, 77, 78, 79, 80, 81, 82, 11, 83, 84]. The primary reason for presenting this development here is to detail the differences among various approximations currently being used, and to clarify the advances our treatment contributes to the field of Rydberg state physics.

The formulation of a many-body problem in terms of relative coordinates gives

rise to an expression for the kinetic energy of the system that involves scalar products of momentum operators associated with different pairs of constituent particles; such terms have been referred to as "mass polarization" [86, 87, 88]. In almost all atoms and small molecules the mass polarization can be treated as a perturbation. However, it is desirable to absorb the perturbative effects of mass polarization into an effective Hamiltonian that describes how the Rydberg electron interacts with the ionic core. One way of doing this is through the use of Jacobi coordinates [89, 90, 11] where the position of each successive particle is defined relative to the center of mass of the previous subsystem.

7.1.1 Transformation Rydberg states of the generalized hydrogen diatomic molecule consist of two nuclei with charges $Z_a e$ and $Z_b e$, a core electron, and a Rydberg electron. The laboratory positions of each particle, respectively, are defined as $\vec{r}_a$, $\vec{r}_b$, $\vec{r}_i$, and $\vec{r}_{Ryd}$ relative to a common origin. The transformation from $\{\vec{r}_a, \vec{r}_b, \vec{r}_i, \vec{r}_{Ryd}\}$ to the Jacobi coordinates $\{\vec{R}_{cm}, \vec{R}, \vec{r}_e, \vec{r}\}$ is advantageous, in that no mass polarization terms arise in the kinetic energy operator. The center of mass of the entire molecule is defined by

$$\vec{R}_{cm} = \frac{M_a \vec{r}_a + M_b \vec{r}_b + m_e \vec{r}_i + m_e \vec{r}_{Ryd}}{M_a + M_b + 2m_e}. \tag{7.1}$$

The relative position of the two nuclei is

$$\vec{R} = \vec{r}_a - \vec{r}_b. \tag{7.2}$$

The position of the core electron relative to the center of mass of the nuclei is

$$\vec{r}_e = \vec{r}_i - \frac{M_a \vec{r}_a + M_b \vec{r}_b}{M_a + M_b}, \tag{7.3}$$

and

$$\vec{r} = \vec{r}_{Ryd} - \frac{M_a\vec{r}_a + M_b\vec{r}_b + m_e\vec{r}_i}{M_a + M_b + m_e} \tag{7.4}$$

is the position of the Rydberg electron relative to the center of mass of the molecular ion.

7.1.2 Kinetic and Potential Operators In Jacobi coordinates the kinetic (T) and potential (V) operators of a generalized hydrogen diatomic molecule are given by

$$\begin{aligned} T \quad &= \frac{1}{2(M_a + M_b + 2m_e)}\vec{P}_{cm}^2 + \frac{M_a + M_b}{2M_aM_b}\vec{P}_R^2 \\ &+ \frac{M_a + M_b + m_e}{2m_e(M_a + M_b)}\vec{P}_e^2 + \frac{M_a + M_b + 2m_e}{2m_e(M_a + M_b + m_e)}\vec{P}_r^2, \end{aligned} \tag{7.5}$$

and

$$\begin{aligned} V \quad &= \frac{Z_aZ_be^2}{R} - \frac{Z_ae^2}{\mid \vec{r}_e - \epsilon_a\vec{R} \mid} - \frac{Z_be^2}{\mid \vec{r}_e + \epsilon_b\vec{R} \mid} \\ &- \frac{Z_ae^2}{\mid \vec{r} - \epsilon_a\vec{R} + \epsilon\vec{r}_e \mid} - \frac{Z_be^2}{\mid \vec{r} + \epsilon_b\vec{R} + \epsilon\vec{r}_e \mid} + \frac{e^2}{\mid \vec{r} - \vec{r}_e + \epsilon\vec{r}_e \mid}. \end{aligned} \tag{7.6}$$

The mass factors in the potential energy, which would normally be associated with mass polarization when non-Jacobian type coordinates are use, are

$$\epsilon_a \equiv \frac{M_b}{M_a + M_b}, \qquad \epsilon_b \equiv \frac{M_a}{M_b + M_a}, \qquad \epsilon \equiv \frac{m_e}{M_a + M_b + m_e}. \tag{7.7}$$

Here ϵ_a and ϵ_b depend only on the masses of the two nuclei, while ϵ also depends on the mass of the electron.

7.1.3 Molecular Ion and Rydberg Hamiltonians Since we are interested in high-ℓ Rydberg states of H_2 and D_2, the full molecular Hamiltonian can be decomposed into largely separate molecular ion and Rydberg electron Hamiltonians:

$$H = T + V = H_{core} + H_{Rydberg}. \tag{7.8}$$

All terms relating to the Rydberg electron, including the electron-ion interaction, are included in the latter. The Hamiltonian for the molecular ion is

$$\begin{aligned} H_{core} \quad &\equiv \frac{M_a + M_b}{2M_a M_b}\vec{P}_R^2 + \frac{Z_a Z_b e^2}{R} \\ &+ \frac{M_a + M_b + m_e}{2m_e(M_a + M_b)}\vec{P}_e^2 - \frac{Z_a e^2}{\mid \vec{r}_e - \epsilon_a \vec{R} \mid} - \frac{Z_b e^2}{\mid \vec{r}_e + \epsilon_b \vec{R} \mid}, \end{aligned} \tag{7.9}$$

and the Hamiltonian for the Rydberg electron is

$$\begin{aligned} H_{Rydberg} \quad &\equiv \frac{M_a + M_b + 2m_e}{2m_e(M_a + M_b + m_e)}\vec{P}_r^2 + \frac{e^2}{\mid \vec{r} - \vec{r}_e + \epsilon\vec{r}_e \mid} \\ &- \frac{Z_a e^2}{\mid \vec{r} - \epsilon_a \vec{R} + \epsilon\vec{r}_e \mid} - \frac{Z_b e^2}{\mid \vec{r} + \epsilon_b \vec{R} + \epsilon\vec{r}_e \mid}. \end{aligned} \tag{7.10}$$

Here it is important to note that H_{core} is the Hamiltonian for a free molecular ion, independent of any Rydberg coordinate. However, $H_{Rydberg}$ is coupled to the molecular ion through its dependence on the internuclear separation $\vec{R}$ and the position $\vec{r}_e$ of the molecular electron. These two Hamiltonians do not commute, of course.

7.1.4 Spherical Expansion of the Rydberg Hamiltonian As in atomic Rydberg systems, the large value of the Rydberg radial coordinate facilitates a perturbative expansion of all electrostatic interactions between the Rydberg electron and the molecular ion. After an expansion of the Rydberg-core interaction into spherical multipoles, the Rydberg Hamiltonian simplifies to

$$H_{Rydberg} \equiv \frac{1}{2}\frac{M_a + M_b + 2m_e}{m_e(M_a + M_b + m_e)}\vec{P}_r^2 + e^2\frac{1 - Z_a - Z_b}{r}$$

$$+e^2\sum_{k>0}\left[N_k r_e^k C^{(k)}(\hat{r}_e) - M_k R^k C^{(k)}(\hat{R})\right]\cdot\frac{C^{(k)}(\hat{r})}{r^{k+1}} \tag{7.11}$$

where the mass factors are

$$N_k \equiv (1-\epsilon)^k - (-1)^k(Z_a + Z_b)\epsilon^k, \tag{7.12}$$

and

$$M_k \equiv Z_a\epsilon_a^k + (-1)^k Z_b\epsilon_b^k. \tag{7.13}$$

For Rydberg states of H_2 this Hamiltonian (in atomic units based on the bare, not reduced, electron mass) becomes

$$H_{Rydberg} \equiv -\frac{1}{2}\frac{2M_p + 2}{2M_p + 1}\vec{\nabla}_r^2 - \frac{1}{r}$$

$$+\sum_{k>0}\left[N_k r_e^k C^{(k)}(\hat{r}_e) - M_k R^k C^{(k)}(\hat{R})\right]\cdot\frac{C^{(k)}(\hat{r})}{r^{k+1}}. \tag{7.14}$$

Here M_p is the proton mass and $m_e = 1$. For this case, N_k and M_k reduce to the simple expressions

$$N_k \equiv (1-\epsilon)^k - 2(-1)^k\epsilon^k, \tag{7.15}$$

and

$$M_k \equiv \left(\frac{1}{2}\right)^k \left(1 + (-1)^k\right). \tag{7.16}$$

To treat Rydberg states of D_2 we need only change the masses in the molecular ion and Rydberg Hamiltonians. The nuclear mass factor M_k is nonzero only when k is *even*.

7.2 Close-Coupling Representation

The theoretical description of a Rydberg diatomic molecule is essentially the same as that for a Rydberg atom, except for the additional vibrational (ν^+) and rotational (N^+) structure. The wavefunction for the entire molecular system can be expanded in a primitive representation $\{\phi_i(\omega)\}$ constructed from the energy eigenstates of the molecular ion and the angular functions of the Rydberg electron

$$\Psi(r,\omega) = \sum_i \phi_i(\omega)\psi_i(r) \tag{7.17}$$

where ω represents all coordinates in the molecular system except the Rydberg radial position. Since we are still considering nonpenetrating, high-ℓ Rydberg states, for which electron spin effects (such as exchange) are negligible, the appropriate coupling scheme is still $(N^+\ell)K$ coupling [35, 36], when molecular hyperfine and spin-rotation splittings can be neglected.

The rotational structure of the molecular ion plays a role analogous to the fine structure of the atomic ions considered ealier. The close-coupling equations once again provide a useful channel structure that facilitates the separation of physically dominant channels from those that play only a perturbative role in the description of a Rydberg molecule. Following the spirit of Chapter 3, we use the standard technique of channel elimination [46] and a Green's function expansion [49, 50] to derive a long-range effective diabatic Hamiltonian that describes how the distant Rydberg electron interacts with the molecular ion. A tensorial analysis similar to that described in Chapter 4 for Eq.(4.40) generates an effective Hamiltonian with operator structure

$$
\begin{aligned}
H_{\mu\mu'} \quad &= \left(E_\mu - E_{\mu_0} - \frac{1}{2\mu_m}\frac{d^2}{dr^2} + \frac{\ell_\mu(\ell_\mu+1)}{2\mu_m r^2} - \frac{1}{r} - \frac{\alpha_s}{2r^4} - \frac{\eta_s}{r^6} \right) \delta_{\mu\mu'} \\
&- \left(\frac{Q}{r^3} + \frac{\alpha_t}{2r^4} + \frac{\eta_t}{r^6} \right) \mathcal{P}^{(2)}_{\mu\mu'} - \left(\frac{\phi}{r^5} + \frac{\lambda_h}{r^6} \right) \mathcal{P}^{(4)}_{\mu\mu'} \\
&+ \left(\frac{\beta_s \mathcal{B}^{(0)}_{\mu\mu'} + \beta_t \mathcal{B}^{(2)}_{\mu\mu'}}{r^6} \right) + \frac{\beta_v}{r^6} \langle \vec{N^+} \cdot \vec{\ell} \rangle_{\mu\mu'} \\
&- 2 \left(\frac{\beta_s \delta_{\mu\mu'} + \beta_t \mathcal{P}^{(2)}_{\mu\mu'}}{r^5} \right) - \frac{d}{dr} \left(\frac{\beta_s \delta_{\mu\mu'} + \beta_t \mathcal{P}^{(2)}_{\mu\mu'}}{r^4} \right) \frac{d}{dr}
\end{aligned} \tag{7.18}
$$

where E_{μ_0} is the lowest ionization threshold in the physical channel subspace, and $\mu_m = \frac{2M_p+1}{2M_p+2}$ is the reduced mass of the Rydberg electron relative to the ion. Likewise, the $\Lambda_{\mu\mu'}$ matrix in Eq.(4.41) is given by

$$
\Lambda_{\mu\mu'} = \delta_{\mu\mu'} + 2 \left(\frac{\beta_s \delta_{\mu\mu'} + \beta_t \mathcal{P}^{(2)}_{\mu\mu'}}{r^4} \right). \tag{7.19}
$$

Here we adopt the convention in which α_s and α_t are the standard scalar and tensor induced dipole polarizabilities, Q and ϕ are the permanent electric quadrupole and hexadecapole moments, and η_s, η_t, and λ_h are higher-order scalar, second-rank tensor, and fourth-rank tensor induced hyperpolarizabilities of the ionic core. Explicit expressions for all terms, including the angular factors $\langle \vec{N^+} \cdot \vec{\ell} \rangle_{\mu\mu'}$, $\mathcal{P}^{(2)}_{\mu\mu'}$, and $\mathcal{P}^{(4)}_{\mu\mu'}$ are given in Appendix B.

As in the atomic case, the β terms represent nonadiabatic effects arising from the radial and angular motion of the Rydberg electron. Here the vector interaction involving β_v couples the total angular momentum N^+ of the molecular ion with the orbital angular momentum ℓ of the Rydberg electron. Interestingly, since the rovibrational states necessarily involve both the massive nuclei and the molecular electron, effects arising from the vector interaction will be much smaller in molecular systems than in atomic systems. In essence,

it is more difficult for a Rydberg electron to "drag" the polarization vector of a massive spinning molecular ion, as opposed to the polarization vector of an atomic ion that involves much lighter electrons. We will return to this point in a couple of sections.

7.3 Levels of Approximation

In order to compute Rydberg state properties of diatomic hydrogen in our formulation, we must determine the permanent electric multipole moments and the induced polarizabilities and hyperpolarizabilities of the molecular ion. The calculation of ionic core properties is a difficult task, but fortunately there are a number of familiar molecular approximations that can be utilized. These approximations make use of the fact that massive nuclei move far more slowly than the molecular electrons.

The wavefunction Ψ_{ion} for the molecular ion can be expanded in products of rovibrational and electronic wavefunctions

$$\Psi_{ion}(\vec{R},\vec{r_e}) = \sum_j F_j(\vec{R})\Phi_j(\vec{R},\vec{r_e}), \tag{7.20}$$

where the electronic wavefunction $\Phi_j(\vec{R},\vec{r_e})$ satisfies the equation

$$\left(-\frac{1}{2}\frac{2M_p+1}{2M_p}\vec{\nabla}_e^2 - \frac{1}{\mid \vec{r_e} - \frac{1}{2}\vec{R} \mid} - \frac{1}{\mid \vec{r_e} + \frac{1}{2}\vec{R} \mid}\right)\Phi_j(\vec{R},\vec{r_e}) = E_j^e(R)\Phi_j(\vec{R},\vec{r_e}). \tag{7.21}$$

An equation for the rovibrational wavefunction $F_i(\vec{R})$ of the nuclei is obtained after projecting out the electronic states in the full molecular ion Schrödinger equation

$$\left(-\frac{1}{M_p}\vec{\nabla}_R^2 + \frac{1}{R} + E_i^e(R)\right)F_i(\vec{R}) - 2\frac{1}{M_p}\sum_j\left[\langle\phi_i \mid \vec{\nabla}_R \mid \phi_j\rangle\cdot\vec{\nabla}_R\right]F_j(\vec{R})$$

$$-\frac{1}{M_p}\sum_j\left[\langle\phi_i \mid \vec{\nabla}_R^2 \mid \phi_j\rangle\right]F_j(\vec{R}) = E_{core}F_i(\vec{R}). \tag{7.22}$$

Various methods can be used to solve these equation, ranging from the Born-Oppenheimer approximation to exact, nonadiabatic methods which treat all coordinates including the internuclear separation R on an equal basis [78, 79, 80, 81, 82, 91, 92, 93, 94, 95, 96, 97, 85]. For clarity, let us review the two most familiar approximate methods that provide solutions for the rovibrational equation: the Born-Oppenheimer approximation and the adiabatic-nuclei approximation.

7.3.1 Born-Oppenheimer Approximation In the Born-Oppenheimer approximation the nuclei are assumed initially to be infinitely massive. The relative separation between the nuclei then becomes a constant parameter. The nuclear momentum operator $-i\vec{\nabla}_R$ is set to zero in this initial step, in Eq.(7.22) leaving

$$\left(-\frac{1}{M_p}\vec{\nabla}_R^2 + \frac{1}{R} + E_i^e(R)\right) F_i^{BO}(\vec{R}) = E_{core}^{BO} F_i^{BO}(\vec{R}) \tag{7.23}$$

as the nuclear rovibrational equation, which contains no coupling among different rovibrational states. The extremely useful Born-Oppenheimer approximation has provided much of the framework used today to understand the low vibrational states of diatomic molecules. However, this approximation must be greatly improved upon to account for modern, high-resolution Rydberg state spectroscopy, which can probe the fine details of the interactions among electronic, vibrational, and rotational degrees of freedom.

7.3.2 Adiabatic Nuclei Approximation The adiabatic-nuclei approximation assumes that the distance between the nuclei varies slowly, but is not entirely negligible compared to the motion of the molecular electrons. In this case Eq.(7.22) reduces to

$$\left(-\frac{1}{M_p}\vec{\nabla}_R^2 + \frac{1}{R} + E_i^e(R) - \frac{1}{M_p}\langle\phi_i \mid \vec{\nabla}_R^2 \mid \phi_i\rangle\right) F_i^{AD}(\vec{R}) = E_{core}^{AD} F_i^{AD}(\vec{R}) \tag{7.24}$$

where the diagonal matrix elements involving $\vec{\nabla}_R$ vanish, since the matrix is skew-symmetric, but the matrix elements involving $\vec{\nabla}_R^2$ survive as corrections due to the relative motion of

the nuclei. While coupling among different rovibrational states is not included at this level of approximation, the energy levels of low rovibrational states are generally accurate to about five significant figures [91, 85]. As we will demonstrate later in this chapter, the adiabatic-nuclei approximation can account for most the physics observed in the recent high-resolution experimental studies of H_2 and D_2 [9].

In our studies of Rydberg states of H_2 and D_2 the rovibrational state of the molecular ion in the physical channel subspace is usually either the ground state or the first rotationally excited state. By the Frank-Condon principle, only excited states that significantly overlap with these low lying states, which have near zero nuclear kinetic energy, will contribute to the matrix elements in the summations for the polarizabilities and hyperpolarizabilities [77, 36]. For this reason, the adiabatic-nuclei approximation can be used to accurately compute low rovibrational induced polarizabilities and hyperpolarizabilities of H_2^+ and D_2^+.

7.4 Core States of H_2^+ and D_2^+

All of our calculations for the H_2^+ and D_2^+ ions are performed using the adiabatic-nuclei approximation. These adiabatic calculations of the induced polarizabilities and hyperpolarizabilities, which involve complete summations over rovibrational states of these molecular ions, are the first of their kind. In almost all previous calculations of these quantities, a "completeness" approximation has been used [98, 99, 100, 101, 19].

7.4.1 Calculation of Electronic States The solution of the electronic equation Eq.(7.21) is most easily performed in prolate spheroidal coordinates (see Appendix D) where the partial differential equation breaks into three separate equations whose solutions are linked only through separation constants. In prolate spheroidal coordinates the electronic Hamiltonian (using atomic units with the bare electron mass) is [78, 79, 80, 81, 82, 77]

$$H_{elec} = -\frac{2}{R^2(\xi^2-\eta^2)}\left\{\frac{\partial}{\partial\xi}(\xi^2-1)\frac{\partial}{\partial\xi}+\frac{\partial}{\partial\eta}(1-\eta^2)\frac{\partial}{\partial\eta}+\frac{(\xi^2-\eta^2)}{(\xi^2-1)(1-\eta^2)}\frac{\partial^2}{\partial\phi^2}\right\}$$

$$-\frac{4\xi}{R}\frac{1}{\xi^2-\eta^2}. \tag{7.25}$$

After electronic wavefunction is expanded as a product

$$\Phi(R,\vec{r_e}) = L(R,\xi)M(R,\eta)N(\phi), \tag{7.26}$$

the electronic equation separates into

$$\left[\frac{\partial}{\partial\xi}(\xi^2-1)\frac{\partial}{\partial\xi} - A + \frac{ER^2}{2}\xi^2 + R\xi(Z_a+Z_b) - \frac{\lambda^2}{\xi^2-1}\right]L(R,\xi) = 0 \tag{7.27}$$

$$\left[\frac{\partial}{\partial\eta}(1-\eta^2)\frac{\partial}{\partial\eta} + A - \frac{ER^2}{2}\eta^2 - R\eta(Z_a-Z_b) - \frac{\lambda^2}{1-\eta^2}\right]M(R,\eta) = 0 \tag{7.28}$$

$$-i\frac{\partial}{\partial\phi}N(\phi) = \lambda N(\phi) \tag{7.29}$$

where λ and A are separation constants and E is the electronic energy of the system. Note that A is a function of λ and E.

The azimuthal equation can be solved analytically, with the result

$$N(\phi) = \frac{1}{\sqrt{2\pi}}e^{i\lambda\phi} \tag{7.30}$$

where $\lambda = 0, \pm1, \pm2, \cdots$. Some of the symmetry properties of the hydrogen diatomic molecular ion are immediately apparent from these equations. Since λ only appears in the

form λ^2 there is a double degeneracy for all nonzero λ states, which is consistent with the azimuthal-symmetry of the electronic Hamiltonian about the internuclear axis. Furthermore, for homonuclear diatomic ions, where $Z_a = Z_b$, the $Z_a - Z_b$ term in the angular $M(R, \eta)$ equation vanishes and the angular equation becomes invariant under reflection ($\eta \rightarrow -\eta$). This invariance translates into angular eigenfunctions that possess either gerade (even) or ungerade (odd) symmetry for each value of the separation constant A.

Solution of the pair of radial $L(R, \xi)$ and angular $N(R, \eta)$ equations requires a little more effort since they are coupled through the separation constant A and the electronic energy E. While there are many ways of solving these equations [78, 79, 80, 81, 82], an efficient and accurate method is to solve each equation using a finite element method (see Appendix E), and iterate the solutions until A and E converge to some desired precision, which in our calculations is ten digits.

7.4.2 Calculation of Rovibrational States The rovibrational states of the molecular ion are obtained by solving the adiabatic-nuclei equation Eq.(7.24), with the electronic energies $E_i^e(R)$, which depend on the internuclear separation R, and the adiabatic corrections arising from the $\vec{\nabla}_R^2$ nuclear operator. A finite element method (see Appendix E) is used to solve these equations. The energy eigenvalues obtained are converged to ten digits, while the core electric multipole moments and the induced polarizabilities and hyperpolarizabilities are converged to only about five digits. (Variational eigenfunctions are typically accurate to only half as many digits as the quantity that is variational, which is the energy in this case.)

7.4.3 Core Parameters and the Vector Hyperpolarizability Until this study, no complete adiabatic calculation of any polarizability or hyperpolarizability had been performed for H_2^+ or D_2^+. The best previous calculations were based on what is loosely called a "clamped nuclei" approximation [98, 99, 100, 101, 19] that neglects the small rovibrational splittings in the energy denominators of the induced polarizabilities and hyperpolarizabilities.

A closure relationship for the rovibrational states can then be used to eliminate the summations over intermediate rovibrational quantum numbers, thereby leaving simple (purely electronic) polarizabilities and hyperpolarizabilities. As with the Born-Oppenheimer approximation, the "clamped nuclei" approximation is unacceptable in the present context, owing to the high resolution attained in Rydberg state spectroscopy.

A few "exact", or nonadiabatic calculations of the permanent electric multipole moments have been performed by Bishop and Moss[102, 93]. However, the first nonadiabatic calculation of the ground state dipole polarizability $\alpha_s = 3.1682$ of H_2^+ has been completed only very recently by Shertzer [103]. This value is still unpublished and should be regarded as preliminary as of this writing. Nevertheless, the new value agrees well with the indirect measurement $\alpha_s = 3.1682(7)$ of Ref.[9]. Thus far, Shertzer's method has only been employed to compute the dipole polarizabilities of the ground rovibrational states of H_2^+ and D_2^+. An extension of Shertzer's method to other ground state or excited rovibrational state polarizabilities and hyperpolarizabilities is likely to be technically difficult, and results are not expected to emerge for some time. For now, our calculation is the most complete treatment of the multipole and induced polarization interactions in H_2 and D_2. It is also the first calculation of the vector hyperpolarizability for a molecular system.

Table 7.1 shows our adiabatic calculation of the ground rovibrational state polarizabilities and hyperpolarizabilities for H_2^+ and D_2^+. These results were obtained by solving the electronic and rovibrational equations using the adiabatic-nuclei approximation. Summations were included over numerous rovibrational states of the molecular ions, until it appeared the series had converged. A total of 180 electronic states of H_2^+ and D_2^+ were computed out to $R = 8a.u.$ to ten digit accuracy. For each electronic potential and each rotational state, 200 rovibrational wavefunctions were computed using the adiabatic-nuclei approximation, also to ten digit accuracy.

Any residual errors in our scalar dipole polarizabilities α_s for H_2^+ and D_2^+, should

be caused by effects of nonadiabatic nuclear motion. In fact, the 0.046 percent difference between the exact and the adiabatic dipole polarizabilities is consistent with the estimates of Bishop [102] and Moss [93] who predicted a 0.043 percent difference between the exact and adiabatic quadrupole moments of $(\nu^+ = 0, N^+ = 1)$ H_2^+. While there are slight differences between the adiabatic calculations and the measured polarizabilities, the adiabatic calculations represent a significant improvement on the "clamped nuclei" approximation which predicts a scalar dipole polarizability $\alpha_s = 3.1730$, with a -0.15 percent difference relative to the exact calculation of Shertzer [103].

In the future we hope to study Rydberg states attached to the anisotropic $(\nu^+ = 0, N^+ = 1)$ H_2^+ ion. With this in mind, we present the first complete adiabatic calculation of the permanent electric multipole moments, polarizabilities and hyperpolarizabilities for this ion in Table 7.2. To our initial surprise, the vector hyperpolarizability β_v is an order of magnitude smaller for the $(\nu^+ = 0, N^+ = 1)$ H_2^+ ion than for the Ne^+ ion studied in Chapter 5. Moreover, β_v is three orders of magnitude smaller than β_s and β_t. Since the H_2^+ molecular ion is generally more polarizable than the Ne^+ ion, we initially expected the vector hyperpolarizability to be much larger, and to play a more significant role in the physics of H_2 Rydberg states. A study of this unexpected result has helped to elucidate the qualitative meaning of the vector interaction.

The explanation lies in the rotational structure of the molecular ion. The adiabatic-nuclei definition of the vector hyperpolarizability given in Appendix B is

$$\beta_{v_\mu} = (-1)^{N^+} N_1^2 \sqrt{\frac{3}{2}} \left[\frac{(2N^+ + 1)}{N^+(N^+ + 1)}\right]^{\frac{1}{2}}$$

$$\sum_\nu (-1)^{N_\nu^+} \frac{(2N_\nu^+ + 1)}{(E_{\mu_0} - E_\nu)^2} \begin{pmatrix} N^+ & 1 & N_\nu^+ \\ 0 & -\lambda_\nu & \lambda_\nu \end{pmatrix} \begin{pmatrix} N_\nu^+ & 1 & N^+ \\ -\lambda_\nu & \lambda_\nu & 0 \end{pmatrix}$$

Table 7.1. Theoretical and experimental [9] parameters (atomic units) for ground state H_2^+ and D_2^+. The theoretical values were computed using a complete summation over adiabatic rovibrational states method, without making the usual "completeness approximation".

H_2^+	α_s	β_s	η_s
Adiabatic Theory	3.1667	1.6938	12.5601
Experiment [9]	3.1681(7)		
Nonadiabatic [103]	3.1682(4)		
Clamped Nuclei Approx. [85]	3.1730		
D_2^+	α_s	β_s	η_s
Adiabatic Theory	3.0708	1.5930	11.8807
Experiment [9]	3.0712(7)		
Nonadiabatic [103]	3.0714(4)		
Clamped Nuclei Approx. [9]	3.0739		

$$\left\{ \begin{array}{ccc} 1 & 1 & 1 \\ N^+ & N^+ & N_\nu^+ \end{array} \right\} \langle \Psi_\mu \mid r_e C^{(1)}_{-\lambda_\nu}(\hat{r}_e) \mid \Psi_\nu \rangle \langle \Psi_\nu \mid r_e C^{(1)}_{-\lambda_\nu}(\hat{r}_e) \mid \Psi_\mu \rangle^*. \tag{7.31}$$

Using the "clamped nuclei" approximation we can binomially expand the energy factor in powers of the vibrational and rotational energy splittings, which are far smaller than the electronic energy differences. Specifically,

$$\frac{1}{(\Delta E_{\mu_0 \nu})^2} = \frac{1}{(\Delta E^{el}_{\mu_0 \nu})^2} - \frac{2\Delta E^{vib}_{\mu_0 \nu}}{(\Delta E^{el}_{\mu_0 \nu})^3} - \frac{2\Delta E^{rot}_{\mu_0 \nu}}{(\Delta E^{el}_{\mu_0 \nu})^3} + \cdots. \tag{7.32}$$

where $\Delta E_{\mu_0 \nu} \equiv E_{\mu_0} - E_\nu$. The electronic ($el$) and vibrational ($vib$) energy differences in this expression contribute nothing to β_v, at this level of approximation, since the summation over the rotational momenta N_ν^+ vanishes. The rotational energy difference on the other hand survives, and provides our desired approximation to leading order. If we replace the rotational energy difference with

$$\Delta E^{rot}_{\mu_0 \nu} = \frac{[N^+(N^+ + 1) - N_\nu^+(N_\nu^+ + 1)]}{2I}, \tag{7.33}$$

where I is the moment of inertia of the diatomic ion, then the vector hyperpolarizability can be expressed in the form

$$\beta_{v_\mu} = \frac{\beta^{\parallel}_{v_\mu} + \beta^{\perp}_{v_\nu}}{2I}. \tag{7.34}$$

Here $\beta^{\parallel}_{v_\mu}$ and $\beta^{\perp}_{v_\nu}$ are parallel and perpendicular electronic hyperpolarizabilities that involve cubed energy denominators. Explicitly

$$\beta^{\parallel}_{v_\mu} = \int d\vec{R} F^*_\mu(\vec{R})\ \beta^{\parallel}_v(R)\ F_\mu(\vec{R}), \tag{7.35}$$

and

$$\beta_{v_\mu}^{\perp} = \int d\vec{R} F_\mu^*(\vec{R})\ \beta_v^{\perp}(R)\ F_\mu(\vec{R}), \tag{7.36}$$

where $F_\mu(\vec{R})$ is an adiabatic rovibrational wavefunction. The radial $\beta_v^{\parallel}(R)$ and $\beta_v^{\perp}(R)$ factors depend only on electronic properties of the molecular ion:

$$\beta_v^{\parallel}(R) = -2N_1^2 \sum_\alpha \frac{D_{X,\alpha 0}^* D_{X,\alpha 0}}{(E_X - E_{\alpha 0})^3}, \tag{7.37}$$

and

$$\beta_v^{\perp}(R) = -2N_1^2 \sum_\alpha \frac{D_{X,\alpha 1}^* D_{X,\alpha 1}}{(E_X - E_{\alpha 1})^3}, \tag{7.38}$$

where N_1 is the electronic mass factor defined in Eq.(7.15), and where the electronic dipole matrix element is defined as

$$D_{X,\alpha\lambda}(R) \equiv \int d\vec{r}_e \Phi_X^*(R,\vec{r}_e) r_e C_{-\lambda}^{(1)}(\hat{r}_e) \Phi_{\alpha\lambda}(R,\vec{r}_e). \tag{7.39}$$

The subscipts X ($\alpha\lambda$) denote the electronic ground (excited) states of H_2^+, and both E_X and $E_{\alpha\lambda}$ depend on the internuclear separation R.

The dependence of the β_{v_μ} expression on the moment of inertia of the molecular ion immediately explains why β_v is approximately one-thousand times smaller than the β_s and β_t hyperpolarizabilities. Moreover, the fact that there is a moment of inertia in this expression for β_v confirms our physical picture of the vector interaction. The origin of the vector interaction is qualitatively different from that of the static polarizabilities. The vector interaction describes how the motion of the Rydberg electron couples with dynamics of the molecular ion. As the distant Rydberg electron revolves around the core, it tries to

"drag" the core polarization vector with it. The comparatively enormous moment of inertia of the molecule resists this drag strongly, thereby minimizing the effect of this "torque". Consequently the dynamic vector interaction is miniscule in molecular Rydberg states.

7.5 Rydberg States of H_2 and D_2

We turn now to the $n = 9$ and 10 Rydberg states of $(\nu^+ = 0, N^+ = 0)$ H_2 and D_2, which have recently been studied experimentally by Jacobson *et al* [9]. In anticipation of new experimental studies of high-ℓ Rydberg states attached to the anisotropic $(\nu^+ = 0, N^+ = 1)$ H_2^+ molecular ion [104], we also present a quantitative investigation of the vector interaction that helps to elucidate its qualitative nature. These results are compared with theoretical calculations of the energy shifts generated by relativistic retardation (Casimir) [19] carried out elsewhere.

7.5.1 Ryberg States of $(\nu^+ = 0, N^+ = 0)$ H_2 and D_2 The experimentally observed spin splittings in the high-ℓ, $n = 9$ and 10 Rydberg states of $(\nu^+ = 0, N^+ = 0)$ H_2 and D_2 were analyzed by the experimental group to extract spinless Rydberg transition frequencies [9, 11, 105]. For these $N^+ = 0$ Rydberg states the hyperfine interaction produces an overall scalar shift that makes no contribution to any of the observed Rydberg intervals. Exchange energies were determined to be less than 0.01 MHz for these high-ℓ Rydberg states. Moreover, refinements made by Jacobson *et al* have improved the signal to noise ratio by a factor of 15 compared with earlier experiments on H_2 [11].

The effective diabatic Hamiltonian in Eq.(7.18) includes all permanent multipole and induced polarization interactions out to radial order $\left(\frac{1}{r}\right)^6$ and out to second-order in the Green's function energy expansion. Since these expansions are finite in extent, care must be taken to ensure that high-order terms contribute a negligible amount to the Rydberg energy intervals under study. Table 7.3 displays the first order energy shifts (MHz) of the $n = 10$, $\ell = 5, 6, 7, 8$ and 9 hydrogenic states arising from various perturbative $\frac{1}{r}$ interactions. The proportionality coefficient is taken to be $1 a.u.$ so that these results can be easily rescaled by

Table 7.2. Theoretical and experimental [11] parameters (atomic units) for $(v^+ = 0, N^+ = 1)$ H_2^+. These parameters are defined in Appendix B and the long range potential is given in Eq.(7.18). The theoretical values were computed using a complete summation over adiabatic rovibrational states method, without making the usual "completeness approximation".

H_2^+	Q	ϕ	λ_h
Adiabatic Theory	1.64285	2.01966	0
Experiment [11]	1.64323(30)		
	α_s	β_s	η_s
Adiabatic Theory	3.17627	1.70230	12.61887
Experiment [11]	3.1787(34)		
Clamped Nuclei Approx. [85]	3.1826		
	α_t	β_t	η_t
Adiabatic Theory	2.67900	2.07061	16.96614
Experiment [11]	2.678(24)		
Clamped Nuclei Approx. [85]	2.6863		
		β_v	
Adiabatic Theory		0.0048231	

the actual coefficients for any Rydberg system. Since our calculation of ionic core properties extends only to inverse radial powers of $\frac{1}{r^6}$, we can accurately predict Rydberg level intervals for ℓ-states for which higher-order $\frac{1}{r^7}$ and $\frac{1}{r^8}$ interactions are negligible. Experimental fits performed by Jacobson *et al* indicate that the coefficient of the scalar $\frac{1}{r^7}$ hyperpolarization interaction is approximately $20 a.u.$. On this basis, Table 7.3 indicates that contributions from this $\frac{1}{r^7}$ interaction and higher-order terms will be negligible for states with $\ell \geq 6$.

Using the theoretical core parameters from Table 7.1, we compute the $n = 9$ and 10 Rydberg intervals (and $\ell > 5$) for the ground rovibrational state of H_2^+ and D_2^+. The results of these calculations are presented in Table 7.4. The agreement between our calculations and the measured intervals is very good, considering the fact that we apply the adiabatic-nuclei approximation to compute all the induced polarizabilities and hyperpolarizabilities. While we do not explicitly compare with the predictions of a "clamped nuclei" calculation in Table 7.4, it is important to know that the error in the polarizabilities and hyperpolarizabilities predicts Rydberg intervals that are larger than the measured intervals by approximately 2 MHz for the $I - K$ transitions. Our calculations reproduce the experimental intervals with an accuracy of 0.3 MHz or better. While this accuracy is still not quite high enough to extract energy shifts due to relativistic retardation from these experiments, it suggests that further improvements in the calculations of the polarizabilities and hyperpolarizabilities of ground state H_2^+ and D_2^+ may clear up the remaining discrepancies, and hopefully improve our quantitative understanding of the non-retardation physics to the desired level.

7.5.2 Analysis of the Vector Interaction and Relativistic Retardation in the $n = 10$ Rydberg States of $(\nu^+ = 0, N^+ = 1)$ H_2 Since the first prediction of the vector interaction one of the most interesting questions in Rydberg state physics has been: what qualitative effect on the spectrum does the vector interaction generate? In order to better understand the nature of this unusual interaction, we compare the relative energy shifts generated by this term with those generated by the more typical even-rank tensorial

Table 7.3. Comparison of the $n = 10$, $\ell = 5, 6, 7, 8$ and 9 energy shifts (MHz) for various powers of $\frac{1}{r}$. Here the proportionality coefficient is taken to be 1.

Radial Dependence	ℓ	Energy Shift (MHz)
$\frac{1}{r^3}$	5	39876.87212000
	6	24101.40622637
	7	15665.91404714
	8	10751.11748333
	9	7695.53672491
$\frac{1}{r^4}$	5	1840.47102092
	6	753.71670381
	7	345.92606584
	8	172.01787973
	9	90.53572618
$\frac{1}{r^5}$	5	100.05735312
	6	27.38796162
	7	8.74266696
	8	3.07174785
	9	1.13169658
$\frac{1}{r^6}$	5	6.14464134
	6	1.10525641
	7	0.24316214
	8	0.05985970
	9	0.01508929
$\frac{1}{r^7}$	5	0.42749565
	6	0.04917661
	7	0.00735501
	8	0.00126020
	9	0.00021556
$\frac{1}{r^8}$	5	0.03447231
	6	0.00243449
	7	0.00024249
	8	0.00002864
	9	0.00000332

Table 7.4. Comparison of computed and measured [9] $n = 10$, $(v^+ = 0, N^+ = 0)$ Rydberg intervals for H_2 and D_2 (all results in MHz).

H_2			
Interval	ΔE^{obs}	ΔE^{theory}	theory-obs
$9I - 9K$	864.563(5)	864.683	0.120
$9K - 9L$	370.696(16)	370.931	0.235
$10I - 10K$	630.795(15)	630.731	-0.064
$10K - 10L$	274.072(20)	274.219	0.147
$10L - 10M$	129.673(20)	129.794	0.121

D_2			
Interval	ΔE^{obs}	ΔE^{theory}	theory-obs
$9I - 9K$	873.27(5)	873.445	0.175
$9K - 9L$	359.58(7)	359.895	0.315
$10I - 10K$	638.01(4)	638.100	0.090
$10K - 10L$	273.07(7)	273.065	-0.005
$10L - 10M$	129.436(14)	129.491	0.055

interaction terms, of second rank (quadrupole and tensor-polarizability) and fourth rank (hexadecapole).

Figure 7.1 displays the pattern of relative energy shifts generated by the operators in our effective long range potential, namely $\langle \vec{N}^+ \cdot \vec{\ell} \rangle_{\mu\mu}$, $\mathcal{P}^{(2)}_{\mu\mu}$, and $\mathcal{P}^{(4)}_{\mu\mu}$, as functions of the total angular momentum N of the system. Here the rotational angular momentum of the ionic core is taken to be $N^+ = 2$ and the orbital momentum of the Rydberg electron is fixed at $\ell = 6$. Each different rank operator expression produces a characteristic pattern of energy level splittings that can be observed experimentally. Specifically, the vector term produces a simple pattern known as the Landé interval rule in spectroscopy [86], with the splitting $E_N - E_{N-1}$ proportional to N. The lowest N state has the most negative shift, assuming the coefficient is positive, and each higher N state rises, which is qualitatively different from the patterns produced by the quadrupole and hexadecapole terms. In the quadrupole case we see a pattern where starting with the $N = 4$ state, which is positive, the next level $N = 5$ moves down just below zero, the next level $N = 6$ moves further down, and then the levels proceed back up to the $N = 7$ state, and finally up to the $N = 8$ state, which is positive. In the hexadecapole case the pattern alternates with four sign changes.

A comparison of the energy shifts produced by the vector interaction and by relativistic retardation is also revealing. Figure 7.2 compares the shifts generated by the vector interaction with the predicted Casimir shifts for the $n = 10$ Rydberg states of $(\nu^+ = 0, N^+ = 1)$ H_2 [19]. Here the molecular core is an anisotropic $(N^+ = 1)$ core and we consider three cases: $\ell = N$, $\ell = N + 1$, and $\ell = N - 1$. When the Rydberg orbital momentum ℓ is the same as the total angular momentum N of the system, or greater by one unit of angular momentum, we see that the vector shifts are negative, while the relativistic shifts are positive. In these two cases, a polarization model that does not include the vector interaction would predict Rydberg energy splittings that are slightly too large compared with experimental observations. When $\ell = N^+ - 1$ both the vector and relativistic shifts are

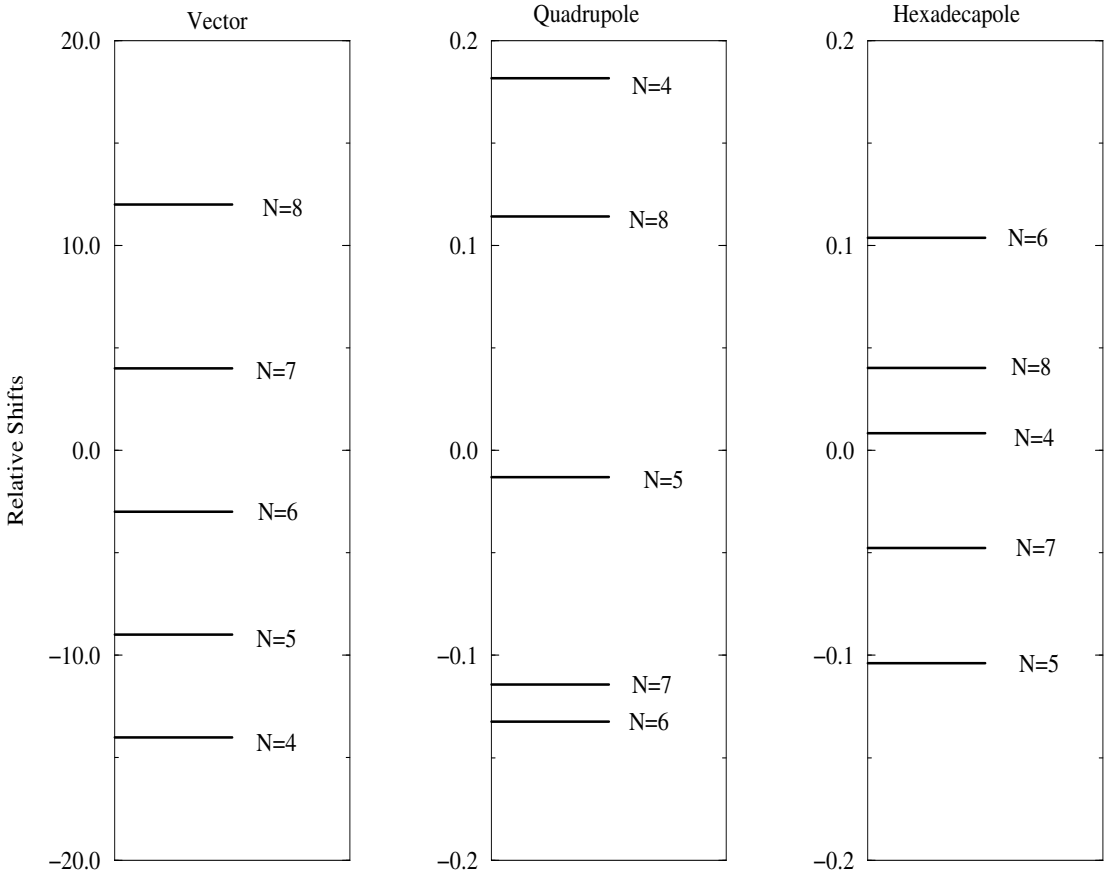

Figure 7.1. Comparison of relative shifts among vector, quadrupole, and hexadecapole operators versus the total angular momentum N. Here $N^+ = 2$ and $L = 6$.

positive, implying that neglect of the vector interaction would generate splittings that are too small.

Figure 7.3 also contrasts the tensorial structure of the vector and Casimir interactions. The N dependence of these two interactions is shown for the $n = 10$, fixed-ℓ Rydberg states of $(\nu^+ = 0, N^+ = 1)$ H_2. The distinct pattern of these energy shifts is similar to the shifts discussed earlier in Figure 7.1. These distinct tensorial patterns should stand out clearly in an experiment.

One additional feature to note is the more rapid decrease in the shifts with increasing ℓ produced by the vector interaction, as compared with those arising from retardation. The origin of this difference lies in their respective radial-dependences, which go as $\frac{1}{r^6}$ and $\frac{1}{r^5}$. Figure 7.4 displays this rapid decrease in the magnitudes of the vector energy shifts most clearly. Shifts due to the vector interaction dominate in the lower ℓ states, while the Casimir shifts dominate in higher ℓ states. Experimentalists aiming for an unambiguous confirmation of relativistic retardation in Rydberg atoms and molecules are advised, based on Figure 7.4, to focus on high $\ell > 6$ states. It would also greatly improve our understanding of the nonrelativistic effects to have measurements of far more energy splittings. The dependences on ℓ and N provide the most detailed information.

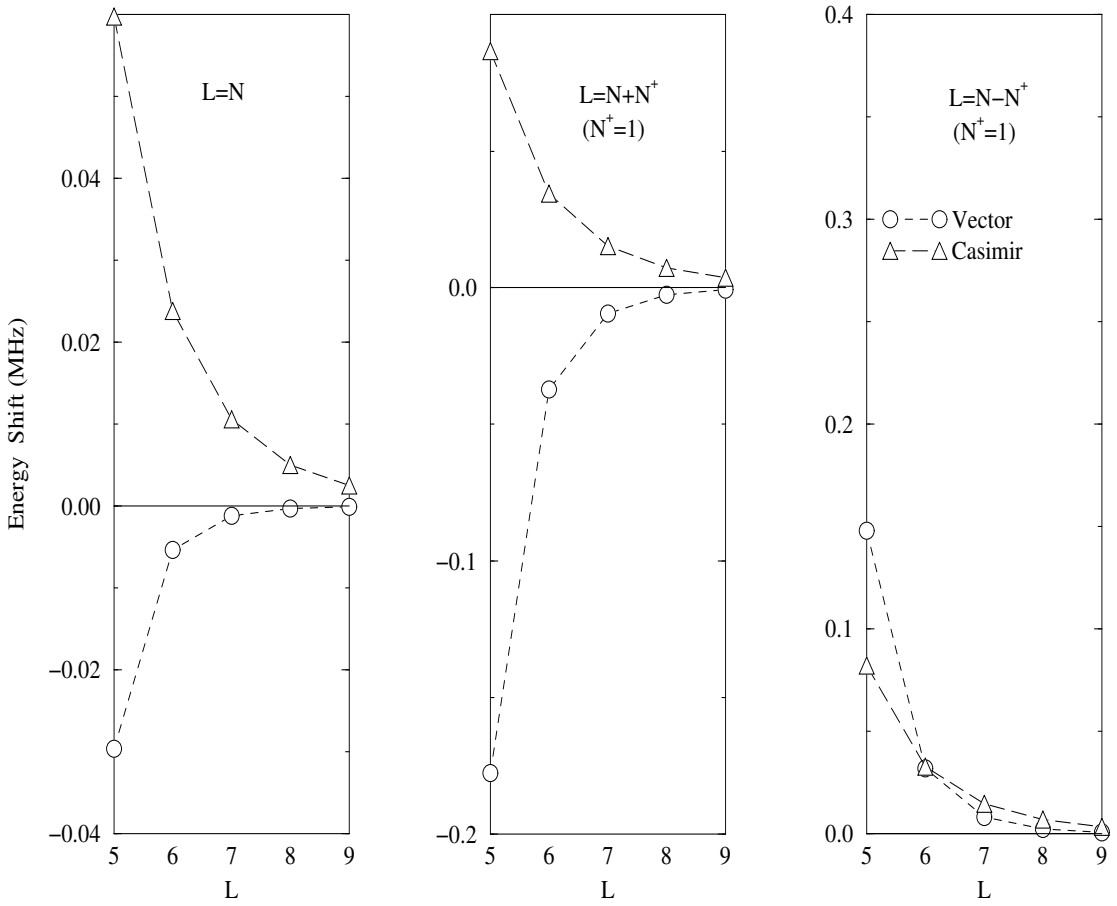

Figure 7.2. Comparison of the vector and Casimir energy shifts [19] in the $n = 10$, ($\nu^+ = 0, N^+ = 1$), $L = N$, $L = N - N^+$, and $L = N + N^+$ states of H_2.

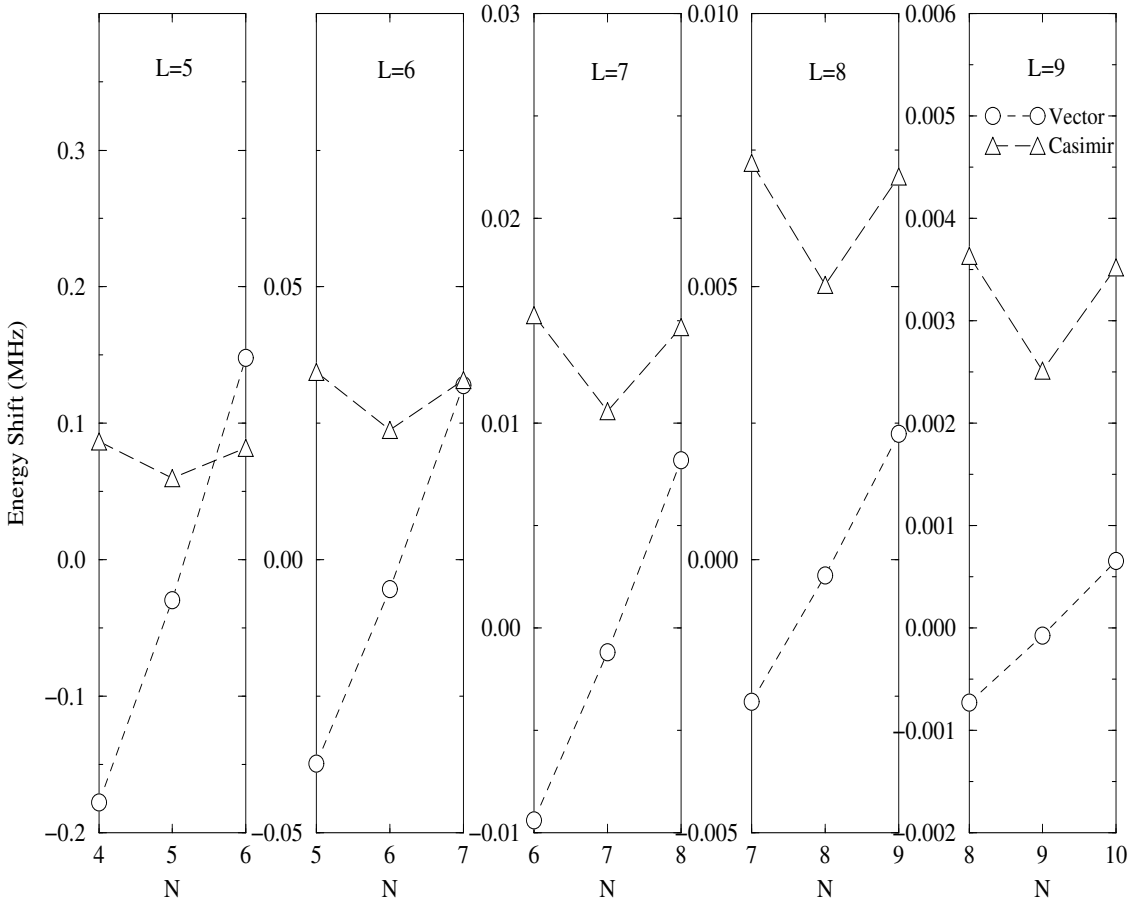

Figure 7.3. Comparison of the vector and Casimir energy shifts [19] in the $n = 10$, ($\nu^+ = 0, N^+ = 1$) states of H_2. Here the splittings for fixed Rydberg orbital momentum L are shown versus the total angular momentum N.

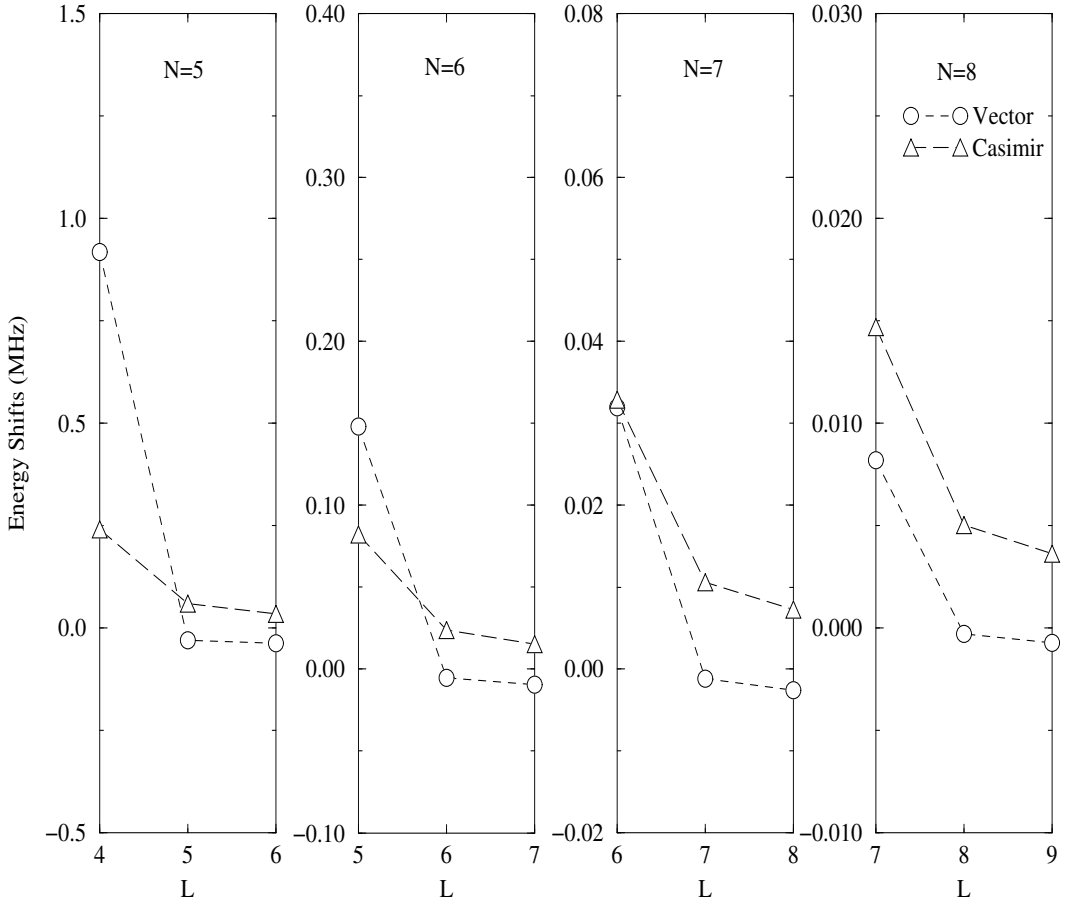

Figure 7.4. Comparison of the vector and Casimir energy shifts [19] in the $n = 10$, ($\nu^+ = 0, N^+ = 1$) states of H_2. Here the splittings for fixed total angular momentum N are shown versus the orbital angular momentum of the Rydberg electron L.

CHAPTER 8

SUMMARY AND REMARKS

In this dissertation, we have developed a new multichannel description of Rydberg state physics that combines the simplicity of long range effective potentials with the multichannel structure of modern scattering theory. At the same time, we have presented systematic adiabatic (and diabatic) derivations of an unusual vector interaction that has intrigued the Rydberg physics community in recent years. Our work demonstrates that the vector interaction describes a coupling among the orbital motion of the Rydberg electron and the internal ionic angular momentum, mediated by the dipole portion of the electron-ion Coulomb force. As the distant Rydberg electron revolves around the core, it tends to "drag" the core polarization vector with it. This drag is hindered by the internal moment of inertia of the ion, and by the moment of inertia of the distant electron (or other charged particle) about the center-of-mass. Stated another way, this interaction reflects the inability of the ionic core to instantaneously adjust to the angular motion of the Rydberg electron.

Our analysis of the $n = 10$ Rydberg states of Ne with orbital angular momenta of $\ell = 5, 6, 7$, and 8 confirmed, for the first time, the existence of an interaction term containing a pseudovector structure. We showed that this pseudovector interaction, in combination with an effective multichannel Hamiltonian, can reproduce observed Rydberg energy intervals in the $n = 10$ range to sub-MHz resolution. Moreover, a χ^2 comparison demonstrated that our description of Rydberg state physics improves on previously-developed perturbative polarization models. *Ab initio* calculations of theoretical values for $\alpha_s, \alpha_t, \beta_v, \cdots$ using multiconfiguration Hartree-Fock atomic wavefunctions confirm that the vector interaction exists and has experimental implications for Rydberg spectra with a distinct pattern of induced

energy splittings.

Our effective Hamiltonian approach was subsequently applied with success in our study of doubly excited, autoionizing $3pnf$ Rydberg states of Mg. The strong coupling among Rydberg states results in an irregular n-dependence of the autoionization rates, which was clearly seen in recent experiments and accurately described by our diabatic Hamiltonian approach. We also investigated variations of the relative orientation of the Rydberg and ionic core angular momenta in a radial adiabatic analysis of Rydberg Mg. The relative orientation of these angular momenta shows dramatic variations in strongly coupled channels, including a "flip", or sign change, in their mutual projection as the Rydberg electron distance from the nucleus changes. We attribute these variations in orientation to the combined effects of anisotropic interactions and the spin-orbit coupling within Mg^+.

Rydberg states of the simple diatomic molecules H_2 and D_2 served as a stringent test of our ability to compute ionic core properties, and to accurately describe Rydberg state physics. The theory and calculations presented are the most extensive, complete adiabatic treatment of H_2^+ and D_2^+ ion properties that has been presented to date. Our calculation of the permanent multipole moments and induced polarizabilities and hyperpolarizabilities for the first rotationally excited state of H_2^+ also provided a novel twist that has helped to elucidate the qualitative meaning of the vector interaction. In addition to being the first calculation of the vector hyperpolarizability for a molecule, the extremely small magnitude of the coefficient, one-thousand times smaller than other induced hyperpolarizabilities of H_2^+, proved to be enlightening. This analysis shows that the vector hyperpolarizability is inversely proportional to the moment of inertia of the diatomic ion. This connection confirms our physical picture of the vector interaction. As the distant Rydberg electron revolves around the core, it tries to "torque" the entire molecular ion. The relatively enormous rotational inertia strongly resists this drag, thereby making the dynamic vector interaction miniscule in Rydberg states of diatomic molecules. When the drag occurs more freely, as in an atomic

ion whose electrons have a very small moment of inertia, the energy associated with the drag shifts Rydberg levels more noticeably.

The $n = 9$ and 10 Rydberg energy intervals with $\ell > 5$ computed for the ground rovibrational states of H_2^+ and D_2^+ reproduce the experimental intervals with an accuracy of 0.3 MHz or better, a significant improvement on earlier calculations based on the "clamped nuclei" approximation. These adiabatic-nuclei calculations are not quite accurate enough yet to extract energy shifts due to relativistic retardation from these experiments. Future work will focus on computing higher order $\frac{1}{r^7}$ and $\frac{1}{r^8}$ hyperpolarization interactions and treating nuclear motion at a nonadiabatic level. An analysis of the energy shifts produced by the vector interaction and relativistic retardation demonstrate that these interactions generate clearly distinct patterns of energy level splittings, whose characteristic tensorial structure should stand out in an experiment. Experimentalists aiming for an unambiguous confirmation of relativistic retardation in Rydberg atoms and molecules should probably focus on high-ℓ Rydberg sates with $\ell > 6$. Moreover, we suggest that future experimental studies attempt to resolve far more energy level splittings, to permit the extraction of yet more information from the ℓ and N dependences of the Rydberg splittings.

BIBLIOGRAPHY

[1] W.E. Lamb and R.C. Retherford, Phys. Rev. **72**, 241 (1947).

[2] W.E. Lamb and R.C. Retherford, Phys. Rev. **79**, 549 (1950).

[3] H. Bethe, Phys. Rev. **72**, 339 (1947).

[4] H. Bethe, L.M. Brown, and J.R. Stehn, Phys. Rev. **77**, 370 (1950).

[5] R.P. Feynman, Rev. Mod. Phys. **20**, 367 (1948); Phys. Rev. **74**, 939, 1430 (1948); Rev. Mod. Phys. **17**, 157 (1945).

[6] J. Schwinger, Phys. Rev. **73**, 416 (1948); Phys. Rev. **74**, 1439 (1948).

[7] S. Tomanaga, Prog. Theoret. Phys. **1**, 27 (1946); Prog. Theoret. Phys. **2**, 101, 198 (1947); Prog. Theoret. Phys. **3**, 1, 101 (1948); Phys. Rev. **74**, 224 (1948).

[8] Wood, C. S., S. C. Bennett, B. P. Masterson, J. L. Roberts, C. E. Tanner, C. E. Wieman, Science **275**, 1759 (1997).

[9] P.L. Jacobson, D.S. Fisher, C.W. Fehrenbach, W.G. Sturrus, and S.R. Lundeen, Phys. Rev. A **56**, R4361 (1997).

[10] R.F. Ward, Jr., W.G. Sturrus, and S.R. Lundeen, Phys. Rev. A **53**, 113 (1996).

[11] W.G. Sturrus, E.A. Hessels, P.W. Arcuni, and S.R. Lundeen, Phys. Rev. A **44**, 3032 (1991).

[12] W.G. Sturrus, E.A. Hessels, P.W. Arcuni, and S.R. Lundeen, Phys. Rev. A **38**, 135 (1988).

[13] W.G. Sturrus, E.A. Hessels, and S.R. Lundeen, Phys. Rev. Lett. **57**, 1863 (1986).

[14] E.A. Hessels, P.W. Arcuni, F.J. Deck, and S.R. Lundeen, Phys. Rev. A **46**, 2622 (1992).

[15] E.A. Hessels, F.J. Deck, P.W. Arcuni, and S.R. Lundeen, Phys. Rev. A **41**, 3663 (1990).

[16] P.W. Arcuni, Z.W. Fu, and S.R. Lundeen, Phys. Rev. A **42**, 6950 (1990).

[17] P.W. Arcuni, E.A. Hessels, and S.R. Lundeen, Phys. Rev. A **41**, 3648 (1990).

[18] L. Spruch, Phys. Today, 37 November (1986).

[19] J.F. Babb and L. Spruch, Phys. Rev. A **50**, 3848 (1994).

[20] A.Dalgarno, G.W.F. Drake, and G.A. Victor, Phys. Rev. **176**,194 (1968).

[21] M.J. Seaton and L. Steenman-Clark, J. Phys. B **10**,2639 (1977).

[22] R.J. Drachman, Phys. Rev. A **26**, 1228 (1982).

[23] W.G Schoenfeld, *Analysis of High-L Rydberg Levels of Silicon from the Solar Spectrum: A Test of the Extended Polarization Model*, PhD. thesis, Univ. of Mass. (1994), unpublished.

[24] Herzberg, G. and Ch. Jungen, J. Chem. Phys. **77**, 5876 (1982).

[25] Jungen, Ch., I. Dabrowski, G. Herzberg, and D. J. W. Kendall, 1989 J. Chem. Phys. **91**, 3926.

[26] Jungen, Ch., I. Dabrowski, G. Herzberg, and M. Vervloet, J. Chem. Phys. **93**, 2289 (1990).

[27] B. Zygelman, Phys. Rev. Lett. **64**, 256 (1990).

[28] R.E. Trees, Phys. Rev. **83** (1951), 756; **84**, 1089 (1951); **85**, 382 (1952).

[29] G. Racah, Phys. Rev. **85**, 381 (1952).

[30] W. Clark, C.H. Greene, and G. Miecznik, Phys. Rev. A **53**, 2248 (1996).

[31] W. Clark and C.H. Greene, Rev. Mod. Phys., (submitted 1998).

[32] B.J. Lyons, J.A. Shanchuck, J. Hostetler, and T.F. Gallagher, Phys. Rev. A **52**, 4586 (1995)

[33] W. Clark and C.H. Greene, Phys. Rev. A **56**, 403 (1997).

[34] W. Clark and C.H. Greene, Phys. Rev. A (in preparation).

[35] L. Pruvost, P. Camus, J.M. Lecomte, C.R. Mahon, and P. Pillet, J. Phys. B **24**, 4723 (1991).

[36] H. Lefebvre-Brion and R.W. Field, *Perturbations in the Spectra of Diatomic Molecules*, Academic Press, New York, 1986.

[37] H. Goldstein, *Classical Mechanics*, Addison-Wesley, Reading, Mass. (1950).

[38] J.D. Jackson, *Classical Electrodynamics*, John Wiley & Sons, New York (1975).

[39] H. Klar and U. Fano, Phys. Rev. Lett. **37**, 1132 (1976).

[40] H. Klar, Phys. Rev. A **15**, 1452 (1977).

[41] V.Aquilanti, S. Cavalli, and M.B. Sevryuk, J. Math. Phys. **35** (2), 536 (1994).

[42] P. M. Morse and H. Feshbach, *Methods of Theoretical Physics* (McGraw-Hill, New York, 1953).

[43] R.N. Zare, *Angular Momentum*. John Wiley & Sons, Inc., New York, 1988.

[44] S. Watanabe and C.H. Greene, Phys. Rev. A **22**, 158 (1980).

[45] Gailitis, M. and R. Damburg, Proc. Phys. Soc. London **82**, 192 (1963).

[46] U. Fano and A.R.P. Rau, *Atomic Collisions and Spectra*. Academic Press, Inc., Orlando, Florida, 1986.

[47] H. Feshbach, Anals of Physics **5**, 357 (1958).

[48] H. Feshbach, Anals of Physics **19**, 287 (1962).

[49] L.S. Rodberg and R.M. Thaler, *Introduction to the Quantum Theory of Scattering*. Academic Press, Inc., New York, 1967.

[50] I. Lindgren and J. Morrison, *Atomic Many-Body Theory*. Springer Verlag, New York, 1982.

[51] D.A. Varshalovich, A.N. Moskalev, and V.K. Khersonskii, *Quantum Theory of Angular Momentum* (World Scientific, Singapore, 1988).

[52] A. Messiah, *Quantum Mechanics Volume II*, John Wiley & Sons, Inc., New York, 1966.

[53] U. Fano and J.H. Macek, Rev. Mod. Phys. **45**, 553 (1973).

[54] R.D. Cowan, *The Theory of Atomic Structure and Spectra*, University of California Press, Berkeley, 1981.

[55] C.H. Greene, *Fundamental Processes of Atomic Dynamics*, Plenum, New York, p105 (1988), C.H. Greene and L. Kim, Phys.Rev.A **38**, 5953 (1988), F. Robicheaux and C. H. Greene, Phys.Rev.A **46**, 3821 (1992)

[56] M. Aymar, C.H. Greene, and E. Luc-Koenig, Rev. Mod. Phys. **68**, 1015-1123 (1996).

[57] L.J. Kovalenko and J.B. Delos, J. Chem. Phys. **107**, 5460 (1997).

[58] L.J. Kovalenko and J.B. Delos, J. Chem. Phys. **107**, 5473 (1997).

[59] A. Hooker, C.H. Greene, and W. Clark, Phys. Rev. A **55**, 4609 (1997).

[60] M.V. Berry, Proc. Roy. Soc. London A **392**, 45 (1984).

[61] F. Wilczek and A. Zee, Phys. Rev. Lett. **52**, 2111 (1984).

[62] J. Moody, A. Shapere, and F. Wilczek, Phys. Rev. Lett. **56**, 893 (1986).

[63] R. Jackiw, Phys. Rev. Lett. **56**, 2779 (1986).

[64] R.G. Littlejohn and S. Weigert, Phys. Rev. A **48**, 924 (1993).

[65] A. Hibbert, M. Le Dourneuf, and Vo Ky Lan, J. Phys. B **10**, 1015 (1977).

[66] D. Sundholm and J. Olsen, Phys. Rev. A **49**, 3453 (1994).

[67] E.S. Chang, W.G. Schoenfeld, E. Biemont, P. Quinet, and P. Palmeri, Physica Scripta **49**, 26 (1994).

[68] C.Froese Fischer, Comp.Phys.Comm. **64**, 369 (1991)

[69] C.E. Moore, *Atomic Energy Levels*, Natl. Stand. Ref. Data. Ser., Nat. Bur. Stand. (U.S.), 35/Volume I, (1971).

[70] C.H. Greene and M. Aymar, Phys. Rev. A **44**, 1773 (1991).

[71] M. Aymar, private communication (1996).

[72] T.F. Gallagher, *Rydberg Atoms*. Cambridge University Press, New York, New York, 1994.

[73] W.C. Martin, and R. Zalubas, J. Phys. Chem. Ref. Data **9**, 4 (1980).

[74] C.E. Moore, *Atomic Energy Levels*, NBS Circular No. 467 (U.S. GPO, Washington, D.C., 1949), Vol. 3.

[75] M.D. Lindsay, C.-J. Dai, L.-T. Cai, T. F. Gallagher, F. Robicheaux, and C. H. Greene Phys. Rev. A **46**, 3789 (1992).

[76] R.T. Pack and J.O. Hirschfelder, J. Chem. Phys. **49**, 4009 (1968).

[77] B. R. Judd *Angular Momentum Theory for Diatomic Molecules*, Academic Press, Inc., New York, 1975.

[78] A. Carrington and R.A. Kennedy, *Gas Phase Ion Chemistry Vol. 3 Ions and Light*, Academic Press, Inc., London (1984).

[79] A. Carrington, I.R. McNAb, and C.A. Montgomerie, J. Phys. B **22**, 3551 (1989).

[80] G. Hunter, B.F. Gray, and H.O. Pritchard, J. Chem. Phys. **45**, 3806 (1966).

[81] G. Hunter and H.O. Pritchard, J. Chem. Phys. **46**, 2146 (1966).

[82] G. Hunter and H.O. Pritchard, J. Chem. Phys. **46**, 2153 (1967).

[83] P.B. Davies, M.A. Guest, and R.J. Stickland, J. Chem. Phys. **93**, 5408 (1990).

[84] P.B. Davies, M.A. Guest, and R.J. Stickland, J. Chem. Phys. **93**, 5417 (1990).

[85] D.M. Bishop and B. Lam, Mol. Phys. **65**, 679 (1988).

[86] I.I. Sobelḿan, *Introduction to the Theory of Atomic Spectra*, Pergamon Press, New York, 1972.

[87] F. Friedrich, *Theoretical Atomic Physics*, Springer-Verlag, New York, 1990.

[88] H.A. Bethe and E.E. Salpeter, *Quantum Mechanics of One- and Two-Electron Atoms*, Academic Press, New York, 1957.

[89] R.J. Drachman, Phys. Rev. A **33**, 2780 (1986).

[90] R.J. Drachman, Phys. Rev. A **37**, 979 (1988).

[91] D.M. Bishop and Lap. M. Cheung, Phys. Rev. A **16**, 640 (1977).

[92] D.M. Bishop and R.W. Wetmore, Mol. Phys. **26**, 145 (1973).

[93] R.E. Moss, Chem. Phys. Lett. **172**, 458 (1990).

[94] W. Kolos and L. Wolniewicz, Rev. Mod. Phys. **35**, 473 (1963).

[95] W. Kolos and L. Wolniewicz, J. Chem. Phys. **41**, 3663 (1964).

[96] W. Kolos and L. Wolniewicz, J. Chem. Phys. **49**, 404 (1968).

[97] L. Wolniewicz and J.D. Poll, J. Chem. Phys. **73**, 6225 (1980).

[98] D.M. Bishop and L.M. Cheung, J. Phys. B **11**, 31333 (1978).

[99] D.M. Bishop and Lap. M. Cheung, J. Phys. B **12**, 3135 (1979).

[100] D.M. Bishop, L.M. Cheung, and A.D. Buckingham, Mol. Phys. **41**, 1225 (1980).

[101] D.M. Bishop and B Lam, Chem. Phys. Lett. **134**, 283 (1987).

[102] D.M. Bishop, Phys. Rev. Lett. **62**, 3008 (1989).

[103] J. Shertzer and J. DeGuzman, (in preparation).

[104] W.G. Sturrus, P.L. Jacobson, and S.R. Lundeen, (in preparation).

[105] R.P. McEachran, C.J. Veenstra, and M. Cohen, Chem. Phys. Lett. **59**, 275 (1978).

[106] E.S. Chang, S. Pulchtopek, and E.E. Eyler, J. Chem. Phys. **80**, 601 (1984).

[107] D.M. Bishop, B. Kirtman, B. Champagne, J. Chem. Phys. **107**, 5780 (1997).

[108] R.J. Drachman, Phys. Rev. A **31**, 1253 (1985).

[109] M. Brieger, Chem. Phys. **89**, 275 (1989).

[110] C.W. Clark and K.T. Taylor, J. Phys. B **15**, 1175 (1982).

[111] G.B. Arfken and H.J. Weber, *Mathematical Methods For Physicists, Forth Edition*, Academic Press, New York, 1995.

[112] M.L. Boas, *Mathematical Methods In The Physical Sciences, Second Edition*, John Wiley & Sons, New York, 1983.

[113] J. Mathews and R.L. Walker, *Mathematical Methods of Physics*, Addison-Wesley Publishing Company, Inc., New York, 1970.

APPENDIX A

PARAMETERS FOR HIGH-ℓ RYDBERG STATES OF LOW-Z ATOMS

Here we give explicit expressions for all radial parameters used in Eqs.(6.1) and (6.2). The constant versions of these radial parameters, those used in Eqs.(4.40) and (4.41), are obtained by taking the limit $r \to \infty$, or by replacing $r_>$ with the radial coordinate r of the Rydberg electron. The summations over i and j in each expression refer to summations over all core electrons. $r_< = min\{r_i, r\}$ and $r_> = max\{r_i, r\}$, where r refers to the Rydberg electron. The summations over γ_ν denote summations over all bound, and integrals over all continuum states of the core that are not degenerate with E_{μ_0}.

The net Coulomb charge seen by the Rydberg electron as a function of the radial distance is

$$C_c(r) = r\langle \gamma_c L_c \parallel \sum_{i=1}^{N_c} \frac{1}{r_>} C^{(0)}(\hat{r}_i) \parallel \gamma_c L_c \rangle - Z. \tag{A.1}$$

The quadrupole moment of the ionic core is

$$Q(r) = -r^3 \begin{pmatrix} L_c & 2 & L_c \\ -L_c & 0 & L_c \end{pmatrix} \langle \gamma_c L_c \parallel \sum_{i=1}^{N_c} \frac{r_<^2}{r_>^3} C^{(2)}(\hat{r}_i) \parallel \gamma_c L_c \rangle. \tag{A.2}$$

The scalar dipole polarizability of the ionic core is

$$\alpha_s(r) = \frac{-2}{3(2L_c+1)} r^4 \sum_{\gamma_\nu, L_\nu} \frac{(-1)^{L_c+L_\nu}}{E_{\mu_0} - E_\nu} \langle \gamma_c L_c \parallel \sum_{i=1}^{N_c} \frac{r_<}{r_>^2} C^{(1)}(\hat{r}_i) \parallel \gamma_\nu L_\nu \rangle$$

$$\langle \gamma_\nu L_\nu \parallel \sum_{j=1}^{N_c} \frac{r_<}{r_>^2} C^{(1)}(\hat{r}_j) \parallel \gamma_c L_c \rangle. \tag{A.3}$$

The second-rank tensor dipole polarizability of the ionic core is

$$\alpha_t(r) = -2\sqrt{\frac{10}{3}}r^4 \begin{pmatrix} L_c & 2 & L_c \\ -L_c & 0 & L_c \end{pmatrix} \sum_{\gamma_\nu, L_\nu} \frac{1}{E_{\mu_0} - E_\nu} \begin{Bmatrix} 2 & L_c & L_c \\ L_\nu & 1 & 1 \end{Bmatrix}$$

$$\langle \gamma_c L_c \parallel \sum_{i=1}^{N_c} \frac{r_<}{r_>^2} C^{(1)}(\hat{r}_i) \parallel \gamma_\nu L_\nu \rangle \langle \gamma_\nu L_\nu \parallel \sum_{j=1}^{N_c} \frac{r_<}{r_>^2} C^{(1)}(\hat{r}_j) \parallel \gamma_c L_c \rangle. \tag{A.4}$$

The scalar hyperpolarizability is

$$\eta_s(r) = \frac{-1}{5(2L_c+1)} \left[\bar{\eta}_s^I(r) + \bar{\eta}_s^{II}(r) \right], \tag{A.5}$$

where

$$\eta_s^I(r) = r^6 \sum_{\gamma_\nu, L_\nu} \frac{(-1)^{L_c+L_\nu}}{E_{\mu_0} - E_\nu} \langle \gamma_c L_c \parallel \sum_{i=1}^{N_c} \frac{r_<^2}{r_>^3} C^{(2)}(\hat{r}_i) \parallel \gamma_\nu L_\nu \rangle$$

$$\langle \gamma_\nu L_\nu \parallel \sum_{j=1}^{N_c} \frac{r_<^2}{r_>^3} C^{(2)}(\hat{r}_j) \parallel \gamma_c L_c \rangle, \tag{A.6}$$

and

$$\eta_s^{II}(r) = -\frac{5}{6} r^6 \sum_{\gamma_\nu, L_\nu} \frac{(-1)^{L_c+L_\nu}}{(E_{\mu_0} - E_\nu)^2} \langle \gamma_c L_c \parallel \sum_{i=1}^{N_c} \frac{r_<}{r_>^2} C^{(1)}(\hat{r}_i) \parallel \gamma_\nu L_\nu \rangle$$

$$\langle \gamma_\nu L_\nu \parallel \sum_{j=1}^{N_c} \left(\frac{d^2}{dr^2} \frac{r_<}{r_>^2} \right) C^{(1)}(\hat{r}_j) \parallel \gamma_c L_c \rangle. \tag{A.7}$$

The tensor hyperpolarizability is

$$\eta_t(r) = \begin{pmatrix} L_c & 2 & L_c \\ -L_c & 0 & L_c \end{pmatrix} \left[\bar{\eta}_t^I(r) + \bar{\eta}_t^{II}(r) + \bar{\eta}_t^{III} \right], \tag{A.8}$$

where

$$\eta_t^I(r) = \sqrt{\frac{10}{7}} r^6 \sum_{\gamma_\nu, L_\nu} \frac{1}{E_{\mu_0} - E_\nu} \begin{Bmatrix} 2 & L_c & L_c \\ L_\nu & 2 & 2 \end{Bmatrix} \langle \gamma_c L_c \parallel \sum_{i=1}^{N_c} \frac{r_<^2}{r_>^3} C^{(2)}(\hat{r}_i) \parallel \gamma_\nu L_\nu \rangle$$

$$\langle \gamma_\nu L_\nu \parallel \sum_{j=1}^{N_c} \frac{r_<^2}{r_>^3} C^{(2)}(\hat{r}_j) \parallel \gamma_c L_c \rangle, \tag{A.9}$$

$$\eta_t^{II}(r) = 2\sqrt{\frac{15}{7}} r^6 \sum_{\gamma_\nu, L_\nu} \frac{1}{E_{\mu_0} - E_\nu} \begin{Bmatrix} 2 & L_c & L_c \\ L_\nu & 1 & 3 \end{Bmatrix} \langle \gamma_c L_c \parallel \sum_{i=1}^{N_c} \frac{r_<}{r_>^2} C^{(1)}(\hat{r}_i) \parallel \gamma_\nu L_\nu \rangle$$

$$\langle \gamma_\nu L_\nu \parallel \sum_{j=1}^{N_c} \frac{r_<^3}{r_>^4} C^{(3)}(\hat{r}_j) \parallel \gamma_c L_c \rangle, \tag{A.10}$$

and

$$\eta_t^{III}(r) = \sqrt{\frac{5}{6}} r^6 \sum_{\gamma_\nu, L_\nu} \frac{1}{(E_{\mu_0} - E_\nu)^2} \begin{Bmatrix} 2 & L_c & L_c \\ L_\nu & 1 & 1 \end{Bmatrix} \langle \gamma_c L_c \parallel \sum_{i=1}^{N_c} \frac{r_<}{r_>^2} C^{(1)}(\hat{r}_i) \parallel \gamma_\nu L_\nu \rangle$$

$$\langle \gamma_\nu L_\nu \parallel \sum_{j=1}^{N_c} \left(\frac{d^2}{dr^2} \frac{r_<}{r_>^2} \right) C^{(1)}(\hat{r}_j) \parallel \gamma_c L_c \rangle. \tag{A.11}$$

The scalar nonadiabatic dipole polarizability is

$$\beta_s(r) = \frac{r^4}{6(2L_c+1)} \sum_{\gamma_\nu, L_\nu} \frac{(-1)^{L_c+L_\nu}}{(E_{\mu_0} - E_\nu)^2} \langle \gamma_c L_c \parallel \sum_{i=1}^{N_c} \frac{r_<}{r_>^2} C^{(1)}(\hat{r}_i) \parallel \gamma_\nu L_\nu \rangle$$

$$\langle \gamma_\nu L_\nu \parallel \sum_{j=1}^{N_c} \frac{r_<}{r_>^2} C^{(1)}(\hat{r}_j) \parallel \gamma_c L_c \rangle. \tag{A.12}$$

The tensor nonadiabatic dipole polarizability is

$$\beta_t(r) = \sqrt{\frac{5}{6}} r^4 \begin{pmatrix} L_c & 2 & L_c \\ -L_c & 0 & L_c \end{pmatrix} \sum_{\gamma_\nu, L_\nu} \frac{1}{(E_{\mu_0} - E_\nu)^2} \begin{Bmatrix} 2 & L_c & L_c \\ L_\nu & 1 & 1 \end{Bmatrix}$$

$$\langle \gamma_c L_c \parallel \sum_{i=1}^{N_c} \frac{r_<}{r_>^2} C^{(1)}(\hat{r}_i) \parallel \gamma_\nu L_\nu \rangle \langle \gamma_\nu L_\nu \parallel \sum_{j=1}^{N_c} \frac{r_<}{r_>^2} C^{(1)}(\hat{r}_j) \parallel \gamma_c L_c \rangle. \tag{A.13}$$

The vector dipole hyperpolarizability is

$$\begin{aligned} \beta_v(r) \quad &= \sqrt{\frac{3}{2}} \frac{r^4}{\sqrt{L_c(L_c+1)(2L_c+1)}} \sum_{\gamma_\nu, L_\nu} \frac{1}{(E_{\mu_0} - E_\nu)^2} \begin{Bmatrix} 1 & L_c & L_c \\ L_\nu & 1 & 1 \end{Bmatrix} \\ & \langle \gamma_c L_c \parallel \sum_{i=1}^{N_c} \frac{r_<}{r_>^2} C^{(1)}(\hat{r}_i) \parallel \gamma_\nu L_\nu \rangle \langle \gamma_\nu L_\nu \parallel \sum_{j=1}^{N_c} \frac{r_<}{r_>^2} C^{(1)}(\hat{r}_j) \parallel \gamma_c L_c \rangle. \end{aligned} \tag{A.14}$$

The angular factors are given by

$$\begin{aligned} \mathcal{A}^{(2)}_{\mu\mu'} \quad &= [(2\ell+1)(2\ell'+1)(2J_c+1)(2J_c'+1)]^{\frac{1}{2}} \\ & (-1)^{J_c'+L_c+S_c} \begin{pmatrix} \ell' & \ell & 2 \\ 0 & 0 & 0 \end{pmatrix} \Big/ \begin{pmatrix} L_c & 2 & L_c \\ -L_c & 0 & L_c \end{pmatrix} \\ & (-1)^{J_c'+K} \begin{Bmatrix} J_c & \ell & K \\ \ell' & J_c' & 2 \end{Bmatrix} \begin{Bmatrix} 2 & L_c & L_c \\ S_c & J_c & J_c' \end{Bmatrix}, \end{aligned} \tag{A.15}$$

and

$$\mathcal{B}^{(0)}_{\mu\mu'} = (\ell(\ell+1)+2)\,\delta_{\mu\mu'}. \tag{A.16}$$

and, finally,

$$\begin{aligned} \mathcal{B}^{(2)}_{\mu\mu'} \quad &= \mathcal{A}^{(2)}_{\mu\mu'} (-1)^{\ell+\ell'} \Big/ \left[\begin{pmatrix} 1 & 1 & 2 \\ 0 & 0 & 0 \end{pmatrix} \begin{pmatrix} \ell' & \ell & 2 \\ 0 & 0 & 0 \end{pmatrix} \right] \\ & \sum_{\ell_\nu} (-1)^{\ell_\nu} \ell_\nu (\ell_\nu+1)(2\ell_\nu+1) \begin{pmatrix} \ell & 1 & \ell_\nu \\ 0 & 0 & 0 \end{pmatrix} \begin{pmatrix} \ell_\nu & 1 & \ell' \\ 0 & 0 & 0 \end{pmatrix} \begin{Bmatrix} 1 & 1 & 2 \\ \ell' & \ell & \ell_\nu \end{Bmatrix} \end{aligned} \tag{A.17}$$

APPENDIX B

CHANNEL PARAMETERS FOR RYDBERG STATES OF H_2 AND D_2

In this appendix we give explicit expressions for all permanent multipole moments and induced polarizabilities and hyperpolarizabilities used in Eqs.(7.18) and (7.19). The summations over ν denote summations over all bound and continuum states Ψ_ν of the molecular ions that are not degenerate with E_{μ_0}. These expressions are formulated specifically for molecular ion wavefunctions computed using the adiabatic nuclei approximation.

The k-th permanent multipole moment of the molecular ion is

$$Q^{(k)}_{mu\mu'} = \langle \Psi_\mu \mid \left(M_k R^k - N_k r_e C^{(k)}_0(\hat{r}_e) \right) \mid \Psi_{\mu'} \rangle \tag{B.1}$$

where the nuclear mass term M_k and the electronic mass term N_k are defined in Chapter 7. The scalar dipole polarizability of the molecular ion is

$$\alpha_{s_{\mu\mu}} = -\frac{2}{3} N_1^2 \sum_\nu \frac{(2N_\nu^+ + 1)}{E_{\mu_0} - E_\nu} \begin{pmatrix} N^+ & 1 & N_\nu^+ \\ 0 & -\lambda_\nu & \lambda_\nu \end{pmatrix}^2 \mid \langle \Psi_\mu \mid r_e C^{(1)}_{-\lambda_\nu}(\hat{r}_e) \mid \Psi_\nu \rangle \mid^2 . \tag{B.2}$$

The second-rank tensor dipole polarizability of the molecular ion is

$$\begin{aligned} \alpha_{t_{\mu\mu'}} &= -10\sqrt{\frac{2}{15}} N_1^2 \Bigg/ \begin{pmatrix} N^+ & 2 & N^{+\prime} \\ 0 & 0 & 0 \end{pmatrix} \\ &\sum_\nu (-1)^{N_\nu^+} \frac{(2N_\nu^+ + 1)}{E_{\mu_0} - E_\nu} \begin{pmatrix} N^+ & 1 & N_\nu^+ \\ 0 & -\lambda_\nu & \lambda_\nu \end{pmatrix} \begin{pmatrix} N_\nu^+ & 1 & N^{+\prime} \\ -\lambda_\nu & \lambda_\nu & 0 \end{pmatrix} \\ &\begin{Bmatrix} 1 & 1 & 2 \\ N^{+\prime} & N^+ & N_\nu^+ \end{Bmatrix} \langle \Psi_\mu \mid r_e C^{(1)}_{-\lambda_\nu}(\hat{r}_e) \mid \Psi_\nu \rangle \langle \Psi_\nu \mid r_e C^{(1)}_{-\lambda_\nu}(\hat{r}_e) \mid \Psi_{\mu'} \rangle^* \end{aligned}$$

(B.3)

The scalar hyperpolarizability is

$$\eta_{s_{\mu\mu}} = -\frac{N_2^2}{5}\sum_{\nu}\frac{(2N_\nu^+ + 1)}{E_{\mu_0} - E_\nu}\begin{pmatrix} N^+ & 2 & N_\nu^+ \\ 0 & -\lambda_\nu & \lambda_\nu \end{pmatrix}^2 \mid \langle \Psi_\mu \mid r_e^2 C^{(2)}_{-\lambda_\nu}(\hat{r}_e) \mid \Psi_\nu \rangle \mid^2$$

$$+N_1^2\sum_{\nu}\frac{(2N_\nu^+ + 1)}{(E_{\mu_0} - E_\nu)^2}\begin{pmatrix} N^+ & 1 & N_\nu^+ \\ 0 & -\lambda_\nu & \lambda_\nu \end{pmatrix}^2 \mid \langle \Psi_\mu \mid r_e C^{(1)}_{-\lambda_\nu}(\hat{r}_e) \mid \Psi_\nu \rangle \mid^2 \qquad \text{(B.4)}$$

The second-rank tensor hyperpolarizability is

$$\eta_{t_{\mu\mu'}} = 5\sqrt{\frac{2}{35}}N_2^2 \Bigg/ \begin{pmatrix} N^+ & 2 & N^{+\prime} \\ 0 & 0 & 0 \end{pmatrix}$$

$$\sum_{\nu}(-1)^{N_\nu^+}\frac{(2N_\nu^+ + 1)}{E_{\mu_0} - E_\nu}\begin{pmatrix} N^+ & 2 & N_\nu^+ \\ 0 & -\lambda_\nu & \lambda_\nu \end{pmatrix}\begin{pmatrix} N_\nu^+ & 2 & N^{+\prime} \\ -\lambda_\nu & \lambda_\nu & 0 \end{pmatrix}$$

$$\begin{Bmatrix} 2 & 2 & 2 \\ N^{+\prime} & N^+ & N_\nu^+ \end{Bmatrix}\langle \Psi_\mu \mid r_e^2 C^{(2)}_{-\lambda_\nu}(\hat{r}_e) \mid \Psi_\nu \rangle\langle \Psi_\nu \mid r_e^2 C^{(2)}_{-\lambda_\nu}(\hat{r}_e) \mid \Psi_{\mu'} \rangle^*$$

$$+5\sqrt{\frac{3}{35}}N_1 N_3 \Bigg/ \begin{pmatrix} N^+ & 2 & N^{+\prime} \\ 0 & 0 & 0 \end{pmatrix}$$

$$\sum_{\nu}(-1)^{N_\nu^+}\frac{(2N_\nu^+ + 1)}{E_{\mu_0} - E_\nu}\begin{pmatrix} N^+ & 1 & N_\nu^+ \\ 0 & -\lambda_\nu & \lambda_\nu \end{pmatrix}\begin{pmatrix} N_\nu^+ & 3 & N^{+\prime} \\ -\lambda_\nu & \lambda_\nu & 0 \end{pmatrix}$$

$$\begin{Bmatrix} 1 & 3 & 2 \\ N^{+\prime} & N^+ & N_\nu^+ \end{Bmatrix}\langle \Psi_\mu \mid r_e C^{(1)}_{-\lambda_\nu}(\hat{r}_e) \mid \Psi_\nu \rangle\langle \Psi_\nu \mid r_e^3 C^{(3)}_{-\lambda_\nu}(\hat{r}_e) \mid \Psi_{\mu'} \rangle^*$$

$$+5\sqrt{\frac{3}{35}}N_3N_1 \Bigg/ \begin{pmatrix} N^+ & 2 & N^{+\prime} \\ 0 & 0 & 0 \end{pmatrix}$$

$$\sum_\nu (-1)^{N_\nu^+} \frac{(2N_\nu^+ + 1)}{E_{\mu_0} - E_\nu} \begin{pmatrix} N^+ & 3 & N_\nu^+ \\ 0 & -\lambda_\nu & \lambda_\nu \end{pmatrix} \begin{pmatrix} N_\nu^+ & 1 & N^{+\prime} \\ -\lambda_\nu & \lambda_\nu & 0 \end{pmatrix}$$

$$\begin{Bmatrix} 3 & 1 & 2 \\ N^{+\prime} & N^+ & N_\nu^+ \end{Bmatrix} \langle \Psi_\mu \mid r_e^3 C_{-\lambda_\nu}^{(3)}(\hat{r}_e) \mid \Psi_\nu \rangle \langle \Psi_\nu \mid r_e C_{-\lambda_\nu}^{(1)}(\hat{r}_e) \mid \Psi_{\mu'} \rangle^*$$

$$-15\sqrt{\frac{2}{15}}N_1^2 \Bigg/ \begin{pmatrix} N^+ & 2 & N^{+\prime} \\ 0 & 0 & 0 \end{pmatrix}$$

$$\sum_\nu (-1)^{N_\nu^+} \frac{(2N_\nu^+ + 1)}{(E_{\mu_0} - E_\nu)^2} \begin{pmatrix} N^+ & 1 & N_\nu^+ \\ 0 & -\lambda_\nu & \lambda_\nu \end{pmatrix} \begin{pmatrix} N_\nu^+ & 1 & N^{+\prime} \\ -\lambda_\nu & \lambda_\nu & 0 \end{pmatrix}$$

$$\begin{Bmatrix} 1 & 1 & 2 \\ N^{+\prime} & N^+ & N_\nu^+ \end{Bmatrix} \langle \Psi_\mu \mid r_e C_{-\lambda_\nu}^{(1)}(\hat{r}_e) \mid \Psi_\nu \rangle \langle \Psi_\nu \mid r_e C_{-\lambda_\nu}^{(1)}(\hat{r}_e) \mid \Psi_{\mu'} \rangle^* \tag{B.5}$$

The fourth-rank tensor hyperpolarizability is

$$\lambda_{h_{\mu\mu'}} = -9\sqrt{\frac{2}{35}}N_2^2 \Bigg/ \begin{pmatrix} N^+ & 4 & N^{+\prime} \\ 0 & 0 & 0 \end{pmatrix}$$

$$\sum_\nu (-1)^{N_\nu^+} \frac{(2N_\nu^+ + 1)}{E_{\mu_0} - E_\nu} \begin{pmatrix} N^+ & 2 & N_\nu^+ \\ 0 & -\lambda_\nu & \lambda_\nu \end{pmatrix} \begin{pmatrix} N_\nu^+ & 2 & N^{+\prime} \\ -\lambda_\nu & \lambda_\nu & 0 \end{pmatrix}$$

$$\begin{Bmatrix} 2 & 2 & 4 \\ N^{+\prime} & N^+ & N_\nu^+ \end{Bmatrix} \langle \Psi_\mu \mid r_e^2 C_{-\lambda_\nu}^{(2)}(\hat{r}_e) \mid \Psi_\nu \rangle \langle \Psi_\nu \mid r_e^2 C_{-\lambda_\nu}^{(2)}(\hat{r}_e) \mid \Psi_{\mu'} \rangle^*$$

$$-\frac{6}{\sqrt{7}}N_1N_3\left/\begin{pmatrix} N^+ & 4 & N^{+\prime} \\ 0 & 0 & 0 \end{pmatrix}\right.$$

$$\sum_\nu(-1)^{N_\nu^+}\frac{(2N_\nu^+ +1)}{E_{\mu_0}-E_\nu}\begin{pmatrix} N^+ & 1 & N_\nu^+ \\ 0 & -\lambda_\nu & \lambda_\nu \end{pmatrix}\begin{pmatrix} N_\nu^+ & 3 & N^{+\prime} \\ -\lambda_\nu & \lambda_\nu & 0 \end{pmatrix}$$

$$\begin{Bmatrix} 1 & 3 & 4 \\ N^{+\prime} & N^+ & N_\nu^+ \end{Bmatrix}\langle\Psi_\mu \mid r_eC^{(1)}_{-\lambda_\nu}(\hat{r}_e)\mid\Psi_\nu\rangle\langle\Psi_\nu\mid r_e^3C^{(3)}_{-\lambda_\nu}(\hat{r}_e)\mid\Psi_{\mu'}\rangle^*$$

$$-\frac{6}{\sqrt{7}}N_3N_1\left/\begin{pmatrix} N^+ & 4 & N^{+\prime} \\ 0 & 0 & 0 \end{pmatrix}\right.$$

$$\sum_\nu(-1)^{N_\nu^+}\frac{(2N_\nu^+ +1)}{E_{\mu_0}-E_\nu}\begin{pmatrix} N^+ & 3 & N_\nu^+ \\ 0 & -\lambda_\nu & \lambda_\nu \end{pmatrix}\begin{pmatrix} N_\nu^+ & 1 & N^{+\prime} \\ -\lambda_\nu & \lambda_\nu & 0 \end{pmatrix}$$

$$\begin{Bmatrix} 3 & 1 & 4 \\ N^{+\prime} & N^+ & N_\nu^+ \end{Bmatrix}\langle\Psi_\mu \mid r_e^3C^{(3)}_{-\lambda_\nu}(\hat{r}_e)\mid\Psi_\nu\rangle\langle\Psi_\nu\mid r_eC^{(1)}_{-\lambda_\nu}(\hat{r}_e)\mid\Psi_{\mu'}\rangle^* \tag{B.6}$$

The scalar nonadiabatic dipole polarizability is

$$\beta_{s_{\mu\bar{\mu}}}\frac{N_1^2}{6}\sum_\nu\frac{(2N_\nu^+ +1)}{(E_{\mu_0}-E_\nu)^2}\begin{pmatrix} N^+ & 1 & N_\nu^+ \\ 0 & -\lambda_\nu & \lambda_\nu \end{pmatrix}^2\mid\langle\Psi_\mu\mid r_eC^{(1)}_{-\lambda_\nu}(\hat{r}_e)\mid\Psi_\nu\rangle\mid^2. \tag{B.7}$$

The second-rank nonadiabatic dipole polarizability is

$$\beta_{t_{\mu\mu'}} = -\sqrt{\frac{5}{3}}N_1^2\left/\begin{pmatrix} N^+ & 2 & N^{+\prime} \\ 0 & 0 & 0 \end{pmatrix}\right.$$

$$\sum_{\nu}(-1)^{N_\nu^+}\frac{(2N_\nu^+ + 1)}{(E_{\mu_0} - E_\nu)^2}\begin{pmatrix} N^+ & 1 & N_\nu^+ \\ 0 & -\lambda_\nu & \lambda_\nu \end{pmatrix}\begin{pmatrix} N_\nu^+ & 1 & N^{+\prime} \\ -\lambda_\nu & \lambda_\nu & 0 \end{pmatrix}$$

$$\begin{Bmatrix} 1 & 1 & 2 \\ N^{+\prime} & N^+ & N_\nu^+ \end{Bmatrix}\langle\Psi_\mu \mid r_e C^{(1)}_{-\lambda_\nu}(\hat{r}_e) \mid \Psi_\nu\rangle\langle\Psi_\nu \mid r_e C^{(1)}_{-\lambda_\nu}(\hat{r}_e) \mid \Psi_{\mu'}\rangle^*. \tag{B.8}$$

The vector hyperpolarizability of the molecular ion is

$$\beta_{v_{\mu\mu}} = (-1)^{N^+} N_1^2\sqrt{\frac{3}{2}}\left[\frac{(2N^+ + 1)}{N^+(N^+ + 1)}\right]^{\frac{1}{2}}$$

$$\sum_{\nu}(-1)^{N_\nu^+}\frac{(2N_\nu^+ + 1)}{(E_{\mu_0} - E_\nu)^2}\begin{pmatrix} N^+ & 1 & N_\nu^+ \\ 0 & -\lambda_\nu & \lambda_\nu \end{pmatrix}\begin{pmatrix} N_\nu^+ & 1 & N^+ \\ -\lambda_\nu & \lambda_\nu & 0 \end{pmatrix}$$

$$\begin{Bmatrix} 1 & 1 & 1 \\ N^+ & N^+ & N_\nu^+ \end{Bmatrix}\langle\Psi_\mu \mid r_e C^{(1)}_{-\lambda_\nu}(\hat{r}_e) \mid \Psi_\nu\rangle\langle\Psi_\nu \mid r_e C^{(1)}_{-\lambda_\nu}(\hat{r}_e) \mid \Psi_\mu\rangle^* \tag{B.9}$$

The angular coupling factors are

$$\mathcal{P}^k_{\mu\mu'} = \langle(N^+\ell)NM_N \mid C^{(k)}(\hat{R})\cdot C^{(k)}(\hat{r}) \mid (N^{+\prime}\ell')N'M_{N'}\rangle$$

$$= \delta_{NN'}\delta_{M_N M'_N}(-1)^{N^+ + N^{+\prime} N}\left[(2N^+ + 1)(2N^{+\prime} + 1)(2\ell + 1)(2\ell' + 1)\right]^{\frac{1}{2}}$$

$$\begin{pmatrix} N^+ & k & N^{+\prime} \\ 0 & 0 & 0 \end{pmatrix}\begin{pmatrix} \ell & k & \ell' \\ 0 & 0 & 0 \end{pmatrix}\begin{Bmatrix} N^+ & \ell & N \\ \ell' & N^{+\prime} & k \end{Bmatrix}, \tag{B.10}$$

and

$$\mathcal{B}^{(0)}_{\mu\mu'} = [\ell(\ell + 1) + 2]\,\delta_{\mu\mu'}, \tag{B.11}$$

and

$$\mathcal{B}^{(2)}_{\mu\mu'} = P^k_{\mu\mu'}(-1)^{\ell+\ell'}\sum_{\ell_\nu}(-1)^{\ell_\nu}\ell_\nu(\ell_\nu+1)(2\ell_\nu+1)$$

$$\begin{pmatrix}\ell & 1 & \ell'\\ 0 & 0 & 0\end{pmatrix}\begin{pmatrix}\ell & 1 & \ell'\\ 0 & 0 & 0\end{pmatrix}\begin{Bmatrix}1 & 1 & 2\\ \ell' & \ell & \ell_\nu\end{Bmatrix}$$

$$\Big/\left[\begin{pmatrix}1 & 1 & 2\\ 0 & 0 & 0\end{pmatrix}\begin{pmatrix}\ell & 2 & \ell'\\ 0 & 0 & 0\end{pmatrix}\right] \tag{B.12}$$

and finally

$$\langle(N^+\ell)NM_N \mid \vec{N}^+\cdot\vec{\ell}\,\mid(N^{+\prime}\ell')N'M_{N'}\rangle = \delta_{NN'}\delta_{M_N M'_N}\delta_{N^+N^{+\prime}}\delta_{\ell\ell'}(-1)^{N+\ell+N^+}$$

$$\left[N^+(N^++1)(2N^++1)\ell(\ell+1)(2\ell+1)\right]^{\frac{1}{2}}\begin{Bmatrix}N^+ & \ell & N\\ \ell' & N^{+\prime} & 1\end{Bmatrix}. \tag{B.13}$$

APPENDIX C

STURMIAN BASIS

The Sturmian Basis is extremely useful in almost any problem involving Coulomb-like potentials. The Sturmian functions $S_{n\ell}^{(k)}(r)$ satisfy the ordinary differential equation [110]

$$\left[-\frac{1}{2}\frac{d^2}{dr^2}+\frac{\ell(\ell+1)}{2r^2}+\frac{k^2}{2}\right]S_{n\ell}^{(k)}(r)=\frac{nk}{r}S_{n\ell}^{(k)}(r) \tag{C.1}$$

where k is a constant that can be chosen to adjust the spatial extent of the Sturmian functions. Provided k is not n-dependent the Sturmians form a $\mathcal{L}^2$ representation.

The Sturmian functions are given explicitly by

$$S_{n\ell}^{(k)}(r)=N(2kr)^{\ell+1}e^{-kr}L_{n-\ell-1}^{(2\ell+1)}(2kr) \tag{C.2}$$

where the $L_{n-\ell-1}^{(2\ell+1)}(2kr)$ are Laguerre functions. To determine the normalization constant N and establish the completeness of the Sturmian functions it is useful to state some of the properties of Laguerre functions. The normalization of the Laguerre functions $\{L_n^{(\alpha)}(x)\}$ [111, 112] is given by

$$\int_0^\infty dx e^{-x}x^{\alpha+1}L_n^{(\alpha)}(x)L_n^{(\alpha)}(x)=\frac{(n+\alpha)!}{n!}(2n+\alpha+1) \tag{C.3}$$

and their orthogonality is given by

$$\int_0^\infty dx e^{-x}x^{\alpha}L_n^{(\alpha)}(x)L_m^{(\alpha)}(x)=\frac{(n+\alpha)!}{n!}\delta_{nm}. \tag{C.4}$$

From the normalization condition for the Laguerre functions it is easy to show that the Sturmian normalization constant is

$$N = \left[\frac{k(n-\ell-1)!}{n(n+\ell)!}\right]^{\frac{1}{2}} \tag{C.5}$$

so that

$$\int_0^\infty dr S_{n\ell}^{(k)}(r) S_{n\ell}^{(k)}(r) = 1. \tag{C.6}$$

In order to show that the Sturmian functions form a complete orthonormal set, as defined by Sturm-Liousville Theory [111, 113], we need to find a weight function such that

$$\int_0^\infty dr \rho(r) S_{n\ell}^{(k)}(r) S_{n\ell}^{(k)}(r) = 0. \tag{C.7}$$

Using the orthogonality condition for Laguerre functions it is easy to show that the Sturmian weight function is given by

$$\rho(r) = \frac{n}{kr}. \tag{C.8}$$

The the formal completeness relation for the Sturmian functions is

$$\sum_{n=\ell+1}^{\infty} \frac{n}{k(rr')^{\frac{1}{2}}} S_{n\ell}^{(k)}(r) S_{n\ell}^{(k)}(r') = \delta(r-r'). \tag{C.9}$$

APPENDIX D

PROLATE SPHEROIDAL COORDINATES

The prolate spheroidal coordinates are particularly useful in the description of two center problems [77, 111]. Let the two centers be located at distances r_a and r_b from a common origin. The orthogonal prolate spheroidal coordinates are defined in terms of a radial coordinates ξ

$$\xi \equiv \frac{r_a + r_b}{R} \qquad \text{with} \;\; 1 \leq \xi < \infty, \tag{D.1}$$

an angular coordinate η

$$\eta \equiv \frac{r_a - r_b}{R} \qquad \text{with} \;\; -1 \leq \eta \leq 1, \tag{D.2}$$

and an azimuthal coordinate ϕ

$$\phi \qquad \text{with} \;\; 0 \leq \phi \leq 2\pi. \tag{D.3}$$

The differential volume elements is

$$d\tau = \frac{R^3(\xi^2 - \eta^2)}{8} d\xi d\eta d\phi. \tag{D.4}$$

The Laplacian is

$$\nabla^2 = \frac{4}{R^2(\xi^2 - \eta^2)} \left\{ \frac{\partial}{\partial \xi}(\xi^2 - 1)\frac{\partial}{\partial \xi} + \frac{\partial}{\partial \eta}(1 - \eta^2)\frac{\partial}{\partial \eta} + \frac{(\xi^2 - \eta^2)}{(\xi^2 - 1)(1 - \eta^2)}\frac{\partial^2}{\partial \phi^2} \right\}. \tag{D.5}$$

The use of prolate spheroidal coordinates in the generalized hydrogen molecular ion facilitates the separation of the electronic Schrödinger equation into three equations coupled by separation constants.

APPENDIX E

FINITE ELEMENT METHOD

The method of finite elements belongs to a class of numerical techniques used to solve ordinary and partial differential equations. In general, the method transforms a set of coupled differential equations into a variational, generalized eigenvalue problem. Depending on how the problem is formulated, a discrete set of bound and continuum energy eigenstates can be obtained, or by chosing the eigenvalue to be the log-derivative of the wavefunction at the boundary of the system, continuous energy eigenstates can be obtained. Here the finite element method for a one-dimensional Schrödinger equation with a restricted configuration space is developed, corresponding to the first case where discrete bound and continuum states are desired.

The Schrödinger equation for an arbitray potential $V(r)$, for $0 \leq r < \infty$, is, in atomic units,

$$\left(-\frac{1}{2}\frac{d^2}{dr^2} + V(r) - E\right)\psi(r) = 0. \tag{E.1}$$

Let us define an integral S

$$S \equiv \int_0^\infty dr\psi(r)\left(-\frac{1}{2}\frac{d^2}{dr^2} + V(r) - E\right)\psi(r). \tag{E.2}$$

Integrating by parts this becomes

$$S = \int_0^\infty dr\left[\psi(r)\left(V(r) - E\right)\psi(r) + \frac{1}{2}\left(\frac{d\psi(r)}{dr}\right)^2\right] + \left[\frac{1}{2}\psi(r)\frac{d\psi(r)}{dr}\right]_0^\infty. \tag{E.3}$$

Now for most problems of interest $lim_{r\to 0}\psi(r) = 0$. However, let us impose the condition that $lim_{r\to\infty}\frac{d\psi(r)}{dr} = 0$ so that the surface term, obtained from the integration by parts, vanishes. This final boundary condition is appropriate for bound states, but discretizes all continuum states (Pseudo States).

Let us now define an action A

$$A \equiv \frac{1}{2}\left(\frac{d\psi(r)}{dr}\right)^2 + \psi(r)\left(V(r) - E\right)\psi(r). \tag{E.4}$$

Then by the Euler-Lagrange equation

$$\frac{dA}{d\psi} - \frac{d}{dr}\frac{dA}{d\left(\frac{d\psi(r)}{dr}\right)} = 2\left(V(r) - E\right)\psi(r) - \frac{d^2}{dr^2}\psi(r) = 0 \tag{E.5}$$

vanishes since the last expression is just the original Schrödinger equation. Thus $\delta S = 0$ and S is a variational equation.

The power of the finite element method is derived by chosing a basis set that provides both computational accuracy and efficiency. Imagine that the interval $0 \leq r < \infty$ is broken into M sectors and that in each sector we expand the wavefunction $\psi(r)$ in a basis. Let us choose the basis to be six polynomials $\{f_i(r)\}$ with the constraints that one is nonzero at any boundary and another has a nonzero derivative at any boundary in a given sector as show in Figure E.1. That is, let us expand the wavefunction as

$$\psi(r) = \sum_{m=1}^{M}\sum_{i=1}^{6} c_i^m f_i^{(m)}(r), \tag{E.6}$$

where the $\{f_i^{(m)}(r)\}$ is a set of six polynomials defined within the m-th sector boundaries. Since $\delta S = 0$

$$\frac{\partial S}{\partial c_i^m} = 0, \tag{E.7}$$

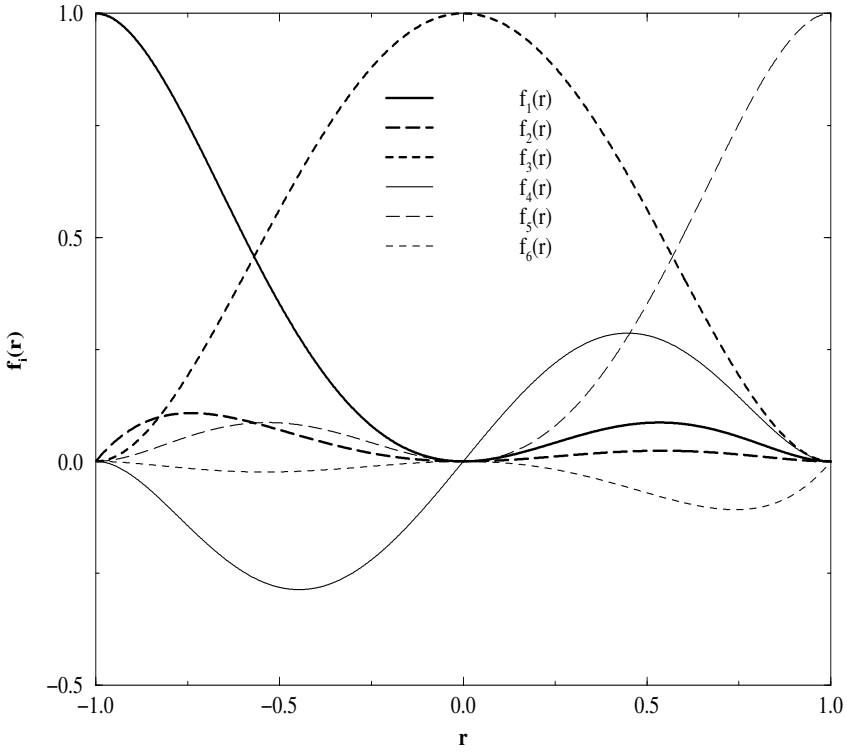

Figure E.1: Polynomial basis set used in finite element method.

where the $\{c_i^m\}$ are interpreted as variational parameters. Substituting the $\psi(r)$ expansion, Eq.[E.6], into the expression for S, Eq.[E.2], and using this partial derivative expression we find the generalized eigenvalue equation

$$\sum_{m=1}^{M}\sum_{j=1}^{6}\int_{r_{m-1}}^{r_m} dr^{(m)}\left[\frac{1}{2}\frac{df_i^{(m)}(r)}{dr}\frac{df_j^{(m)}(r)}{dr}+f_i^{(m)}(r)V(r)f_j^{(m)}(r)\right]c_j^m$$

$$= E\sum_{m=1}^{M}\sum_{j=1}^{6}\int_{r_{m-1}}^{r_m} dr f_i^{(m)}(r)f_j^{(m)}(r)c_j^m. \tag{E.8}$$

Since we have chosen to partition the configurations space, in addition to expanding the wavefunction in a discrete basis, the wavefunction and its derivative must be forced to be continuous across each sector boundary. As a result, not all of the c_i^m coefficients are independent. However, the nature of the polynomial basis set ensures that in any sector only the first two coefficients are coupled to the previous sector, and the last two coefficients are coupled to the next sector.

The wavefunction and its derivative in the m th sector are

$$\psi^{(m)}(r) = \sum_{i=1}^{6} c_i^m f_i^{(m)}(r), \tag{E.9}$$

$$\frac{d}{dr}\psi^{(m)}(r) = \sum_{i=1}^{6} c_i^m \frac{df_i^{(m)}}{dr}(r). \tag{E.10}$$

Continuity of the wave function between sectors m and $m+1$, at the boundary coordinate r_m, is given by

$$\sum_{i=1}^{6} c_i^m f_i^{(m)}(r_m) = \sum_{j=1}^{6} c_j^{m+1} f_j^{(m+1)}(r_m) \tag{E.11}$$

and the continuity of the derivative of the wavefunction across the boundary is

$$\sum_{i=1}^{6} c_i^m \frac{df_i^{(m)}}{dr}(r_m) = \sum_{j=1}^{6} c_j^{m+1} \frac{df_j^{(m+1)}}{dr}(r_m). \tag{E.12}$$

From these equations and the choice of our polynomial basis, the relationship among the sector coefficients is

$$c_5^m = c_1^{m+1} \qquad \text{and} \qquad c_6^m = c_2^{m+1}. \tag{E.13}$$